

Dissertation

submitted to the
Combined Faculties for the Natural Sciences and for Mathematics
of the
Ruperto-Carola University of Heidelberg, Germany
for the degree of
Doctor of Natural Sciences

put forward by

Simon Schettler

born in Poughkeepsie, USA

Oral examination: July 21st, 2015

A Model with Two Periods of Inflation

Referees: PD Dr. Jürgen Schaffner-Bielich
Prof. Dr. Matthias Bartelmann

Abstract

In this work a scenario with two subsequent periods of inflationary expansion in the very early Universe is examined. The model is based on a potential motivated by symmetries being found in field theory at high energy. For various parameter sets of the potential the spectra of scalar and tensor perturbations that are expected to originate from this scenario are calculated. Also the beginning of the reheating epoch connecting the second inflation with thermal equilibrium is studied. Both is done in comparison with standard potentials leading to accelerated cosmic expansion. Perturbations with wavelengths leaving the horizon around the transition between the two inflations are special: It is demonstrated that the power spectrum at such scales deviates significantly from expectations based on measurements of the cosmic microwave background (CMB). This supports the conclusion that parameters for which this part of the spectrum leaves observable traces in the CMB must be excluded. Parameters entailing a very efficient second inflation correspond to standard small-field inflation and can meet observational constraints. Particular attention is paid to the case where the second inflation leads solely to a shift of the observable spectrum from the first inflation. A viable scenario requires this shift to be small.

In dieser Arbeit wird ein Szenario mit zwei aufeinanderfolgenden Phasen inflationärer Expansion im sehr frühen Universum untersucht. Das Potential zu diesem Modell stützt sich auf Symmetrien, die für Feldtheorien bei hoher Energie relevant sind. Für verschiedene das Potential bestimmende Parametersätze werden die Spektren skalarer und tensorieller Störungen berechnet, die durch die Inflationen in diesem Modell entstehen. Außerdem wird der Beginn des Reheating untersucht, das den Übergang von der Inflation zur anschließenden Big-Bang-Expansion im thermischen Gleichgewicht bildet. Die Ergebnisse werden jeweils mit Rechnungen zu den klassischen inflationären Potentialen verglichen. Störungen auf Längenskalen, die um den Übergang zwischen den zwei Inflationen herum den Horizont verlassen, zeigen ungewöhnliches Verhalten: Die Ergebnisse zeigen, dass das Leistungsspektrum für diese Wellenlängen signifikant von den Erwartungen abweichen, die sich aus Beobachtungen des kosmischen Mikrowellenhintergrundes (CMB) ergeben. Dies lässt den Schluss zu, dass Parametersätze, für die dieser Teil des Spektrums im CMB beobachtbar ist, ausgeschlossen werden müssen. Die Ergebnisse aus Parametersätzen, die zu sehr starker Expansion während der zweiten Inflation führen, liegen teils im durch die Beobachtungen erlaubten Bereich. Die Fälle, bei denen die zweite Inflation ausschließlich zu einer Verschiebung des beobachtbaren Spektrums aus der ersten Inflation führt, werden eingehender untersucht. Die Beobachtungen fordern eine möglichst kleine Verschiebung.

Contents

1. Introduction	1
2. Some aspects of the theory of relativity	5
2.1. Special relativity	5
2.2. General relativity	6
2.2.1. Important quantities	6
2.2.2. The Friedmann–Robertson–Walker spacetime	8
2.2.3. Basics of metric fluctuations	10
2.2.4. Primordial spectra of scalar fluctuations	16
2.2.5. Primordial spectra of tensor fluctuations	18
3. Elements of field theory	19
3.1. Equations for flat and FRW spacetimes	19
3.2. Symmetries and conserved currents	21
3.3. Chiral symmetry for two flavors of fermions	22
3.4. Quantum chromodynamics	24
3.4.1. The Lagrange density of QCD	25
3.4.2. Symmetries and other properties	26
3.5. Effective theories of strong interactions	32
3.5.1. Mesonic states and their chiral transformation	32
3.5.2. Chiral symmetry breaking	33
3.5.3. Linear sigma model	34
3.5.4. The dilaton field in string theory	36
3.5.5. Linear sigma model with dilaton	38
4. Hot Big Bang cosmology	41
4.1. Evolution of the universe after inflation	41
4.2. A cosmic timeline	42
4.3. Problems of pure Big Bang	43
4.3.1. Horizon problem	44
4.3.2. Flatness problem	45
4.3.3. Monopole problem	45
4.3.4. Primordial perturbations	46
5. Inflation	47
5.1. Short history of cosmological inflation	47
5.2. Inflation as a solution to cosmological problems	49
5.3. Inflation driven by a homogeneous scalar field	51

5.3.1.	Slow-roll inflation	52
5.3.2.	Large-field inflation	53
5.3.3.	Hilltop inflation	55
5.3.4.	Hybrid inflation	57
5.4.	Inflation and the origin of fluctuations	59
5.4.1.	Scalar perturbations	59
5.4.2.	Tensor perturbations	65
5.4.3.	The spectra of fluctuations after slow-roll inflation	65
5.5.	Examples and observations	67
5.6.	A universe without inflation?	74
6.	Fluctuations after two periods of inflation	77
6.1.	The potential and its simplification	77
6.2.	Evolution of the homogeneous mode	79
6.3.	Scalar and tensor perturbations	81
6.4.	Compatibility with measurements	84
7.	Fluctuations produced after inflation: Preheating	89
7.1.	Initial vacuum fluctuations	89
7.2.	Periodically changing mass and the Mathieu equation	91
7.2.1.	Broad and narrow parametric resonance	91
7.2.2.	Transmission and reflection coefficients	97
7.2.3.	Evolution of the particle number	99
7.2.4.	Particle production in Minkowski spacetime	102
7.3.	Effects of the Hubble expansion	103
7.4.	Preheating within $\lambda\phi^4$ theory	107
7.5.	Preheating after hilltop inflation	109
7.5.1.	Slow roll and oscillations of the homogeneous field	109
7.5.2.	Tachyonic preheating	111
7.5.3.	Parametric resonance	114
7.6.	Preheating within a model with two periods of inflation	115
8.	Conclusion	119
Appendix A.	Equations of linearized General Relativity	125
A.1.	Linearized Einstein tensor	125
A.2.	Conformal transformations	126
A.3.	Linearization within FRW background	127
A.4.	Linearized evolution equations	128
Appendix B.	LATTICEASY	131
B.1.	General lattice issues	131
B.2.	The implementation of vacuum fluctuations	132
B.3.	Staggered leapfrog method	134
B.4.	Particle number density of classical fields	135
Appendix C.	An auxiliary calculation	137

1. Introduction

After countless attempts to understand our world as a whole and yet many years and centuries after scientific methods have been adopted as the way of learning from nature, in the early twentieth century Albert Einstein's invention of the general theory of relativity laid the foundation of modern cosmology. This chapter lists some of the most important steps, leading to Einstein's insight and afterwards to cosmology supported by precision measurements. The presentation relies on information from Refs. [2, 53, 82, 83, 116].

As other branches of science, cosmology emerged from prehistoric myths. Even among the early archeological evidence of mankind, such as the paintings in the caves of Lascaux and Altamira, some have been interpreted as symbols and reproductions of observations in the night sky. Much later, around 5500 years ago, megalithic cultures left their monuments to be marveled at by civilizations to come. It is assumed that for example the arrangements in Stonehenge have been built also in the context of astronomical observations.

About 4500 year-old, written documents from ancient Egypt and Mesopotamia give much more details on the belief about the cosmos in these cultures. It is not based on observation, of course, but on religious traditions. Also in Indian and Greek culture, cosmology maintained the character of a creation myth, often complemented by the assumption of cyclic processes of generation and destruction. It should be mentioned that the approach to cosmology is in contrast with a more scientific treatment of astronomy in ancient Mesopotamia.

A major step towards modern science has been made by Greek philosophers from 600 B.C. onward. They tried to understand natural phenomena in terms of general laws leaving behind the belief in personal gods being responsible for them. Examples are the Milesian philosophers Thales and Anaximander, who already made considerations of symmetry: Taken to be at the center of the universe the Earth should be immobile. This can be seen as an example that reasoning has been accepted as a possible way towards insight, regardless of whether the result seems doubtful from a modern view. A more religious school was established by the Pythagoreans. However, it should be mentioned that they promoted the assumption of a spherical Earth not being at the center of the universe. Around 430 B.C., this was a major new concept.

Astronomy had become an important field of observation and theory in ancient Greece. In contrast, being more elusive to observation, cosmology left the area of interest for a long time. Let us leave the presentation of ancient ideas of the cosmos by stating that Plato and Aristotle argued in favor of Earth as the center of the universe. As a

Chapter 1. Introduction

consequence, the observed motions of the planets were not easy to understand. Nevertheless, the picture of the central immobile Earth and of planets moving on complicated paths was not questioned in the following centuries.

Nicolaus Cusanus (1401–1464) speculated about the infinity of the cosmos and argued that the Earth is not the center of the universe. Nicolaus Copernicus (1473–1543) is famous for breaking with this tradition. His assumption of the sun as the center of the universe can be dated back at least to the time around the year 1512. Giordano Bruno (1548–1600) went even further and stated for example that from each point in space the universe looks the same. This bold assertion is known as the cosmological principle today. At that time it proved difficult for many scientists to accept a heliocentric world. This changed during the seventeenth century when Galileo Galilei (1564–1642) observed the phases of Venus and Johannes Kepler (1571–1630) published his discovery of a new star, contradicting the assumed invariability of the fixed star sphere.

The heliocentric picture has been accepted and the Milky Way has proven to consist of single stars when Isaac Newton (1642–1727) developed the first theory of gravity. Published in 1687, his “*Philosophiae Naturalis Principia Mathematica*” were a first step towards a unification of forces: Gravity on Earth could be explained by the same equations as Kepler’s laws of planetary motion. It is well-known that Newtonian mechanics is sufficient to explain many phenomena and is applicable to a large range of scales. Newton thought of the universe as being static and tried to find the mechanism which prevents the distribution of stars from collapsing. However, such problems could not be solved with the methods of the time.

Immanuel Kant (1724–1804) speculated about the cosmos outside our galaxy and assumed that the known nebulae could be distant galaxies. This was also to back the cosmological principle of homogeneity on large scales.

Serious doubts about the contemporary view on the universe were raised by Heinrich Wilhelm Olbers (1758–1840) in 1823 when he considered the darkness of the night sky contradictory to the assumption that the universe is static and infinite in both space and time. A few years earlier, Carl Friedrich Gauss (1777–1855) has written to him about his speculations on alternatives to Euclidean geometry. Bernhard Riemann (1826–1866) identified three possibilities—flat space, positive curvature and negative curvature—as candidates for a viable geometry of the universe at a given moment in time. He pointed out that a three-dimensional space with positive curvature can be finite and unbounded and that this might be the case in our universe. On this basis Karl Friedrich Zöllner (1834–1882) could overcome Olbers’ paradox without putting bounds to time and space of the universe. In 1900 Karl Schwarzschild (1873–1916) put limits on the spatial curvature using the parallax of distant stars [118]. However, curvature of space was beyond the interest of physics and astronomy of the time.

In 1913 Albert Einstein (1879–1955) appreciated the benefit of Riemann’s work with regard to the inclusion of gravity into his special theory of relativity. The general theory of relativity (GR) from 1915 was successfully tested during the solar eclipse in 1919. It did not show its value for cosmology because the generally accepted picture of the cosmos

still had the dimensions of the Milky Way within a void surrounding. Application of GR to cosmology was stimulated by Schwarzschild and Willem de Sitter (1872–1934). In 1917 Einstein’s result included the cosmological constant such that a stationary state is possible [45].

However, GR did not play an important role for astronomers in the following years. Most important for many scientists were the size of the Milky Way and the nature of the nebulae, topics which were discussed at the Great Debate in 1920. This was settled by Hubble’s observation of Cepheid variables in the Andromeda Nebula. Using Henrietta Leavitt’s [86] relation of the period and the luminosity of those pulsating stars, he could show that this structure is located far beyond the range of the Milky Way. This supported the picture of an “island universe” with several similar structures surrounding our galaxy. A further issue backing this picture was raised by Vesto Melvin Slipher’s (1875–1969) observation of Doppler shifts in the spectral lines of nebulae receding from us [119]. In 1922 Alexander Friedmann (1888–1925) realized the theoretical possibility of an expanding cosmological solution of Einstein’s equation and also considered a beginning of the evolution with zero radius [54]. A similar result was obtained in 1927 by Georges Lemaitre (1894–1966) who ascribed the redshift of the nebulae to an effect of cosmological expansion [87]. He is considered as the inventor of the Big Bang scenario. Lemaitre’s work became known only after Edwin Hubble (1889–1953), who himself was unaware of these results, published his empirical studies on the linear relation between redshifts and distances in 1929, see Ref. [72]. Compared to the modern value, he obtained a far too large proportionality constant between distance and redshift: In the later interpretation, this means that he obtained much bigger recession velocities than accepted today. Also Hubble’s work was not seen as groundbreaking at that time. Big Bang models became more popular in the 1940’s: In 1948, George Gamow (1904–1968), Ralph Alpher (1921–2007), and, for the sake of naming, Hans Bethe (1906–2005) published their “ $\alpha\beta\gamma$ theory” of Big Bang nucleosynthesis. In the 1950’s the theory became less popular because nucleosynthesis in stars and novae was found as an explanation for the existence of heavier elements which could not be synthesized in the early universe.

A serious competitor was the steady state theory which extended the cosmological principle to the assumption of homogeneity in time. Thus it avoided the age paradox being a problem of the Big Bang models. However, starting in 1964 with the discovery of the cosmic microwave background (CMB) by Arno Penzias (*1933) and Robert Woodrow Wilson (*1936), the steady state theory became disfavored by most scientists. Robert Dicke (1916–1997) and James Peebles (*1935) interpreted the radiation as a relic of the early universe [44, 110].

An important ingredient to Big Bang cosmology was added in the 1990’s, when observations of supernovae suggested a recent acceleration of the universe. For this discovery, Saul Perlmutter (*1959), Brian Schmidt (*1967), and Adam Riess (*1969) shared the Nobel Prize in 2011. Their method uses type Ia supernovae as standard candles similar to the use of Cepheids earlier. The acceleration is attributed to the fact that vacuum energy gives the dominant contribution to the energy content of the universe today.

The latest developments in cosmology were due to the increasingly accurate observations of the CMB fluctuations. Important projects in this respect were the space-based measurements of COBE (Cosmic Background Explorer), WMAP (Wilkinson Microwave Anisotropy Probe), and Planck [1]. COBE showed in 1992 the anisotropy of the CMB on scales larger than 10° . The measurements have been improved dramatically by WMAP since 2001 and by Planck since 2009. The details of the CMB anisotropies permit a much deeper understanding of the cosmic history.

Today, the CMB fluctuations are explained by various mechanisms. One of them gives rise to the primeval spectra of density fluctuations and gravitational waves which is later imprinted on the background radiation of photons. This mechanism is called inflation. Since the key issue of this work is the inflationary scenario in the early universe its historical development is given some extra space in Section 5.2.

This thesis has the following structure: In Chapter 2 some basic notions of the theory of relativity are introduced. Then cosmological perturbations and their characterizing spectra are presented.

The discussion of cosmological inflation makes use of some concepts of field theory. For example, with regard to the motivation of the potential, symmetries in field theories play an important role. These concepts are the main topic of Chapter 3.

In Chapter 4 a timeline of the universe after inflation is given and the observational problems arising for a scenario without inflation are discussed.

Chapter 5 reviews three classic scenarios of inflation together with their observable consequences before the details of a model with two subsequent inflationary periods are described in Chapter 6.

This work also includes calculations of particle spectra originating from the decay of the inflaton field after inflation. More precisely, Chapter 7 gives a presentation of lattice computations, which concern the early, non-perturbative phase of this decay. Such a period of strong particle production is called “preheating”. It precedes (or is sometimes also included into) the stage of reheating that leads to a state of thermal equilibrium. When equilibrium is reached, the hot Big Bang evolution of the universe begins. The calculations on preheating are done for the same potentials that are considered with respect to the production of fluctuations during inflation.

The presentation ends with some remarks on the conclusions that can be drawn and with hints to related and possible future work.

Throughout the thesis, units with $c = k_B = \hbar = 1$ are used. The Planck mass is $m_{\text{Pl}} = 1/G \approx 1.2 \cdot 10^{19} \text{GeV}$. The signature of the metric is $(+, -, -, -)$. If not stated differently, dots denote derivative with respect to cosmic time. Primes are used for derivatives with respect to conformal time with the exceptions V' , V'' , and U' , where the derivative of the potentials is taken with respect to a scalar field. In this thesis our Universe is called universe. A persistent distinction according to the degree of uniqueness in the corresponding context seemed too contrived to me.

2. Some aspects of the theory of relativity

2.1. Special relativity

In special relativity the notion of a distance in space is extended to spacetime. The generalized concept is called the spacetime interval and up to an overall sign, which depends on convention, it is defined as

$$ds^2 = dt^2 - dx^2 - dy^2 - dz^2. \quad (2.1)$$

With the metric tensor $\eta_{\mu\nu} = \text{diag}(1, -1, -1, -1)$ this equation is conveniently written as

$$ds^2 = \eta_{\mu\nu} dx^\mu dx^\nu. \quad (2.2)$$

Here and throughout this thesis the Einstein convention implies summation over each pair of identical indices. Coordinates (t, x, y, z) , in which the spacetime interval can be written as above, are called Minkowski coordinates. They set up an inertial frame. Different inertial frames are connected by coordinate transformations. Besides reversal of coordinates, these transformations are elements of the Poincaré group, which consists of translations and Lorentz transformations $\Lambda \in SO(1, 3)$. The defining property of the latter is the invariance of the metric,

$$\Lambda^\alpha_\mu \Lambda^\beta_\nu \eta_{\alpha\beta} = \eta_{\mu\nu}, \quad (2.3)$$

where the entries of the transformation matrix Λ are spacetime independent. The coordinates in the new frame are

$$\tilde{x}^\mu = \Lambda^\mu_\nu x^\nu, \quad (2.4)$$

and the transformation matrix can be written as

$$\Lambda^\mu_\nu = \frac{\partial \tilde{x}^\mu}{\partial x^\nu}. \quad (2.5)$$

Under such a transformation a scalar field stays the same:

$$\tilde{\phi}(\tilde{x}) = \phi(x). \quad (2.6)$$

The components of any (contravariant) vector field with upper indices, $A^\mu(x)$, behave as in Eq. (2.4):

$$\tilde{A}^\mu(\tilde{x}) = \frac{\partial \tilde{x}^\mu}{\partial x^\nu} A^\nu(x). \quad (2.7)$$

Upper indices can be lowered by contraction with the metric,

$$B_\mu(x) = \eta_{\mu\nu} B^\nu(x), \quad (2.8)$$

obtaining a covariant vector. The result of a contraction $A^\mu B_\mu$ is a scalar and does not change under Lorentz transformations. So the transformation of B_μ has to be inverse to that of A^μ ,

$$\tilde{B}_\mu(\tilde{x}) = \frac{\partial x^\nu}{\partial \tilde{x}^\mu} B_\nu(x). \quad (2.9)$$

The way of a particle through spacetime is called its worldline. It can be parameterized by the time τ measured by an observer moving with the particle: $x^\mu(\tau)$. Then the 4-velocity of the particle is

$$u^\mu = \frac{dx^\mu}{d\tau}. \quad (2.10)$$

The 4-momentum is

$$p^\mu = m u^\mu = (E, \mathbf{p}), \quad (2.11)$$

with particle mass m , energy E and momentum \mathbf{p} . The second version is valid also for massless particles. If not single particles but fluids are considered, the velocity and momentum fields $u^\mu(x^\mu)$ and $p^\mu(x^\mu)$ replace the last two functions. Energy and momentum of a fluid are more properly accounted for with the help of the energy–momentum tensor $T^{\mu\nu}$. For a perfect fluid it can be written in terms of u^μ , the energy density ρ and the pressure p ,

$$T^{\mu\nu} = (\rho + p)u^\mu u^\nu - p\eta^{\mu\nu}. \quad (2.12)$$

The metric with upper indices $\eta^{\mu\nu}$ can be thought of as the inverse of $\eta_{\mu\nu}$, but it has the same numerical entries in Minkowski spacetime. Energy–momentum conservation is written as

$$\partial_\mu T^{\mu\nu} = 0. \quad (2.13)$$

2.2. General relativity

2.2.1. Important quantities

In combination with quantum mechanics, special relativity is able to treat the dynamics of the forces in the standard model of particle physics. However it is not suitable to handle gravity. To include gravitational effects the notion of inertial coordinates within Minkowski spacetime has to be abandoned. Instead, spacetime is viewed as a

more general, curved manifold which is described using a metric $g_{\mu\nu}(x)$. The interval Eq. (2.2) is replaced by

$$ds^2 = g_{\mu\nu}(x)dx^\mu dx^\nu. \quad (2.14)$$

Because in general the choice of a global inertial system is not possible, Lorentz transformations lose their specific character. One considers the much bigger class of diffeomorphic transformations of coordinates

$$x^\mu \longrightarrow \tilde{x}^\mu(x^\nu). \quad (2.15)$$

The transformation laws as written in Eqs. (2.6), (2.7), and (2.9) can be adopted without change. Tensors with multiple indices transform like products of according numbers of co- and contravariant vectors.

Raising and lowering indices is done with the metric $g_{\mu\nu}$ and its inverse $g^{\mu\nu}$. The determinant

$$\det g_{\mu\nu} = g < 0 \quad (2.16)$$

is used to define the diffeomorphism invariant measure $\sqrt{-g}d^4x$ for integration. To describe dynamics within curved spacetime also an appropriate derivative is needed: Tensors that are defined on different points of a manifold need to be (parallel) transported to the same point. Only then they can be subtracted from each other in order to calculate a derivative. The parallel transport is only along a small distance, and so its effect is taken to be linear. Put together, a derivative transforming a tensor into a tensor can be defined as

$$\nabla_\nu A^\mu(x) = \partial_\nu A^\mu(x) + \Gamma_{\rho\nu}^\mu(x)A^\rho(x) \quad (2.17)$$

and is called covariant derivative. The (non-tensorial) quantities $\Gamma_{\rho\nu}^\mu$ are called the Christoffel symbols. They constitute the connection within general relativity (GR) and they are calculated as

$$\Gamma_{\nu\lambda}^\mu = \frac{1}{2}g^{\mu\rho}(\partial_\nu g_{\rho\lambda} + \partial_\lambda g_{\rho\nu} - \partial_\rho g_{\nu\lambda}). \quad (2.18)$$

The covariant derivative is defined with the help of parallel transport. It can be used to quantify curvature because in curved space parallel transport depends non-trivially on the path which is chosen between two points. The following commutator of two covariant derivatives (acting on the vector A^ρ) corresponds to the difference of parallel transport along two paths that are both piecewise along one coordinate:

$$[\nabla_\mu, \nabla_\nu]A^\rho = (\nabla_\mu \nabla_\nu - \nabla_\nu \nabla_\mu)A^\rho = A^\sigma R_{\sigma\mu\nu}^\rho. \quad (2.19)$$

It can be checked that it is a linear transformation and all derivatives of the vector field A^ρ cancel. This yields the Riemann tensor,

$$R_{\nu\rho\sigma}^\mu = \partial_\rho \Gamma_{\nu\sigma}^\mu - \partial_\sigma \Gamma_{\nu\rho}^\mu + \Gamma_{\lambda\rho}^\mu \Gamma_{\nu\sigma}^\lambda - \Gamma_{\lambda\sigma}^\mu \Gamma_{\nu\rho}^\lambda, \quad (2.20)$$

Chapter 2. Some aspects of the theory of relativity

as a characterization of curvature. The Ricci tensor $R_{\mu\nu}$ and the Ricci scalar R are defined via contractions of the Riemann tensor:

$$R_{\mu\nu} = R_{\mu\sigma\nu}^{\sigma}, \quad R = R_{\mu\nu}g^{\mu\nu}. \quad (2.21)$$

The action that defines GR is the Hilbert action with Lagrangian \mathcal{L} proportional to R ,

$$S_H = -\frac{m_{\text{Pl}}^2}{16\pi} \int d^4x \sqrt{-g} R. \quad (2.22)$$

Variation with respect to the metric yields the left hand side of the Einstein equation

$$R_{\mu\nu} - \frac{1}{2}Rg_{\mu\nu} = \frac{8\pi}{m_{\text{Pl}}^2} T_{\mu\nu}. \quad (2.23)$$

From the calculation of the Riemann tensor it is seen that it contains second derivatives of the metric. However, doing the variation of S_H shows that this does not lead to higher derivatives in the equation of motion: Eq. (2.23) is a differential equation of second order.

The right hand side of Eq. (2.23) stems from the action of the matter field content of spacetime. This action should be added to S_H . The result of variation with respect to the metric is found to be the energy–momentum tensor $T_{\mu\nu}$. For example the Lagrangian of a scalar field

$$\mathcal{L} = \frac{1}{2}g^{\mu\nu}\partial_{\mu}\phi\partial_{\nu}\phi - V(\phi) \quad (2.24)$$

gives

$$T_{\mu\nu} = \partial_{\mu}\phi\partial_{\nu}\phi - g_{\mu\nu}\mathcal{L}. \quad (2.25)$$

Because the Einstein tensor,

$$G_{\mu\nu} = R_{\mu\nu} - \frac{1}{2}Rg_{\mu\nu}, \quad (2.26)$$

is divergenceless, energy–momentum conservation,

$$\nabla_{\mu}T^{\mu\nu} = 0, \quad (2.27)$$

is consistent with the Einstein equation (2.23). In terms of energy density ρ , pressure p and the local velocity field u^{μ} the energy–momentum tensor (2.25) is written as

$$T_{\mu\nu} = (\rho + p)u^{\mu}u^{\nu} - pg^{\mu\nu}. \quad (2.28)$$

This is the general form for an ideal fluid.

2.2.2. The Friedmann–Robertson–Walker spacetime

General relativity is the framework which is used to describe the cosmological evolution, and from observations it is known that our universe is isotropic and homogeneous in

space on large scales. Then the theory of maximally symmetric spaces states that space-time can be described as a 3-dimensional sphere, plane or hyperboloid which evolves in time. The metric of such a space can be cast into the form

$$dl^2 = \frac{dr^2}{1 - \kappa r^2/R^2} + r^2(d\theta^2 + \sin^2 \theta d\phi^2), \quad (2.29)$$

where κ is +1 for the sphere, 0 for the plane and -1 for the hyperboloid. R is the radius of the sphere: Thought of as embedded in a 4-dimensional space with coordinates $x_{(i)}$, the equation for the sphere and the hyperboloid would be

$$x_{(1)}^2 + x_{(2)}^2 + x_{(3)}^2 + x_{(4)}^2 = R^2 \quad (2.30)$$

and

$$x_{(1)}^2 - x_{(2)}^2 - x_{(3)}^2 - x_{(4)}^2 = R^2, \quad (2.31)$$

respectively. Including the time coordinate, the metric is

$$ds^2 = dt^2 - a^2(t)\gamma_{ij}dx^i dx^j, \quad (2.32)$$

where $\gamma_{ij}dx^i dx^j$ stands for the spatial part, Eq. (2.29), and $a(t)$ is the scale parameter. The right hand side of Eq. (2.32) is called the Friedmann–Robertson–Walker (FRW) or Friedmann–Lemaître–Robertson–Walker (FLRW) metric. The use of conformal time η with

$$d\eta = \frac{dt}{a(t)} \quad (2.33)$$

simplifies many calculations. Furthermore, spatial curvature can be neglected on large scales. So the metric is written as

$$ds^2 = a^2(\eta)(d\eta^2 - \delta_{ij}dx^i dx^j). \quad (2.34)$$

The scale-factor $a(\eta)$ is a non-vanishing function. So, by definition, this metric is related to the Minkowski metric $\eta_{\mu\nu}$ by a conformal transformation. For better clarity, let us list the following properties:

$$g_{\mu\nu} = a^2(\eta)\eta_{\mu\nu}, \quad g^{\mu\nu} = a^{-2}(\eta)\eta^{\mu\nu}, \quad \sqrt{-g} = a^4(\eta). \quad (2.35)$$

The next step is to determine the behavior of $a(t)$ and of the field content of spacetime. This is done with the help of Eq. (2.23) whose 00-component reads

$$R_{00} - \frac{1}{2}g_{00}R = 3 \left(\frac{\dot{a}^2}{a^2} + \frac{\kappa}{a^2} \right) \quad (2.36)$$

(left hand side) and

$$T_{00} = (p + \rho)u_0u_0 - g_{00}p = \rho \quad (2.37)$$

(right hand side). With the definition of the Hubble parameter,

$$H(t) = \frac{\dot{a}(t)}{a(t)}, \quad (2.38)$$

this gives the (first) Friedmann equation,

$$H^2 = \frac{8\pi}{3m_{\text{Pl}}^2}\rho - \frac{\kappa}{a^2}. \quad (2.39)$$

For later reference, some further consequences—not always independent from each other—are listed in the following: Equation (2.23) exists also in a slightly different variant,

$$R_{\mu\nu} = \frac{8\pi}{m_{\text{Pl}}^2} \left(T_{\mu\nu} - \frac{1}{2} T g_{\mu\nu} \right), \quad (2.40)$$

which is obtained by taking the trace in the original version and using therein the result again. Its 00-component,

$$\frac{\ddot{a}}{a} = -\frac{4\pi}{3m_{\text{Pl}}^2}(\rho + 3p), \quad (2.41)$$

is sometimes called the second Friedmann equation. Using conformal time, the first Friedmann equation reads

$$\frac{a'^2}{a^4} = \frac{8\pi}{3m_{\text{Pl}}^2}\rho - \frac{\kappa}{a^2} \quad (2.42)$$

and, together with the second one, the Raychaudhuri equation,

$$2\frac{a''}{a^3} - \frac{a'^2}{a^4} = -\frac{8\pi}{m_{\text{Pl}}^2}p - \frac{\kappa}{a^2}, \quad (2.43)$$

is obtained. The Friedmann equations are complemented by energy–momentum conservation (2.27), which takes on the forms

$$\dot{\rho} = -3H(\rho + p) \quad \text{and} \quad \rho' = -3\frac{a'}{a}(\rho + p) \quad (2.44)$$

when using cosmic and conformal time, respectively. To fix the behavior of the medium and the scale factor in the homogeneous and isotropic case, the last equation needed is the equation of state,

$$p = p(\rho). \quad (2.45)$$

Some examples will be discussed in Chapter 4. The rest of this chapter is devoted to fluctuations in the metric and the fluid.

2.2.3. Basics of metric fluctuations

Fluctuations of the metric (2.34) are included as a spacetime dependent tensor $h_{\mu\nu}$. It is defined by the equation

$$g_{\mu\nu} = a^2(\eta)\gamma_{\mu\nu} = a^2(\eta_{\mu\nu} + h_{\mu\nu}(x)). \quad (2.46)$$

The homogeneous part of the metric is $\bar{g}_{\mu\nu} = a^2\eta_{\mu\nu}$. The entries of $h_{\mu\nu}$ are taken to be small and calculations are done up to terms of linear order. This means that the indices of $h_{\mu\nu}$ (and of other small quantities as well) are raised and lowered with the

unperturbed metric $\eta_{\mu\nu}$. In addition this entails a simple expression for the inverse of $\gamma_{\mu\nu}$,

$$\gamma_{\mu\nu}^{-1} = \gamma^{\mu\nu} = \eta^{\mu\nu} - h^{\mu\nu}, \quad (2.47)$$

and likewise for $g_{\mu\nu}$,

$$g_{\mu\nu}^{-1} = g^{\mu\nu} = \frac{1}{a^2} (\eta^{\mu\nu} - h^{\mu\nu}). \quad (2.48)$$

Gauge transformations. The tensor $h_{\mu\nu}$ is not completely fixed by (2.46). Rather, the invariance of GR under coordinate transformations allows for various splittings of the metric into background and fluctuations. The corresponding coordinate systems are linked up by “small” changes of coordinates which are called gauge transformations. More precisely, gauge transformations are induced by arbitrary infinitesimal functions $\xi^\mu(x)$ as

$$\tilde{x}^\mu = x^\mu + \xi^\mu(x), \quad (2.49)$$

such that

$$\tilde{g}^{\mu\nu}(\tilde{x}) = \frac{\partial \tilde{x}^\mu}{\partial x^\lambda} \frac{\partial \tilde{x}^\nu}{\partial x^\rho} g^{\lambda\rho}(x) = g^{\mu\nu}(x) + g_{(0)}^{\nu\lambda} \partial_\lambda \xi^\mu + g_{(0)}^{\mu\lambda} \partial_\lambda \xi^\nu, \quad (2.50)$$

where unperturbed quantities are labeled with a zero. The calculation is done to first order in the perturbations and in ξ^μ . On the other hand a Taylor expansion gives

$$\tilde{g}^{\mu\nu}(\tilde{x}) \approx g_{(0)}^{\mu\nu}(\eta) + \xi^\sigma \partial_\sigma g_{(0)}^{\mu\nu}(x) + \delta \tilde{g}^{\mu\nu}(\tilde{x}) \quad (2.51)$$

$$\approx \tilde{g}^{\mu\nu}(x) + \xi^\sigma \partial_\sigma g_{(0)}^{\mu\nu}(x), \quad (2.52)$$

where the first two terms of the first step add up to the background metric in the new coordinate system and the third one is the perturbation. The result is equated to the right hand side of (2.50), where the metric is split similarly as

$$g^{\mu\nu}(x) = g_{(0)}^{\mu\nu}(\eta) + \delta g^{\mu\nu}(x). \quad (2.53)$$

Then one has

$$\tilde{g}^{\mu\nu}(x) \approx g^{\mu\nu}(x) - \xi^\sigma \partial_\sigma g_{(0)}^{\mu\nu}(x) + g_{(0)}^{\nu\lambda} \partial_\lambda \xi^\mu + g_{(0)}^{\mu\lambda} \partial_\lambda \xi^\nu. \quad (2.54)$$

In this line the derivative of the metric can be replaced by Christoffel symbols (and metrics) because the corresponding covariant derivative vanishes. They are reorganized into conformal derivatives of ξ^μ such that one obtains

$$\tilde{g}^{\mu\nu}(x) = g^{\mu\nu}(x) + \nabla^\mu \xi^\nu(x) + \nabla^\nu \xi^\mu(x) \quad (2.55)$$

to first order in the perturbation. Equation (2.50) allows for immediate use of (2.48) to leave the gauge transformation of the metric fluctuation,

$$\tilde{h}^{\mu\nu}(x) = h^{\mu\nu}(x) - 2\eta^{\mu\nu} \xi^\sigma \frac{\partial \sigma a}{a} - \partial^\mu \xi^\nu - \partial^\nu \xi^\mu. \quad (2.56)$$

It will be used to simplify the calculation of perturbations.

Helicity decomposition. Since the FRW metric is spatially homogeneous and fluctuations are considered only to linear order, the treatment of Fourier transformed quantities is adequate. For example the metric fluctuation is written as

$$h^{\mu\nu}(\eta, \mathbf{x}) = \int d^3k e^{i\mathbf{k}\mathbf{x}} h^{\mu\nu}(\eta, \mathbf{k}), \quad (2.57)$$

where the quantities \mathbf{x} , \mathbf{k} , and η are all conformal. For each Fourier mode, \mathbf{k} sets a direction in momentum space, which permits a further decomposition according to the transformation properties under rotations around the axis \mathbf{k} . This amounts to the consideration of irreducible representations of the symmetry group $SO(2)$. They have definite helicity, which is the eigenvalue with respect to the generating angular momentum operator. The helicity of quantities being independent from momentum or with proportionality to k_i or $k_i k_j$ is zero. They are called scalar perturbations. The helicity eigenvalue of vector perturbations is 1 up to a phase. Under rotations around \mathbf{k} they transform like transverse vectors, i.e. vectors in the plane orthogonal to \mathbf{k} . Tensor perturbations can be constructed from products of two vectors being orthogonal to \mathbf{k} which entails helicity 2. They give rise to gravitational waves.

The Einstein equations do not mix helicity in the linear case: The corresponding operations comprise time derivatives and, in momentum representation, multiplication with k_i , which both leave the behavior under rotations around \mathbf{k} unchanged. Of course, these considerations lose their validity if nonlinearities need to be considered.

The decomposition of each momentum mode \mathbf{k} of the metric can be written as

$$h_{00} = 2\Phi \quad (2.58)$$

$$h_{0i} = ik_i Z + Z_i^T \quad (2.59)$$

$$h_{ij} = -2\Psi\delta_{ij} - 2k_i k_j E + i(k_i W_j^T + k_j W_i^T) + h_{ij}^{TT}. \quad (2.60)$$

In the following, the gauge freedom (2.56) is used to set

$$h_{0i} = 0, \quad E = 0. \quad (2.61)$$

The first condition can be achieved by choosing ξ^0 appropriately. Then one can still use gauge transformations that leave $h_{0i} = 0$ invariant. These are derived from functions ξ^μ with

$$\partial^0 \xi^i + \partial^i \xi^0 = 0. \quad (2.62)$$

This equation is for example fulfilled by $\xi^\mu(\eta, \mathbf{x})$ obtained from any function $\sigma(\eta, \mathbf{x})$ through

$$\xi^0 = \partial^0 \sigma(\eta, \mathbf{x}) \quad \text{and} \quad \xi^i = -\partial^i \sigma(\eta, \mathbf{x}) \quad (2.63)$$

Such a transformation has the following effect on the spatial part of $h^{\mu\nu}$:

$$\tilde{h}^{ij} = h^{ij} - 2\partial^i \partial^j \sigma - 2\frac{a'}{a} \delta^{ij} \sigma'. \quad (2.64)$$

The choice $\sigma = E$ leaves $\tilde{E} = 0$ in the new metric.

It can be concluded that the scalar Z and the transverse vector Z_i^T will not be considered. Likewise the vectorial quantity W_i^T will be disregarded since vector perturbations follow decaying solutions and are not expected to leave any observable traces. So it is

$$h_{00} = 2\Phi, \quad h_{0i} = 0, \quad h_{ij} = -2\Psi\delta_{ij} + h_{ij}^{TT}. \quad (2.65)$$

The tensor h_{ij}^{TT} is transverse and traceless. So, for each momentum mode one has

$$k_i h_{ij}^{TT}(\mathbf{k}) = k_j h_{ij}^{TT}(\mathbf{k}) = 0. \quad (2.66)$$

Evolution of scalar perturbations. The linearized Einstein tensor in terms of scalar metric perturbations is calculated in App. A. Then, in order to write down the linearized Einstein equation, the energy–momentum tensor of the perturbed cosmological medium is needed. Starting point is the energy–momentum tensor of an ideal fluid with energy density $\hat{\rho} = \bar{\rho} + \delta\rho$, pressure $\hat{p} = \bar{p} + \delta p$, and local 4-velocity $\hat{u}^\mu = \bar{u}^\mu + \delta u^\mu$,

$$T_\nu^\mu = (\hat{\rho} + \hat{p})\hat{u}^\mu\hat{u}_\nu - \delta_\nu^\mu\hat{p}. \quad (2.67)$$

As in the case of metric perturbations, the calculation is done up to linear order in the inhomogeneities $\delta\rho$, δp , and δu^μ . The 4-velocity is characterized by

$$g_{\mu\nu}u^\mu u^\nu = 1. \quad (2.68)$$

Because the spatial components of u^μ are small and the same is true for the off-diagonal entries of the metric, one is left with

$$g_{00}u^0u^0 = 1 \quad \text{or} \quad g^{00}u_0u_0 = 1, \quad (2.69)$$

giving

$$u^0 = \frac{1}{a\sqrt{1+2\Phi}} \approx \frac{1}{a}(1-\Phi) \quad \text{and} \quad u_0 = \frac{a}{\sqrt{1-2\Phi}} \approx a(1+\Phi). \quad (2.70)$$

The components of T_ν^μ are

$$T_0^0 = \hat{\rho} = \bar{\rho} + \delta\rho, \quad (2.71)$$

$$T_i^0 = -(\bar{\rho} + \bar{p})v^i = -(\bar{\rho} + \bar{p})v_i, \quad (2.72)$$

$$\text{and} \quad T_j^i = -\delta_j^i\hat{p} \quad (2.73)$$

to first order. In these equations the physical velocity $v^i = au^i$ and $v_i = +\delta_{ij}v^j$ have been defined. For the linearized Einstein equation only the perturbations,

$$\delta T_0^0 = \delta\rho, \quad \delta T_i^0 = -(\bar{\rho} + \bar{p})v_i, \quad \delta T_j^i = -\delta_j^i\delta p, \quad (2.74)$$

are needed. The perturbed Einstein equation and energy–momentum conservation equation are derived to linear order in App. A. As shown there, the results for the 00-, the 0i-,

and the spatial components of the Einstein equation as well as the 0- and i -components of the conservation equation are given by

$$\Delta\Phi - 3\frac{a'}{a}\Phi' - 3\frac{a'^2}{a^2}\Phi = \frac{4\pi a^2}{m_{\text{Pl}}^2}\delta\rho, \quad (2.75)$$

$$\Phi' + \frac{a'}{a}\Phi = -\frac{4\pi}{m_{\text{Pl}}^2}(\bar{\rho} + \bar{p})v, \quad (2.76)$$

$$\Phi'' + 3\frac{a'}{a}\Phi' + 2\frac{a''}{a}\Phi - \frac{a'^2}{a^2}\Phi = \frac{4\pi a^2}{m_{\text{Pl}}^2}\delta\rho, \quad (2.77)$$

$$((\bar{\rho} + \bar{p})v_i)' + \partial_i\delta p + (\bar{\rho} + \bar{p})\left(4\frac{a'}{a}v_i + \partial_i\Phi\right) = 0, \quad (2.78)$$

$$\delta\rho' + 3\frac{a'}{a}(\delta\rho + \delta p) + (\bar{\rho} + \bar{p})(3\Phi' + \partial_i v_i) = 0, \quad (2.79)$$

respectively. For $a = 1$, the first equation reduces to the Poisson equation for the Newtonian potential. Note that the sources in the Einstein equation refer to the total fluid. By contrast, energy–momentum conservation (Eqs. (2.78) and (2.79)) holds for each component separately, as long as interactions between the fluids can be neglected. The master equation for the potential Φ is obtained by multiplying (2.75) with the sound speed squared, $u_s^2 = \delta p/\delta\rho$ and adding the result to (2.77). Then it is

$$\Phi_k'' + 3\frac{a'}{a}(1 + u_s^2)\Phi_k' + \left\{2\frac{a''}{a} - \frac{a'^2}{a^2}(1 - 3u_s^2)\right\}\Phi_k + u_s^2 k^2 \Phi_k = 0 \quad (2.80)$$

for the modes with comoving momentum \mathbf{k} . This equation can be simplified using

$$2\frac{a''}{a} = \frac{8\pi a^2}{3m_{\text{Pl}}^2}(\rho - 3p) \quad \text{and} \quad \frac{a'^2}{a^2} = \frac{8\pi a^2}{3m_{\text{Pl}}^2}\rho, \quad (2.81)$$

which are obtained from Eqs. (2.42) and (2.43). Under the assumption

$$p = u_s^2 \rho \quad (2.82)$$

the expression in curly brackets is then seen to vanish. One is left with the wave equation

$$\Phi_k'' + 3\frac{a'}{a}(1 + u_s^2)\Phi_k' + u_s^2 k^2 \Phi_k = 0. \quad (2.83)$$

Three scales are important for the behavior of the solutions to this equation: The Hubble horizon H^{-1} , which is of the order of the distance traveled by light since the Big Bang; the sound horizon $u_s H^{-1}$, which is the corresponding distance covered by a sound wave; and the wavelength $\lambda = 2\pi/k$. If the wavelength is much larger than the sound horizon,

$$u_s k \ll H a, \quad (2.84)$$

the last term in Eq. (2.83) can be neglected and there is a constant solution. Oscillation sets in when the inequality (2.84) is valid in the opposite direction. This is possible in a radiation dominated epoch, as is observed for example in the traces of baryon acoustic oscillations in the CMB. Further discussion of the important issue of structure formation can be found in the literature.

Evolution of tensor perturbations. The equation of motion for the tensor perturbations (2.85) is derived in the Appendix, see Eq. (A.46).

$$(h_{ij}^{TT})'' + 2\frac{a'}{a}(h_{ij}^{TT})' - \Delta h_{ij}^{TT} = -\frac{16\pi a^2}{m_{\text{Pl}}^2}\Pi_{ij}^{TT} \quad (2.85)$$

In the ideal fluid approximation the right hand side is zero because the anisotropic stress vanishes. Then this equation describes the free propagation of a gravitational wave as long as the wavelength is much smaller than the Hubble radius. A spectrum of gravitational waves is expected to be produced during inflation (Section 5). To calculate this spectrum it is necessary to know their action S_{TT} which can be obtained from the Hilbert action (2.22) by expansion to second order in the tensor perturbation h_{ij}^{TT} . The result

$$S_{TT} = \frac{m_{\text{Pl}}^2}{64\pi} \int d^4x a^2 \left\{ (\partial_\eta h_{ij}^{TT})^2 - \partial_k h_{ij}^{TT} \partial_k h_{ij}^{TT} \right\} \quad (2.86)$$

is valid for ideal fluids. A further decomposition of each mode into the basis of two polarizations e_{ij}^+ and e_{ij}^\times ,

$$h_{ij}^{TT} = \sum_{A=+,\times} e_{ij}^{(A)} h^{(A)}, \quad (2.87)$$

streamlines the notation somewhat for the action,

$$S_{TT} = \sum_{A=+,\times} \frac{m_{\text{Pl}}^2}{64\pi} \int d^3x d\eta a^2 \left\{ (\partial_\eta h^{(A)})^2 - \partial_i h^{(A)} \partial_i h^{(A)} \right\}, \quad (2.88)$$

as well as for the resulting equation of motion,

$$\partial_\eta^2 h^{+,\times} + 2\frac{a'}{a}\partial_\eta h^{+,\times} - \Delta h^{+,\times} = 0. \quad (2.89)$$

In contrast to the case of scalar perturbations, the solution to this equation is governed solely by the Hubble horizon and by the wavelength k of the mode in question. A mode well outside the horizon fulfills

$$k \ll Ha, \quad \text{or, equivalently,} \quad k \ll \frac{a'}{a}, \quad (2.90)$$

which can be directly used to identify the relevant contributions to Eq. (2.89). Hence, in the superhorizon regime one solves the equation

$$h_k'' + 2\frac{a'}{a}h_k' = 0 \quad (2.91)$$

and identifies, besides a decaying solution, the behavior of a tensor perturbation outside the horizon to be time independent. When the universe is not inflating, i.e. when

$$\ddot{a} < 0 \quad \Leftrightarrow \quad \frac{d}{dt}Ha < 0, \quad (2.92)$$

then modes that are outside the horizon will at some time enter the horizon. Then Eq. (2.91) has to be replaced by

$$h_k'' + k^2 h_k = 0 \quad (2.93)$$

and the solution is an oscillating gravitational wave.

2.2.4. Primordial spectra of scalar fluctuations

Regarding scalar fluctuations, this work is confined to the discussion of the adiabatic mode. For a medium in local thermal equilibrium being described with the help of a metric in conformal Newtonian gauge, the defining property of the adiabatic mode is

$$\begin{aligned}\delta\rho_\lambda(\mathbf{x}, \eta) &= \frac{\partial\rho_\lambda}{\partial T}\delta T(\mathbf{x}, \eta) \\ \delta p_\lambda(\mathbf{x}, \eta) &= \frac{\partial p_\lambda}{\partial T}\delta T(\mathbf{x}, \eta),\end{aligned}\tag{2.94}$$

for fluctuations over scales exceeding the Hubble radius. The index λ identifies the component in question. Equation (2.94) suggests that the composition of the cosmic medium is the same throughout spacetime and the only independent fluctuation is in temperature. This is in contrast to the isocurvature mode in which the fluctuations are independent for different particle species. Observations do not show evidence for perturbations in the isocurvature mode.

In order to generalize the definition of the adiabatic mode to a medium out of thermal equilibrium, δT can be replaced by the function $\epsilon(\mathbf{x}, \eta)T'(\eta)$ with the result

$$\begin{aligned}\delta\rho_\lambda(\mathbf{x}, \eta) &= \rho'_\lambda\epsilon(\mathbf{x}, \eta), \\ \delta p_\lambda(\mathbf{x}, \eta) &= p'_\lambda\epsilon(\mathbf{x}, \eta).\end{aligned}\tag{2.95}$$

The purpose of this section is to establish a quantity that characterizes the strength of fluctuations before they enter the horizon. It will be seen that there are two equivalent possibilities, ζ_k and \mathcal{R}_k , that are both constant outside the horizon, i.e. for $k \ll aH$.

To obtain a suitable definition, Eq. (2.79) is considered in the superhorizon approximation, $\partial_i v_i = 0$. With Eq. (2.95) one has

$$(\rho'_\lambda\epsilon)' + 3\frac{a'}{a}(\rho'_\lambda + p'_\lambda)\epsilon - 3\Phi'(\rho_\lambda + p_\lambda) = 0\tag{2.96}$$

and repeated use of (2.44) leaves

$$\Phi' = -\left(\frac{a'}{a}\epsilon\right)'.\tag{2.97}$$

The conclusion is that the quantity

$$\zeta = -\Phi - \frac{a'}{a}\epsilon = -\Phi + \frac{\delta\rho_{\text{tot}}}{3(\rho_{\text{tot}} + p_{\text{tot}})}\tag{2.98}$$

is constant as long as the mode has not entered the horizon. The second equality is obtained with Eqs. (2.44) and (2.95). The subscript refers to the total medium.

The definition of \mathcal{R} is equal to that of ζ with $-\epsilon$ replaced by

$$v_{\text{tot}} = \frac{\sum(\rho_\lambda + p_\lambda)v_\lambda}{\sum(\rho_\lambda + p_\lambda)},\tag{2.99}$$

so,

$$\mathcal{R} = -\Phi + \frac{a'}{a}v_{\text{tot}}. \quad (2.100)$$

For negligible k in the superhorizon regime it is $\zeta = \mathcal{R}$ because the result in the calculation

$$\zeta - \mathcal{R} = \frac{\delta\rho_{\text{tot}}}{3(\rho_{\text{tot}} + p_{\text{tot}})} - \frac{a'}{a}v_{\text{tot}} = -\frac{m_{\text{Pl}}^2}{12\pi a^2} \frac{k^2\Phi}{(\rho_{\text{tot}} + p_{\text{tot}})} \quad (2.101)$$

can be taken to vanish as well. So, both \mathcal{R} and ζ are adequate and equivalent measures for scalar fluctuations before horizon entry. Their physical interpretation is given in the rest of this section. For this purpose the perturbations are considered in the comoving reference frame, which means $v_{\text{tot}} = 0$. It follows from Eq. (2.74) that switching into this frame is achieved by the gauge transformation (2.56) when the function $\xi(x^\mu)$ obeys

$$\partial_0\xi_i = -\partial_i\xi_0 = v_i : \quad (2.102)$$

Applying the transformation (2.54) to the energy–momentum tensor leads to

$$\tilde{T}_i^0(x) = T_i^0(x) - \xi^\sigma\partial_\sigma T_i^0(x) + T_i^\rho\partial_\rho(x)\xi^0 - T_\lambda^0\partial_i(x)\xi^\lambda \quad (2.103)$$

So the transformation of the perturbation is to first order

$$\delta\tilde{T}_i^0(x) = \delta T_i^0(x) + T_i^i(x)\partial_i\xi^0 - T_0^0(x)\partial_i\xi^0, \quad (2.104)$$

where the index i should not be summed over. Now Eq. (2.74) is used to replace the fluctuations observing

$$\delta T_i^0 = -(\bar{\rho} + \bar{p})v_i \quad \text{and} \quad \delta\tilde{T}_i^0 = -(\bar{\rho} + \bar{p})\tilde{v}_i, \quad (2.105)$$

which entails (2.102) as a conclusion. It should be stated that this gauge transformation preserves $h_{0i} = 0$, which is the condition for Eq. (2.100) to be valid. So, as an intermediate step towards the interpretation of \mathcal{R} , note that $\mathcal{R} = -\Phi$ in the comoving gauge, and that “comoving” has the meaning of $v_{\text{tot}} = 0$ in this context.

The next step is to calculate the curvature of a hypersurface of constant time in these coordinates. First, the calculation is done for the metric γ_{ij} , which is defined according to the beginning of Section 2.2.3. So, one has $a(\eta) \equiv 1$. From Eq. (A.8) in three dimensions one has

$$R^{(3)}(\gamma) = \partial_i\partial_j h_{ij} + \partial_i\partial_i h_{jj}. \quad (2.106)$$

The only scalar contribution comes from

$$h_{ij} = -2\Psi\delta_{ij} + 2\partial_i\partial_j E \quad (2.107)$$

and reads

$$R^{(3)}(\gamma) = 4\partial_i\partial_i\Psi \equiv 4\Delta\Psi. \quad (2.108)$$

Restoring the scale parameter by use of the conformal transformation (A.18) gives an additional factor $1/a^2$ and for ideal fluids it is $\Psi = -\Phi$, see Section A.4. Therefore, the comoving reference frame ($v_{tot} = 0$) implies equal-time hypersurfaces with curvature

$$R^{(3)} = -\frac{4}{a^2}\Delta\mathcal{R}, \quad (2.109)$$

representing the physical interpretation of \mathcal{R} . Observations do not require higher correlation functions than $\langle\mathcal{R}(\mathbf{k}_1)\mathcal{R}(\mathbf{k}_2)\rangle$ for the description of $\mathcal{R}(\mathbf{k})$, which means that they are consistent with the assumption that $\mathcal{R}(\mathbf{k})$ is a random Gaussian field. It is completely determined by its power spectrum $\mathcal{P}_{\mathcal{R}}(k)$ through

$$\langle\mathcal{R}(\mathbf{k})\mathcal{R}(\mathbf{k}')\rangle = \frac{\mathcal{P}_{\mathcal{R}}(k)}{4\pi k^3}\delta(\mathbf{k} + \mathbf{k}'). \quad (2.110)$$

The fluctuations of $\mathcal{R}(\mathbf{x})$ then obey the equation

$$\langle\mathcal{R}^2(\mathbf{x})\rangle = \int_0^\infty \frac{dk}{k}\mathcal{P}_{\mathcal{R}}(k). \quad (2.111)$$

Their amplitudes are more conveniently quantified by

$$\Delta_{\mathcal{R}}(k) = \sqrt{\mathcal{P}_{\mathcal{R}}(k)}. \quad (2.112)$$

Within the standard picture of structure formation these spectra originate in a period of accelerated expansion in the early universe, called inflation (see Chapter 5). In Chapters 5 and 6 the spectra will be computed for different models of inflation.

2.2.5. Primordial spectra of tensor fluctuations

In analogy to the case of scalar perturbations, the tensor modes are quantified by their power spectra. Despite of lacking observational evidence one can try to describe the tensor modes as a Gaussian random field with a power spectrum defined by

$$\langle h^{(A)}(\mathbf{k})h^{(B)}(\mathbf{k}')\rangle = \frac{1}{2}\delta_{AB}\frac{\mathcal{P}_T(k)}{4\pi k^3}\delta(\mathbf{k} + \mathbf{k}'). \quad (2.113)$$

As in the last section, the amplitude is characterized by

$$\Delta_T = \sqrt{\mathcal{P}_T} \quad (2.114)$$

and the power spectrum is connected to the fluctuations in space through

$$\sum_A \left\langle \left(h^{(A)}(\mathbf{k}) \right)^2 \right\rangle = \int_0^\infty \frac{dk}{k}\mathcal{P}_T(k). \quad (2.115)$$

In these equations the notation of Section 2.2.3 has been used. Also the tensor power spectrum is discussed for different inflationary scenarios in Chapters 5 and 6.

3. Elements of field theory

The purpose of this chapter is mainly to prepare the background for the presentation of the theory of inflation and to motivate the potential which is later used for an inflationary scenario. So, it is far from a well-balanced account on the vast field of (quantum) field theory but instead concentrates on some indispensable basics needed for this work. Since the potential that will be used later on is rooted in effective potentials of strong interactions, the presentation will also include some aspects of quantum chromodynamics. This chapter follows Refs. [79] and [100] with additional reference to [111, 120] and other sources given in the following.

3.1. Equations for flat and FRW spacetimes

A field theory is defined by its action, which in curved spacetime and for a single scalar field $\phi(\mathbf{x}, t)$ may be written as

$$S = \int d^4x \sqrt{-g} \mathcal{L} = \int d^4x \sqrt{-g} \left(\frac{1}{2} g^{\mu\nu} \partial_\mu \phi \partial_\nu \phi - V(\phi) \right), \quad (3.1)$$

where the Lagrange density \mathcal{L} is the expression in brackets and a canonic kinetic term is assumed. The equation of motion is obtained by variation with respect to the field and its derivative $\partial_\mu \phi$. Using the FRW metric (2.32), the result is

$$\ddot{\phi} + 3H\dot{\phi} + \frac{\partial V(\phi)}{\partial \phi} = 0 \quad \text{or} \quad \phi'' + 2\frac{a'}{a}\phi' + a^2 \frac{dV(\phi)}{d\phi} = 0 \quad (3.2)$$

for a homogeneous field using cosmic and conformal time, respectively. As in chapter 2, conformal time is defined by $d\eta = dt/a$. The energy-momentum tensor is obtained by varying the action with respect to the metric,

$$T_{\mu\nu} = \frac{2}{\sqrt{-g}} \frac{\delta S}{\delta g^{\mu\nu}} = \partial_\mu \phi \partial_\nu \phi - g_{\mu\nu} \mathcal{L}. \quad (3.3)$$

The energy density $\rho = T_{00}$ and the pressure $p = T_{ii}$ ¹ are

$$\rho = \frac{1}{2} \dot{\phi}^2 + V(\phi), \quad p = \frac{1}{2} \dot{\phi}^2 - V(\phi) \quad (3.4)$$

¹No sum over the spatial index i is intended here.

in the homogeneous case. Inserting the energy density into the Friedmann equation (2.39) leaves

$$H^2 = \frac{8\pi}{3m_{Pl}^2} \left(\frac{1}{2} \dot{\phi}^2 + V(\phi) \right). \quad (3.5)$$

In flat spacetime the equation of motion is

$$\partial_\mu \partial^\mu \phi + \frac{\partial V}{\partial \phi} = 0. \quad (3.6)$$

The calculations, on which this thesis is built, have been done with real scalar fields. However, the motivation of the employed model relies on symmetries including spinor fields, which are used to describe fermions. Therefore, a short glimpse at some of their basic properties is now included.

A spinor ψ is a four-component object used to describe the dynamics of fermionic fields. The Lagrange density of a free fermionic field with mass m is

$$\mathcal{L} = \bar{\psi}(i\gamma^\mu \partial_\mu - m)\psi \quad (3.7)$$

leading to the equation of motion

$$(i\gamma^\mu \partial_\mu - m)\psi = 0. \quad (3.8)$$

The 4×4 Dirac matrices γ^μ are defined as

$$\gamma^0 = \begin{pmatrix} \mathbb{1} & 0 \\ 0 & -\mathbb{1} \end{pmatrix}, \quad \gamma^i = \begin{pmatrix} 0 & \tau^i \\ -\tau^i & 0 \end{pmatrix}, \quad (3.9)$$

with the 2×2 identity matrix

$$\mathbb{1} = \begin{pmatrix} 1 & 0 \\ 0 & 1 \end{pmatrix}, \quad (3.10)$$

and the 2×2 Pauli matrices

$$\tau^1 = \begin{pmatrix} 0 & 1 \\ 1 & 0 \end{pmatrix}, \quad \tau^2 = \begin{pmatrix} 0 & -i \\ i & 0 \end{pmatrix}, \quad \tau^3 = \begin{pmatrix} 1 & 0 \\ 0 & -1 \end{pmatrix}. \quad (3.11)$$

The Pauli matrices obey the (anti-)commutation relation

$$[\tau^i, \tau^j] = 2i\epsilon^{ij}_k \tau^k, \quad \{\tau^i, \tau^j\} = 2\delta^{ij} \mathbb{1}_{2 \times 2}. \quad (3.12)$$

The Lagrange density (3.7) is invariant under Lorentz transformations if $\bar{\psi} := \psi^\dagger \gamma^0$. There are other representations of the Dirac matrices as well. The essential property is the anticommutator relation

$$\{\gamma^\mu, \gamma^\nu\} = \gamma^\mu \gamma^\nu + \gamma^\nu \gamma^\mu = 2\eta^{\mu\nu}, \quad (3.13)$$

where $\eta^{\mu\nu}$ is the Minkowski metric Eq. (2.2).

3.2. Symmetries and conserved currents

For the construction of effective models in particle or nuclear physics, symmetries are often used as a guiding principle. If the microscopic theory exhibits a symmetry, one can try to mimic its dynamics by transferring the symmetric behavior under a certain transformation to the effective fields that are used to describe the system. This section presents symmetry transformations that reflect phenomena observed in strong interactions.

First, it is demonstrated that invariance of the Lagrange density $\mathcal{L}(\phi)$ under a continuous symmetry transformation, $\phi \rightarrow \phi + \delta\phi$, leads to a conserved current. This is the statement of Noether's theorem [106]. The symmetry assumption is written as the first equality in

$$\begin{aligned}
 0 &= \mathcal{L}(\phi + \delta\phi) - \mathcal{L}(\phi) \\
 &= \frac{\partial\mathcal{L}}{\partial\phi}\delta\phi + \frac{\partial\mathcal{L}}{\partial(\partial_\mu\phi)}\delta(\partial_\mu\phi) \\
 &= \left(\partial_\mu\frac{\partial\mathcal{L}}{\partial(\partial_\mu\phi)}\right)\delta\phi + \frac{\partial\mathcal{L}}{\partial(\partial_\mu\phi)}\partial_\mu\delta\phi \\
 &= \partial_\mu\left(\frac{\partial\mathcal{L}}{\partial(\partial_\mu\phi)}\delta\phi\right) \equiv \partial_\mu J^\mu,
 \end{aligned} \tag{3.14}$$

and an expansion is applied in the second one. The third line is obtained using the equation of motion

$$\frac{\partial\mathcal{L}}{\partial\phi} - \partial_\mu\frac{\partial\mathcal{L}}{\partial(\partial_\mu\phi)} = 0 \tag{3.15}$$

for the first term, and commuting the derivative ∂_μ and the variation δ in the second term. The last line in (3.14) contains the definition of the conserved current,

$$J^\mu = \frac{\partial\mathcal{L}}{\partial(\partial_\mu\phi)}\delta\phi. \tag{3.16}$$

The zero component J^0 is the density of the conserved charge related to the symmetry,

$$Q = \int d^3x J^0 \quad \Rightarrow \quad \frac{d}{dt}Q = 0. \tag{3.17}$$

In the case of invariance under spacetime translations, the conserved current is the energy–momentum tensor. However, this presentation concentrates on internal symmetries, which are inherent to specific combinations of fields in the Lagrange density. Important symmetries of this kind correspond to unitary transformations, as it is the case for rotations and translations in spacetime. An infinitesimal unitary² transformation of a number of fields ϕ_i can be written as

$$\phi_i \rightarrow (\delta_{ij} - i\vartheta^a T_{ij}^a) \phi_j \equiv U_{ij} \phi_j \tag{3.18}$$

² The group of unitary $N \times N$ matrices is called $U(N)$; it is $U \in U(N) \Leftrightarrow U^\dagger = U^{-1}$. The group of special unitary $N \times N$ matrices is called $SU(N)$; the additional requirement is $\det(U) = +1$.

with implied summation over the index a of the real infinitesimal ϑ^a and the traceless hermitian³ matrices or operators T_{ij}^a . A transformation with finite ϑ is obtained by repeated use of (3.18), which results in

$$\vec{\phi} \rightarrow \exp(-i\vartheta^a T^a) \vec{\phi}. \quad (3.19)$$

The T^a form a basis of the generators of the unitary transformations (3.18). The vector space of these generators is additionally equipped with a map similar to Eq. (3.12), which makes it an algebra. Each generator comes with a conserved current,

$$J^{\mu,a} = -i \frac{\partial \mathcal{L}}{\partial(\partial_\mu \phi_i)} T_{ij}^a \phi_j, \quad (3.20)$$

and the resulting conserved charge. As an aside it should be mentioned that the highly successful standard model of particle physics is built on the direct product of three unitary symmetry groups, $U(1) \times SU(2) \times SU(3)$.

The following gives a short account on the symmetries that are important for effective theories in nuclear physics. They can be crucial even if they are not exact in nature, as is the case for chiral symmetry. Therefore, let us write down the effect of a symmetry breaking contribution \mathcal{L}_{sb} to the Lagrange density on the conservation of J^μ : The calculation (3.14) yields

$$\partial_\mu J^\mu = \delta \mathcal{L}_{sb}, \quad (3.21)$$

which gives a direct relation of the symmetry breaking of the Lagrange density to the non-conservation of the current.

3.3. Chiral symmetry for two flavors of fermions

A system of two sorts (flavors) of massless non-interacting fermions is described by the Lagrange density

$$\mathcal{L} = i\bar{\psi}_u \gamma^\mu \partial_\mu \psi_u + i\bar{\psi}_d \gamma^\mu \partial_\mu \psi_d, \quad (3.22)$$

where the indices can be read as “up” and “down”. If both flavors are combined into the spinor $\psi = (u, d)$, one can consider the “vector transformation” Λ_V , which rotates the two components into each other. Of course, this presentation is alluding to the situation in nuclear physics, where quarks and mesons are allocated the quantum numbers isospin, strangeness and others. Then the u- and d-quarks are interpreted as the same particle within two quantum states with isospin plus and minus one half. The transformation Λ_V and also the axial vector transformation described below act on this space of isovectors. The action on the two components of ψ is given by

$$\begin{aligned} \psi &\xrightarrow{\Lambda_V} \exp\left(-i\vartheta^a \frac{\tau^a}{2}\right) \psi \approx \left(1 - i\vartheta^a \frac{\tau^a}{2}\right) \psi \\ \Rightarrow \bar{\psi} &\xrightarrow{\Lambda_V} \exp\left(+i\vartheta^a \frac{\tau^a}{2}\right) \bar{\psi} \approx \left(1 + i\vartheta^a \frac{\tau^a}{2}\right) \bar{\psi}. \end{aligned} \quad (3.23)$$

³ A Hermitian matrix A fulfills $A^\dagger = A$.

3.3. Chiral symmetry for two flavors of fermions

From this one gathers that the Lagrange density itself is invariant because the exponents commute with γ^μ . The conserved “vector current” $V^{\mu,a}$ associated with the transformation is found from Eq. (3.16) to be

$$V^{\mu,a} = \bar{\psi} \gamma^\mu \frac{\tau^a}{2} \psi. \quad (3.24)$$

The axial vector transformation Λ_A can be studied when the matrix

$$\gamma^5 := i\gamma^0\gamma^1\gamma^2\gamma^3\gamma^4 = \begin{pmatrix} 0 & \mathbb{1}_{2 \times 2} \\ \mathbb{1}_{2 \times 2} & 0 \end{pmatrix} \quad (3.25)$$

with

$$\{\gamma^5, \gamma^\mu\} = 0, \quad \gamma^5 \gamma^5 = \mathbb{1}_{4 \times 4} \quad (3.26)$$

is introduced.⁴ Λ_A is defined as the first line in

$$\begin{aligned} \psi &\xrightarrow{\Lambda_A} \exp\left(-i\gamma^5 \vartheta^a \frac{\tau^a}{2}\right) \psi \approx \left(1 - i\gamma^5 \vartheta^a \frac{\tau^a}{2}\right) \psi \\ \Rightarrow \bar{\psi} &\xrightarrow{\Lambda_A} \bar{\psi} \exp\left(-i\gamma^5 \vartheta^a \frac{\tau^a}{2}\right) \approx \bar{\psi} \left(1 - i\gamma^5 \vartheta^a \frac{\tau^a}{2}\right). \end{aligned} \quad (3.27)$$

In the second line the order of the terms becomes important, because γ^5 and γ^0 anti-commute rather than commute, see (3.26). When calculating the modification of the Lagrange density, however, a further sign change occurs due to the γ^μ in the kinetic terms in Eq. (3.22). Once more, this gives invariance of the Lagrange density. Therefore, also the axial current

$$A^{\mu,a} = \bar{\psi} \gamma^\mu \gamma^5 \frac{\tau^a}{2} \psi \quad (3.28)$$

is conserved. Taken together, the two symmetries constitute the chiral symmetry $SU(2)_V \times SU(2)_A$.

However, considering a system of quarks, one deals with particles of finite mass; and whereas a mass term in the Lagrange density,

$$\mathcal{L}_m = -m_u \bar{\psi}_u \psi_u - m_d \bar{\psi}_d \psi_d, \quad (3.29)$$

respects invariance under Λ_V , it breaks the axial symmetry. From Eqs. (3.21) and (3.29) the symmetry breaking is seen to be proportional to the masses. So, chiral symmetry can be regarded as a useful guide as long as quark masses are small. For the light quarks (up and down) with masses of a few MeV compared to the QCD scale $\Lambda_{\text{QCD}} \sim 200$ MeV this is indeed the case. The following linear combination of the generators of vector and axial transformations,

$$\tau_L = \frac{1}{2}(1 - \gamma^5) \frac{\tau}{2} \quad \text{and} \quad \tau_R = \frac{1}{2}(1 + \gamma^5) \frac{\tau}{2}, \quad (3.30)$$

⁴ As Eq. (3.9) the result in Eq. (3.25) depends on the representation.

can be seen to commute, which means that they act independently of each other. The generator $\tau_{L,R}$ belongs to the subgroup $SU(2)_{L,R}$, respectively, the cartesian product of which is the full $SU(2)$,

$$SU(2) = SU(2)_L \times SU(2)_R. \quad (3.31)$$

Because the projection operators

$$P_L = \frac{1}{2}(1 - \gamma^5) \quad \text{and} \quad P_R = \frac{1}{2}(1 + \gamma^5) \quad (3.32)$$

are used in the definitions (3.30), a transformation generated by one of the τ_L and τ_R projects on a state with definite chirality. The indices stand for left- and right-handedness, respectively.

3.4. Quantum chromodynamics

Quantum chromodynamics (QCD) is widely accepted as the theory of strong interactions. It describes interactions between quarks and gluons by introducing color charge as a new quantum number. In this framework, a quark can carry one of the three colors “red,” “green,” and “blue,” which is another distinguishing property adding to the quantum number “flavor” that comes in the six different types

up, charm, top,
down, strange, bottom/beauty.

In correspondence to the leptons, the quarks are organized into three generations, which are indicated by the column structure of the list above. However, let us stick to color dynamics here:

The strong interaction is symmetric under the color transformation $SU(3)_C$ that rotates states of different color charge into each other. So, each quark flavor q^f can be represented by a spinor triplet of different color states.⁵

$$q^f = \begin{pmatrix} q_r^f \\ q_g^f \\ q_b^f \end{pmatrix}. \quad (3.33)$$

As in the electroweak theory, the interaction is introduced by allowing for spacetime dependence of the symmetry transformation. This is phrased as turning the global $SU(3)$ into a local, “gauge” transformation. In order to keep the Lagrange density invariant, the derivative has to be turned into a covariant one. This is in correspondence to the covariant derivative of GR and, historically, it has been done earlier in a similar way for the $U(1)$ symmetry of quantum electrodynamics (QED). Then it is natural to permit a separate term governing the dynamics of the new field which is also in analogy

⁵In the following these are indicated by r , g and b , respectively.

to QED. The only difference in the notation is an additional index a . It is needed because the algebra of the generators of $SU(3)$ is an eight-dimensional vector space. In the fundamental representation it is the vector space of traceless, hermitian 3×3 matrices. A conventional basis is the collection of Gell-Mann matrices λ^1 to λ^8 ,

$$\begin{aligned} & \begin{pmatrix} 0 & 1 & 0 \\ 1 & 0 & 0 \\ 0 & 0 & 0 \end{pmatrix}, \quad \begin{pmatrix} 0 & -i & 0 \\ i & 0 & 0 \\ 0 & 0 & 0 \end{pmatrix}, \quad \begin{pmatrix} 1 & 0 & 0 \\ 0 & -1 & 0 \\ 0 & 0 & 0 \end{pmatrix}, \quad \begin{pmatrix} 0 & 0 & 1 \\ 0 & 0 & 0 \\ 1 & 0 & 0 \end{pmatrix}, \\ & \begin{pmatrix} 0 & 0 & -i \\ 0 & 0 & 0 \\ i & 0 & 0 \end{pmatrix}, \quad \begin{pmatrix} 0 & 0 & 0 \\ 0 & 0 & 1 \\ 0 & 1 & 0 \end{pmatrix}, \quad \begin{pmatrix} 0 & 0 & 0 \\ 0 & 0 & -i \\ 0 & i & 0 \end{pmatrix}, \quad \frac{1}{\sqrt{3}} \begin{pmatrix} 1 & 0 & 0 \\ 0 & 1 & 0 \\ 0 & 0 & -2 \end{pmatrix}. \end{aligned} \quad (3.34)$$

These represent a three-dimensional generalization of the Pauli matrices, Eq. (3.11). The normalization of the generators T^a is chosen as

$$T^a = \frac{1}{2} \lambda^a, \quad (3.35)$$

such that

$$\text{tr} (T^a T^b) = \frac{1}{2} \delta^{ab}. \quad (3.36)$$

3.4.1. The Lagrange density of QCD

Let us now examine the ingredients out of which the QCD Lagrange density,

$$\mathcal{L}_{\text{QCD}} = \sum_f \bar{q}_f (i\gamma^\mu D_\mu - m_f) q_f - \frac{1}{4} F_{\mu\nu}^a F^{a,\mu\nu}, \quad (3.37)$$

is built. Note that the comma in the index does not indicate a derivative but only separates the two types of indices. Then, it should be mentioned that, since they are fermions, the behavior of the quark fields, q_f , under Lorentz transformations is governed by the spinor representation of the Lorentz group $SO(1,3)$, which leaves the combination $\bar{q}q$ invariant. The indices μ and ν are Lorentz indices and their contraction leads to Lorentz invariance as well. The conformal derivative D_μ is defined as

$$D_\mu = \partial_\mu + igT^a G_\mu^a \equiv \partial_\mu + igG_\mu. \quad (3.38)$$

In order to keep the kinetic term of the quarks invariant under the gauge transformation

$$q_f \rightarrow \exp(-i\varepsilon^a(x)T^a) q_f \equiv U q_f, \quad (3.39)$$

the transformation of the field G_μ is introduced as

$$G_\mu \rightarrow U G_\mu U^{-1} - \frac{i}{g} U (\partial_\mu U^{-1}). \quad (3.40)$$

The field G_μ is the gauge field of QCD. It represents the eight gluons. They are bosons, which are the field quanta of the strong interaction. The field strength tensor is

Chapter 3. Elements of field theory

constructed from the gauge field G_μ . It is a vector in the algebra and a tensor in color space, too:

$$F_{\mu\nu} = T^a F_{\mu\nu}^a \quad (3.41)$$

where the index a runs from 1 to 8. It is defined as a generalization to the QED case by adding a component proportional to the commutator, which is necessary in order to preserve gauge invariance:

$$F_{\mu\nu} = \partial_\mu G_\nu - \partial_\nu G_\mu + ig [G_\mu, G_\nu]. \quad (3.42)$$

From this equation it is seen that the gluons themselves are charged under the strong interaction. The Lagrange density contains terms with three or four gluons and the coupling constant g . They show that gluons interact with each other, as opposed to photons. The components

$$F_{\mu\nu}^a = \partial_\mu G_\nu^a - \partial_\nu G_\mu^a - gf^{abc} G_\mu^b G_\nu^c \quad (3.43)$$

contain the structure constants f^{abc} of $SU(3)$, which are given by

$$[T^a, T^b] = if^{abc} T^c. \quad (3.44)$$

It can be shown that the field strength tensor (3.42) transforms as

$$F_{\mu\nu} \rightarrow U F_{\mu\nu} U^{-1}, \quad (3.45)$$

such that the last term in Eq. (3.37) is invariant because it is a trace. Altogether, the conclusion is that the Lagrange density (3.37) is indeed symmetric under $SU(3)_C$ gauge transformations. Arguing the other way round, one can state that the gauge symmetry guarantees a universal coupling strength to all particle fields with color charge. This is because the coupling g is not only present in the covariant derivative but also in the definition of the field strength. Then it is clear, that this argument is only valid for a non-vanishing commutator in Eq. (3.42), i.e. for a non-Abelian gauge group.

3.4.2. Symmetries and other properties

Quantum chromodynamics is built around the central assumption of the existence of a local $SU(3)$ symmetry acting on a new degree of freedom called color. However, there are further symmetries and characteristics of the physics of strong interactions, which prove important when effective, simplifying theories shall be found, that nevertheless incorporate the essence of QCD. Some of them will be discussed in this section:

Global $U(1)$ symmetry. Obviously, the QCD Lagrange density is invariant under the global $U(1)$ symmetry

$$q \xrightarrow{U(1)} \exp(-i\varphi)q \quad (3.46)$$

leading to baryon number conservation: The conserved current is

$$J_B^\mu = \bar{q}(x)\gamma^\mu q(x) \quad (3.47)$$

and the baryon number

$$B = \int d^3x q^\dagger q \quad (3.48)$$

is the conserved charge. For massless quarks the Lagrange density is also symmetric under the axial $U_A(1)$ transformation,

$$q \xrightarrow{U_A(1)} \exp(-i\gamma^5\varphi)q, \quad (3.49)$$

but it has been shown that this symmetry is broken by quantum effects. This is known as the Adler-Bell-Jackiw anomaly [8, 9, 74, 111].

Global $SU(2)$ flavor symmetry. In Section 3.3 the chiral transformation of quarks has been presented. Chiral $SU(2)$ symmetry is a substantial feature of QCD although it is only approximately realized and in addition spontaneously broken. Nevertheless, the quark masses m_u and m_d are small, and the corresponding vector current (3.24) is conserved to good approximation. Also the axial vector current (3.28) is at least partially conserved. The zero component of the first one is the isospin charge

$$Q_i = \int d^3x V_i^0 = \int d^3x \psi^\dagger \frac{\tau_i}{2} \psi. \quad (3.50)$$

More on chiral $SU(2)$ symmetry will be said in the Sections to follow.

Global $SU(3)$ flavor symmetry. Including the strange quark q_s , one could ask for a possible $SU(3)$ flavor symmetry. Since the strange quark is considerably heavier than the up and down quarks [107],

$$m_u \approx m_d \approx 3.4\text{MeV}, \quad m_s \approx 94\text{MeV}, \quad (3.51)$$

the axial $SU(3)_A$ is not a good symmetry. However, the transformation $SU(3)_V$, though likewise broken explicitly due to the differences in the masses listed above, can still be successfully utilized in order to structure hadrons containing strange quarks. Their quantum numbers and their corresponding behavior in nuclear reactions can be understood from their arrangement in multiplets of $SU(3)_V$.

Asymptotic freedom. It is known from QED that the effective coupling constant, experienced by electrically charged particles in scattering experiments, depends on the momentum transfer q . This can be seen by calculating the contribution from the individual Feynman graphs that are relevant in this process. If q is large enough, the contribution of the exchange of one photon, as represented by the Feynman diagram 3.1(a) is significantly corrected by terms of higher order in the coupling constant

$$\alpha_{\text{QED}} = \frac{e^2}{4\pi} \sim \frac{1}{137}. \quad (3.52)$$

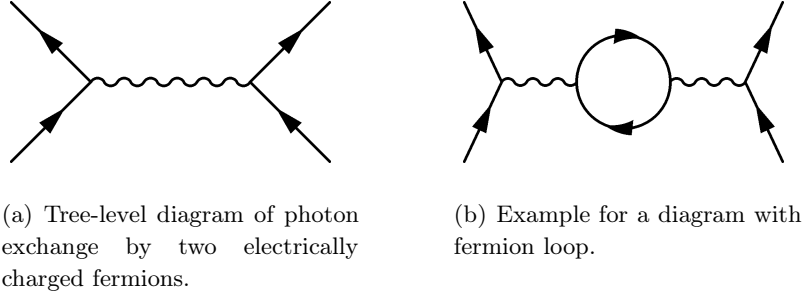


Figure 3.1.: Two diagrams from the calculation of fermion-fermion scattering in QED. The fermions (for example electrons or positrons) exchange a photon represented by the wiggly line (left). To higher order in the coupling, more complicated diagrams contribute. The example on the right-hand side is called a vacuum polarization diagram. It reduces the value if the effective coupling experienced by the particles.

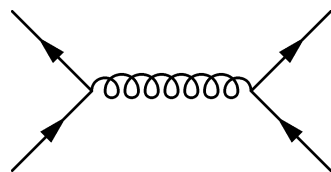
An example is the diagram 3.1(b), which belongs to the terms characterizing the vacuum polarization. It describes the short-term decay of the exchanged photon into a fermion–antifermion pair. This leads to a shielding of the charge in analogy to the shielding by a dielectric medium. It is also phrased as the running of the coupling. The situation in QCD is different because the gluons do not only mediate the strong interaction but carry color charge themselves. Also 3- and 4-gluon vertices are possible, which leads to Feynman diagrams as the one depicted in Fig. 3.2(c). The interaction of gluons among each other entails an anti-shielding contribution. The effect of the color charge of the gluons can be interpreted as a distribution of the quark color. If the momentum exchange between two scattering quarks is large, then they penetrate each other’s color cloud and, therefore, are subject only to a part of the charge. This phenomenon is known as asymptotic freedom because it leads to the fact that quarks inside hadrons behave almost like non-interacting particles. This is seen for example in deep inelastic scattering experiments using leptons and hadrons.

The value of the coupling constant α_s is obtained from scattering experiments and from lattice calculations, see Ref. [19]. Due to the effects mentioned above, this coupling varies with energy scale. The cited reference gives the value

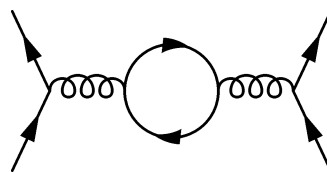
$$\alpha_s(m_Z) = 0.1184 \pm 0.0007 \tag{3.53}$$

at the scale of the Z-boson mass $m_Z \approx 90$ GeV. The running of α_s is quantified by the β -function. Once again referring to the Particle Data Group [17], the functional dependency can be cited as

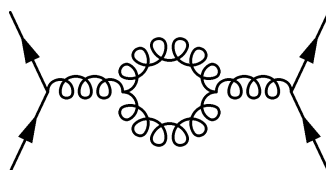
$$\begin{aligned} \mu^2 \frac{d\alpha_s}{d\mu^2} &= \beta(\alpha_s) \\ &= -(b_0\alpha_s^2 + b_1\alpha_s^3 + b_2\alpha_s^4) \\ &\approx -\frac{33 - 2n_f}{12\pi} \alpha_s^2, \end{aligned} \tag{3.54}$$



(a) Tree-level diagram of quark-quark scattering. The exchanged gluon is depicted by the curly line.



(b) Higher order diagram with quark loop.



(c) This diagram is only possible in the non-Abelian case, because it implies charged exchange particles.

Figure 3.2.: Feynman diagrams contributing to the quark-quark scattering cross-section. Diagram (c) belongs to the contributions which reduce the effective coupling for high momentum-transfer.

where the numerical values b_1 and b_2 from the given reference have been waived in the last line. To be precise, the variable μ is not exactly the momentum transfer q between two scattering particles but the renormalization scale. For the purpose of this thesis let us simply take $\mu = q$. The most important feature is the negative sign of the derivative (3.54) which is in contrast to the QED case. It leads to both asymptotic freedom and the confinement of color charge described in the next paragraph.

Confinement. Experiments have not only lead to the finding of asymptotic freedom but have also revealed its counterpart at large distances, the confinement of quarks and gluons into color-neutral objects. Quarks and gluons are never observed as separate particles but instead are always found to be bound in hadrons.

An effective description of this situation is given by the Bag Model [33, 43], which assigns a higher value of energy density to the inside of hadrons. This is said to contain the perturbative vacuum as opposed to the non-perturbative QCD vacuum outside the hadron “bags”. In a first approximation the quarks inside the bags are assumed to be only subject to the confining boundary of the bag and to behave otherwise as free particles. The energy difference of both vacua is fixed by the bag constant B . It can be estimated by comparing the pressure from the kinetic energy of the quarks inside the bag with the pressure from the energy difference of the two vacua.

Within this picture the QCD phase transition to the deconfined phase of the quark-gluon plasma can be understood in the following way: With higher temperature the kinetic pressure inside the bags rises and the bags expand until they overlap with neighboring ones. Similarly, this merging of bags can occur when the hadron density rises and a number of bags is forced into a smaller and smaller volume.

Scale invariance. In the limit of massless quarks, there is no dimensionful parameter left in the QCD Lagrange density. Then the physics stays exactly the same when the unit of length is changed. However, this invariance is spoiled by the renormalization of QCD. Then the scale Λ_{QCD} occurs as the energy scale, for which the running coupling constant grows large: Coming from large energies, at Λ_{QCD} any perturbative treatment of QCD breaks down and low-energy QCD has to rely on different methods such as lattice calculations and effective models. The presentation in this paragraph is based on [36]. For comparison, also [21] has been used.

First, we must take a short detour and include a few lines about some basics of scale symmetry: The change of the physical scale, which is also called a dilatation or a conformal transformation, can be written as

$$\Lambda_\varphi : x^\mu \rightarrow e^{2\varphi} x^\mu, \quad \varphi \in \mathbb{R}. \quad (3.55)$$

Note, that this is no coordinate transformation, leaving invariant any reasonable field theory, but a true transformation of spacetime. A more general type of conformal transformation with spacetime dependent parameter φ is introduced in Appendix A. Assuming that a spacetime dependent field $\phi(x)$ transforms linearly under Λ_φ , one writes

$$\begin{aligned} \Lambda_\varphi : \phi(x) &\rightarrow e^{2\varphi D} \phi(e^{2\varphi} x) \\ &\approx (1 + 2\varphi D) (\phi(x) + \partial_\mu \phi 2\varphi x^\mu) \\ &\approx \phi(x) + 2\varphi (D + x^\mu \partial_\mu) \phi(x) \end{aligned} \quad (3.56)$$

with some operator D . From this, one defines the change of the field under a transformation as

$$\delta\phi = (D + x^\mu \partial_\mu) \phi(x). \quad (3.57)$$

The following choice of D renders many theories of massless fields invariant under Λ_φ , as long as only dimensionless couplings are contained:

$$D\phi = \phi \quad \text{for bosonic fields } \phi \text{ and} \quad (3.58)$$

$$D\psi = \frac{3}{2}\psi \quad \text{for fermionic fields } \psi. \quad (3.59)$$

For example the potentials ϕ^4 , and $\bar{\psi}\psi\phi$ transform by

$$\begin{aligned} \delta(\phi^4) &= 4\phi^3 \delta\phi = 4\phi^3 (1 + x^\mu \partial_\mu) \phi = (4 + x^\mu \partial_\mu) \phi^4 \quad \text{and} \\ \delta(\bar{\psi}\psi\phi) &= \left\{ \left(\frac{3}{2} + x^\mu \partial_\mu \right) \bar{\psi} \right\} \psi\phi + \bar{\psi} \left\{ \left(\frac{3}{2} + x^\mu \partial_\mu \right) \psi \right\} \phi + \bar{\psi}\psi (1 + x^\mu \partial_\mu) \phi \\ &= (4 + x^\mu \partial_\mu) \bar{\psi}\psi\phi, \end{aligned} \quad (3.60)$$

both of which are seen vanish upon partial integration. One may conclude that products of fields are invariant as long as their scaling dimensions D add up to four. Kinetic terms as $\partial_\mu\phi\partial^\mu\phi/2$ or $\bar{\psi}i\gamma^\mu\partial_\mu\psi$ are found to be invariant as well:

$$\delta\left(\frac{1}{2}\partial_\mu\phi\partial^\mu\phi\right) = \partial_\mu\{(1+x^\nu\partial_\nu)\phi\}\partial^\mu\phi \quad (3.61)$$

$$= \partial_\mu\phi\partial^\mu\phi + \{(1+x^\nu\partial_\nu)\partial_\mu\phi\}\partial^\mu\phi \quad (3.62)$$

$$= \partial_\mu\phi\partial^\mu\phi + \left(1 + \frac{1}{2}x^\nu\partial_\nu\right)\partial_\mu\phi\partial^\mu\phi = 0 \quad (3.63)$$

$$\delta(\bar{\psi}i\gamma^\mu\partial_\mu\psi) = \left(\frac{3}{2} + x^\nu\partial_\nu\right)\bar{\psi}i\gamma^\mu\partial_\mu\psi + \bar{\psi}i\gamma^\mu\partial_\mu\left(\frac{3}{2} + x^\nu\partial_\nu\right)\psi = 0. \quad (3.64)$$

In the fermion case the result is obtained from partial integration of one of the terms. However the scaling dimension is not always equal to the mass dimension of dimensional analysis. Indeed, masses and dimensionful couplings themselves do not transform under the scaling, which is the reason for the scale symmetry breaking of mass terms like

$$\frac{1}{2}m^2\phi^2 \quad \text{or} \quad m\bar{\psi}\psi. \quad (3.65)$$

Finishing the detour on scale transformations, let us now have a look on the QCD Lagrange density in terms of its scaling behavior. It is clear from the analysis above that the gluon part is invariant because every term contains altogether four derivatives or gluon fields. Only the quark mass terms transform non-trivially.

Then one could assume that QCD is still approximately symmetric under scale transformations because the quark masses are small. However this is not the case because the approximate symmetry is broken by an anomaly in quantum dynamics [37]. This does not mean that the use of considering scale transformations is lost: Inside hadrons for example, scale symmetry is approximately restored and is used in effective descriptions [27, 76].

Trace anomaly. Scale symmetry is connected to the trace of the energy–momentum tensor. A prominent example is QED, which is traceless and symmetric under scale transformations. For strongly interacting matter this trace is non-zero because of an anomaly [39]. The Bag Model, which has been mentioned earlier in this Section, ascribes the energy density B to the perturbative vacuum inside hadrons. Since the equation of state in these volumes is that of vacuum, one obtains $4B$ as the trace of the energy–momentum tensor. On the other hand, QCD calculations yield a proportionality to the gluon condensate [39],

$$T^\mu_\mu = \frac{\beta_{\text{QCD}}}{2g}\langle F_{\mu\nu}^a F^{\mu\nu,a}\rangle, \quad \text{with} \quad \alpha_s = \frac{g^2}{4\pi}. \quad (3.66)$$

Again, the comma is only meant to separate the two types of indices and does not denote a derivative. Furthermore, one can define the energy–momentum tensor such that it is

connected to the Noether current of dilatation symmetry J_D^μ by

$$J_D^\mu = x_\nu T^{\nu\mu} : \quad (3.67)$$

Because of $\partial_\mu x_\nu = \eta_{\mu\nu}$, one then obtains that the trace of the energy–momentum tensor is zero if the scale current is conserved.

So, it is seen that the dilatation symmetry is connected with the gluon condensate and the trace of the energy momentum tensor. This motivates the introduction of a new field, the dilaton $\chi(x)$ as the supposed Goldstone boson of this symmetry. As already mentioned above, quantum effects break scale symmetry and the dilaton is not expected to be massless or light [76]. Nevertheless, the dilaton has been considered as a pseudo-Goldstone boson and identifications with observed mesonic resonances have been made [67]. The dilaton field can be used to match the scaling properties of the linear sigma model terms to the corresponding ones in QCD [32, 99, 109]. Thus the dilaton field is associated with the gluon condensate, which breaks scale invariance and leaves the rest of the theory approximately scale-free when a phase transition leads to its disappearance. Likewise, the dilaton is expected to undergo a phase transition from a finite value at low temperatures to $\chi = 0$ in the high-temperature phase. An effective model of QCD including a dilaton field will be introduced in Section 3.5.5.

3.5. Effective theories of strong interactions

3.5.1. Mesonic states and their chiral transformation

The first experimental evidences supporting the chiral nature of nuclear forces came from the nuclear beta decay. Although it is a process due to the weak interaction, it allows for the conclusion that chiral symmetry is approximately realized in the strong interaction. Therefore, effective nuclear theories are constructed such that their behavior under chiral transformations can be easily controlled. It will be seen that these models permit perfectly symmetric behavior under chiral transformations as well as spontaneous and explicit symmetry breaking. In the following the linear sigma model will serve as example. Its potential couples nucleons or quarks with the mesonic pion and sigma fields π^a and σ . Guided by their transformation behavior they can be built from quark fields as

$$\pi^a = i\bar{\psi}\tau^a\gamma^5\psi, \quad \text{and} \quad \sigma = \bar{\psi}\psi. \quad (3.68)$$

The τ_i makes the pion transform as a vector under isospin rotations and the γ^5 contributes negative parity. Vector mesons with Lorentz index can be constructed by including γ^μ . The chiral transformation of the mesons arises from the transformation of the quark

spinors: Equations (3.23) and (3.27) give

$$\begin{aligned}
 \pi^a &= i\bar{\psi}\tau^a\gamma^5\psi \xrightarrow{\Lambda_V} i\bar{\psi}\left(1 + i\vartheta^b\frac{\tau^b}{2}\right)\tau^a\gamma^5\left(1 + i\vartheta^c\frac{\tau^c}{2}\right)\psi \\
 &= i\bar{\psi}\tau^a\gamma^5\psi + \frac{1}{2}\bar{\psi}\gamma^5[\tau^a, \tau^b]\vartheta^b\psi \\
 &= i\bar{\psi}\tau^a\gamma^5\psi + i\vartheta^b\epsilon^{abc}\bar{\psi}\gamma^5\tau^c\psi
 \end{aligned} \tag{3.69}$$

to linear order in ϑ^a . This can be written as an isospin rotation of the pion by the angle ϑ^a ,

$$\vec{\pi} \xrightarrow{\Lambda_V} \vec{\pi} + \vec{\vartheta} \times \vec{\pi}. \tag{3.70}$$

The axial transformation,

$$\pi^a = i\bar{\psi}\tau^a\gamma^5\psi \xrightarrow{\Lambda_A} i\bar{\psi}\tau^a\gamma^5\psi + \vartheta^a\bar{\psi}\psi, \tag{3.71}$$

is obtained using the anticommutation relation in (3.12). Again, one can also write

$$\vec{\pi} \xrightarrow{\Lambda_A} \vec{\pi} + \vec{\vartheta}\sigma. \tag{3.72}$$

The transformation of the sigma meson is obtained similarly. Like the mass term in the example of Section 3.3, it transforms trivially under vector transformations. Axial transformations rotate the σ and the π^a fields into each other, see also Eq. (3.72),

$$\sigma \xrightarrow{\Lambda_V} \sigma, \quad \sigma \xrightarrow{\Lambda_A} \sigma - \vec{\vartheta}\vec{\pi}. \tag{3.73}$$

The results on mesonic transformations need to be borne in mind when the dynamics of the effective theory is to respect the desired chiral behavior.

3.5.2. Chiral symmetry breaking

As stated in Section 3.4, chiral $SU(2)$ symmetry is approximately realized in the QCD Lagrange density. However, this symmetry does not become manifest in the mesonic mass spectrum: Chiral partners as the σ and the π mesons or the vector mesons ρ_μ and $a_{1\mu}$ do not have approximately the same masses—as they should, following the naive expectation. The solution to this apparent problem is a spontaneous breaking of chiral symmetry in addition to the explicit one that comes from the comparatively small current quark masses.

A symmetry is termed spontaneously broken if it is obeyed by the Lagrange density but not respected by the ground state. So, violation of chiral symmetry need not pose a problem in the low energy hadronic regime as long as a phase transition occurs at higher energies, where chiral symmetry is restored. In the chirally restored phase mesons and also nucleons should be massless.

There is the following specialty about spontaneously broken symmetries; it is formulated by the Goldstone theorem [56, 57]: It states that any spontaneously broken

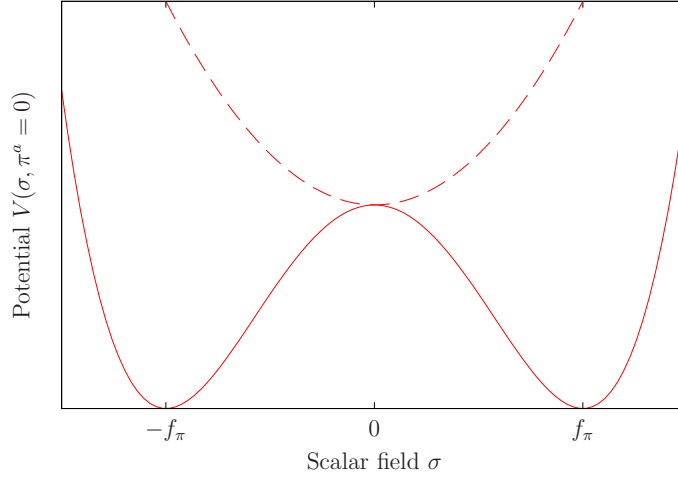


Figure 3.3.: Potential of the linear sigma model in the $\pi^a = 0$ plane. The potential should be thought of as rotationally symmetric around the $\sigma = 0$ axis. Whereas the potential is chirally symmetric, the ground state, $\sigma = f_\pi$, $\pi^a = 0$, is not. At high temperatures the effective potential (dashed line) does not allow symmetry breaking.

continuous symmetry leads to a massless bosonic mode carrying the same quantum numbers as the generator of the symmetry. They are called Goldstone bosons. In the case of chiral symmetry this part is attributed to the pions. For an exact symmetry the pions should be massless. This is obviously not the case. However, since chiral symmetry is subject to an explicit breaking by the non-zero quark masses, one should not expect zero mass but a comparatively small one. This is satisfied by the pion masses.

From experiment it is known that pions are pseudo-scalar particles, which means that they obtain a minus sign under parity transformations. This is consistent with their origin from axial symmetry breaking because the factor of γ^5 in Eq. (3.28) makes the accordant charge a pseudo-scalar as well.

3.5.3. Linear sigma model

An important example of an effective theory of strong interactions is the linear sigma model [55] with the Lagrangian

$$\begin{aligned} \mathcal{L} = & \frac{1}{2} \partial_\mu \pi^a \partial^\mu \pi^a + \frac{1}{2} \partial_\mu \sigma \partial^\mu \sigma + i \bar{\psi} \gamma^\mu \partial_\mu \psi \\ & + g_\pi \bar{\psi} (\sigma + i \gamma^5 \tau^a \pi^a) \psi - \frac{\lambda}{4} ((\vec{\pi}^2 + \sigma^2) - f_\pi^2)^2, \end{aligned} \quad (3.74)$$

which is examined in the following: It is composed of standard kinetic terms for the (pseudo) scalar fields π^a and σ and the fermion ψ in the first line, and of interaction terms in the second one. The π^a and the σ are thought of as the meson fields from Section 3.5.1. Depending on the phase, the spinor ψ can be interpreted either as nucleon

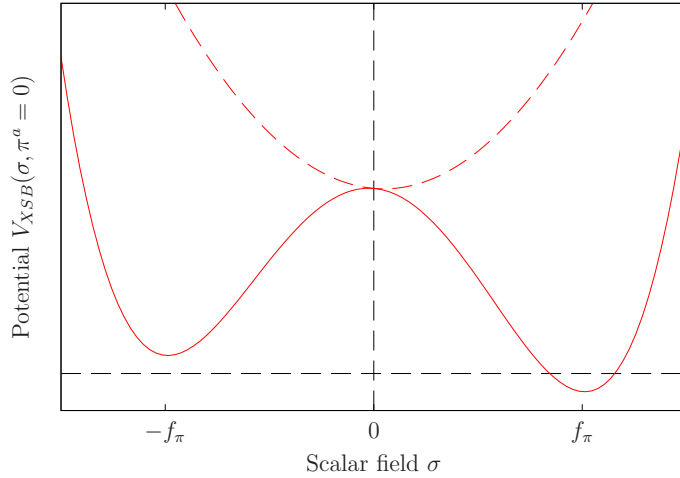


Figure 3.4.: Potential of the linear sigma model in the $\pi^a = 0$ plane as in Fig. 3.4, but here with small symmetry breaking term linear to σ . In the minimum the potential has non-vanishing curvature in π direction (vertical to the drawing plane), which generates the pion mass. The effective potential above the critical temperature is indicated by the dashed red line.

or as quark field. For $SU(2)$ it consists of the two components for proton and neutron or for up and down quark, as the case may be.

Now, the invariance under chiral transformations should be checked: Equations (3.70), (3.72), and (3.73) give the invariance of the last term,

$$(\vec{\pi}^2 + \sigma^2) \xrightarrow{\Lambda_V, \Lambda_A} (\vec{\pi}^2 + \sigma^2). \quad (3.75)$$

The first term in the second line transforms in the same manner because of the identification (3.68). The kinetic terms of the mesons share the same structure (3.75) and the free fermion Lagrange density has already been seen to be invariant.

The minimum of the potential lies in a circle of radius f_π in field space, see Fig. 3.4. In the ground state this value is assumed by the scalar σ because as opposed to the pion field, its quantum numbers are the same as of vacuum. So, the chirally symmetric circle of the potential, $\vec{\pi}^2 + \sigma^2 = f_\pi^2$, is replaced by the choice $\sigma = f_\pi$, $\vec{\pi} = 0$ for the ground state. Of course, there will be fluctuations around these values. In accordance with the Goldstone theorem, there is a direction in field space with vanishing curvature of the potential. The fluctuations into these directions are interpreted as (massless) pions, whereas the radial fluctuations correspond to massive sigma particles.

The small masses of the pions have their origin in the small masses of the light quarks, which explicitly break chiral symmetry. From Eqs. (3.29) and (3.68), the quark mass terms are seen to be equivalent to a term linear in the sigma field. This suggests to introduce such a linear potential in order to take explicit symmetry breaking into consideration. Taking this into account, the potential of the model,

$$V = \frac{\lambda}{4} ((\vec{\pi}^2 + \sigma^2) - f_\pi^2)^2, \quad (3.76)$$

is replaced by

$$V_{\text{sb}} = \frac{\lambda}{4} ((\vec{\pi}^2 + \sigma^2) - v_0^2)^2 - f_\pi m_\pi^2 \sigma, \quad (3.77)$$

where the choice of

$$v_0 = f_\pi \left(1 - \frac{m_\pi^2}{2\lambda f_\pi^2} \right) \quad (3.78)$$

and of the symmetry breaking term leaves the minimum at $\sigma = f_\pi$ to leading order in the parameter $f_\pi m_\pi^2$. The pion mass calculated from this potential is m_π . The nucleon mass in the ground state is read from Eq. (3.74),

$$m_N = g_\pi \sigma_0 = g_\pi f_\pi \quad (3.79)$$

and, as for the pion mass, the value of m_N is retained here.

3.5.4. The dilaton field in string theory

The most prominent occurrence of a dilaton field is not in effective theories of the strong interaction but in string theory. The following short description of its role in this field of physics is based on information gathered from the textbooks and reviews [15, 16, 108, 115, 128].

String theory is an approach to describe the physical world based on one-dimensional objects called strings. As opposed to the case of point particles, the motion of a string through spacetime is not described by a world-line but by a two-dimensional world-sheet. Hence, the action of a free string is not the length of the world-line, but the area of the world-sheet. It is called the Nambu–Goto action S_{NG} . Depending on whether the string in question is open or closed, its world-sheet takes the form of a ribbon or a tube. The degrees of freedom of a string are allocated to translation, rotation and various modes of vibration. The fluctuations of a vibrating string correspond to ripples of the world-sheet. For both types of string, open and closed, these excitations are subject to boundary conditions, which lead to discrete spectra of energy states. The goal is to identify these string excitations with particle spectra known from the standard model and its extensions. While in general there are many obstacles on the way towards a stringy basis of testable field theoretical models, string theory shows some qualities that have stimulated continuous research interest over the last decades.

A nice property of perturbative calculations in string theory is that the number of Feynman diagrams to each order is reduced with respect to field theory. In addition, the spreading of point-like vertices in field theory to areas of meeting world-sheets in string theory avoids divergences in the calculation of the diagrams.

As will be indicated in the following, a hint at a major plus is already seen when quantizing the excitations of a closed string: In this case the creation and annihilation operators come in pairs, corresponding to right-moving and left-moving waves,

$$a_n^{i\dagger}, \bar{a}_n^{i\dagger} \quad \text{and} \quad a_n^i, \bar{a}_n^i. \quad (3.80)$$

3.5. Effective theories of strong interactions

The index n labels the possible wavelengths and the index i specifies the direction of the embedding space into which the mode is oscillating. The various ground states differ by their non-vibrational degrees of freedom. They are annihilated by any annihilation operator, and all states of the string are obtained by repeated use of the creation operators. Then, a more thorough analysis yields a matching condition connecting the occupation numbers of right-movers and left-movers. Altogether, this gives the spectrum of particles that have their origin in the vibration of the string.

The vacuum state corresponds to a particle with negative mass squared, a tachyon. This entails an unstable vacuum. While also arising in the theory of open strings, it can be avoided when fermionic states are included.

The first excited state is obtained by the action of two creation operators because of the matching condition mentioned above. It can be written as

$$\sum_{i,j} R_{ij} a_1^{i\dagger} \bar{a}_1^{j\dagger} |\text{string vacuum}\rangle, \quad (3.81)$$

where the indices i and j now both label the spatial direction of the embedding. The state, on which the creators act, is the vacuum state in the sense that it shows no excitation of the vibration modes, but it is not constrained with respect to translation and rotation of the string. The arbitrary quadratic matrix R_{ij} can be decomposed into three contributions:

1. The symmetric-traceless part is a massless spin-two state. It is interpreted as the graviton giving rise to Einstein gravity in certain limits of the theory. This is part of the reason why string theory is called a viable way to a quantum theory of gravitation.
2. The antisymmetric part yields the Kalb–Ramond field $B_{\mu\nu}$. It is a generalization of the vector potential of electrodynamics. For bosonic field theory without fermions it turns out that this field is massless only in $25+1$ dimensions. This is a necessary condition for Poincaré invariance. It can be shown that the particle content also includes exchange bosons of non-Abelian gauge theories.
3. The trace of R_{ij} leads to one single state. This massless scalar state is called the dilaton. It occurs in all perturbative string theories. It will be discussed below.

The inclusion of fermions is achieved in superstring theory in the framework of supersymmetry: The coordinates of the world-sheet are interpreted as bosonic fields, and corresponding fermion fields need to be introduced. For example this is possible with two-dimensional spinor fields on the world-sheet, as it is done within the Ramond–Neveu–Schwarz formalism.

In superstring theory there are no tachyonic states in the particle spectrum, and the number of required spacetime dimensions is reduced to 10. However, also in this case a compactification of 6 dimensions to small and therefore unobservable scales is necessary.

The dilaton field plays an important role for string interactions. To see this we leave string theory as the generalization of ordinary quantum mechanics of particles to one-dimensional objects and we take a glimpse on what could yield a string field theory, after a second quantization. This is no fully developed theory yet, but at least there is a recipe for the computation of Feynman diagrams [108]. On this basis it can be shown that the dilaton field occurs in the string scattering amplitudes. The simplest example is the vacuum amplitude, which is calculated as a path integral over world-sheet coordinates x and world-sheet metrics γ_{ij} . The γ_{ij} are introduced as auxiliary fields in order to facilitate quantization, which is difficult in the original Nambu–Goto action. The resulting action is the Polyakov action S_P . The result for the vacuum amplitude is the path integral

$$Z = \sum_t \left(e^{\phi_0} \right)^{-\chi(t)} \int_{\{\Sigma_t\}} \mathcal{D}x \mathcal{D}\gamma e^{-S_P \Sigma_t}. \quad (3.82)$$

As usual, the integrand is the exponential of an action. The integral is split into a sum over different topologies t and a remaining integral over all world-sheets with the topology in question. The Euler characteristic $\chi(t)$ counts holes and other topological features. Its negative value can be interpreted as the loop order of a diagram and the exponential in front is seen to play the role of a coupling constant. The vacuum expectation value of the dilaton field, ϕ_0 , occurs here because it is present as a prefactor of the world-sheet metric. As such, it controls the extent, the dilatation, of the world sheet. The apparent dilatation symmetry of the Polyakov action is broken by anomalies, just as in the case of QCD. As far as string theory is concerned it should be stressed, that the string coupling

$$g = e^{\phi_0} \quad (3.83)$$

is not a constant given as an input. Instead, it is the result of a dynamical process, namely of the dilaton’s rolling into its minimum. It is assumed that the dilaton acquires a mass through spontaneous supersymmetry breaking in certain vacua. From the QCD perspective this looks quite familiar: It has been shown that the gluon condensate gives rise to an anomalous trace of the energy–momentum tensor, thereby breaking scale invariance. In an effective approach the gluon condensate is described by a scalar field with corresponding behavior. This field should undergo a symmetry-breaking phase transition somewhere around the QCD energy scale mimicking the condensation of gluons. We will return to this point in the next section.

3.5.5. Linear sigma model with dilaton

For the calculations to this thesis a potential has been used that is derived from the linear sigma model for strong interactions (3.74). When explicit symmetry breaking is taken into account, its potential includes the term linear in the sigma field, as in Eq. (3.77). In the discussion of scale invariance in Section 3.4.2, it has been argued, that the high-energy dynamics of any theory is expected to be scale invariant. From QCD, however, we know that this is an approximation which is valid only for the classical theory. For the

3.5. Effective theories of strong interactions

effective description of strongly interacting matter this has the following consequence: Effective theories of QCD try to keep as many properties of QCD as possible while being as simple as possible. So, one should try to mimic the behavior of QCD under scale transformations as closely as possible by simple means. Such an approach is followed by the authors of [22, 32, 99, 109], which has been mentioned at the end of Section 3.4.2. Here the scalar dilaton field is used to confer the expected transformation property on the individual terms of the action. Therefore, the original potential (3.77) is written as

$$\begin{aligned}
 V_{\text{sb}} = & \frac{\lambda}{4} (\vec{\pi}^2 + \sigma^2)^2 - v_0^2 (\vec{\pi}^2 + \sigma^2) \left(\frac{\chi}{v}\right)^2 - f_\pi m_\pi^2 \sigma \left(\frac{\chi}{v}\right)^2 \\
 & + k \left(\frac{\chi}{v}\right)^4 + \frac{1}{4} \chi^4 \ln \left(\frac{\chi^4}{v^4}\right),
 \end{aligned} \tag{3.84}$$

where the constant k is introduced and v is the minimum of the dilaton potential. From comparison with the above discussion of scale symmetry, it is clear that not every contribution to this potential is invariant. Indeed, the first two terms are, whereas the third transforms non-trivially, as expected from a mass term. (Recall that σ is treated as $\bar{\psi}\psi$.) The second line contains a pure dilaton potential. Up to a constant, it is the same as the one displayed in Fig. 5.3. The logarithm of χ is not scale symmetric and gives a non-zero trace of the energy-momentum tensor. It becomes important when the dilaton evolves from the flat maximum at $\chi = 0$ to one of the two minima at $|\chi| = v$. This implies spontaneous scale symmetry breaking during the cooling of the system, which is similar to the breaking of chiral symmetry: When the dilaton potential is included, the part that breaks scale symmetry is small for high temperatures⁶ because the value of χ is small compared to v . It gets large for low temperatures where the logarithm gives a sizeable contribution. This is the effective description of gluon condensation at low temperatures. It imitates the formation of the scale-symmetry breaking gluon condensate.

To make use of this potential in the context of cosmological inflation, it has been simplified: The third, symmetry breaking term has been omitted and the chiral fields $\vec{\pi}$ and σ have been reduced to one, ϕ . In that sense, the computations have been done on the chiral circle. Finally, a vacuum contribution has been included to keep the potential positive. After renaming the constants, the potential now reads

$$V(\phi) = V_0 + \frac{1}{4} \lambda_0 \chi^4 \left(\ln \left| \frac{\chi}{v} \right| - \frac{1}{4} \right) + \frac{1}{4} \lambda_1 \phi^4 - \frac{1}{4} \lambda_2 \chi^2 \phi^2 \tag{3.85}$$

with

$$V_0 = \frac{1}{16} \lambda_0 v^4 \exp(\lambda_2^2 / \lambda_0 \lambda_1). \tag{3.86}$$

We will return to it in Eq. (6.1). As it will be shown, within such a potential two inflationary periods are possible.

⁶It is the pion mass term.

4. Hot Big Bang cosmology

This chapter deals with some important fundamentals of cosmology. It is based on Refs. [60] and [101]. After the presentation of a few basic equations on redshift and the time dependence of energy density, Section 4.2 will introduce the most important epochs in the evolution of the universe after inflation and reheating. This is the history of the hot Big Bang. Then it will be shown that there are observations that are difficult to explain within this scenario. In the next chapter, an elegant solution to these problems is considered. It is the aforementioned scenario of cosmological inflation.

4.1. Evolution of the universe after inflation

The rate of expansion of the universe can be characterized by the Hubble parameter, which is defined in terms of the scale parameter $a(t)$,

$$H = \frac{\dot{a}}{a}. \quad (4.1)$$

Its value today is approximately $H_0 \approx 70 \text{ km/s Mpc}$. It gives the timescale of the universe, $t = 1/H_0 \approx 1.4 \cdot 10^{10} \text{ yrs}$, and the lengthscale $l = 1/H_0 \approx 4.3 \cdot 10^3 \text{ Mpc}$. The physical wavelength λ_{ph} of a photon is redshifted as the universe expands: Starting from an initial value λ_i at time t_i it grows like

$$\lambda_{\text{phys}}(t) = \frac{a(t)}{a(t_i)} \lambda_i. \quad (4.2)$$

The redshift z is then defined to fulfill

$$\frac{\lambda_{\text{phys}}}{\lambda_i} = 1 + z. \quad (4.3)$$

Frequency and wavenumber decrease correspondingly. The majority of the photons in the universe today belongs to the CMB. They are not in thermal equilibrium anymore but they nevertheless show an almost perfect Planck spectrum. It is not entirely perfect because of small fluctuations of relative size 10^{-5} – 10^{-4} , which will be important for the following chapters. However, it still can be seen as a Planck spectrum to a very good approximation. This is because these photons once were in thermal equilibrium and redshift preserves the Planck distribution. The temperature that corresponds to this distribution is subject to redshift as well. According to this statement, a high

temperature should be expected immediately after reheating, gradually decreasing to the present value $T_0 \approx 2.73$ K.

After the decay of the inflaton field, the energy content of the universe is dominated by radiation. This period is followed by a matter dominated epoch and finally by today's era of vacuum domination. This sequence results from the different equation of state of the corresponding media. To see this let us collect the equations connecting ρ , t , η , H , and a for each type of medium.⁷ Energy–momentum conservation and the second Friedmann equation, (2.41, 2.43, 2.44), are used to calculate the entries of the three last columns in

	Radiation	Matter	Vacuum
p	$\frac{1}{3}\rho$	0	$-\rho$
a	$a_0 t^{1/2}$	$a_0 t^{2/3}$	$a_0 e^{Ht}$
a	$a_0 \eta$	$a_0 \eta^2$	$-\frac{1}{\eta H}$
H	$\frac{1}{2t}$	$\frac{2}{3t}$	const.
ρ	a^{-4}	a^{-3}	const.,

where the entry in each column equals the quantity in the same line of the first column. So, it is seen that the energy density of radiation decays most rapidly with growing scale parameter. Vacuum energy density does not decay at all. Then one expects the primordial radiation dominated era to be followed by matter domination, finally ending with the vacuum dominated universe of today.

4.2. A cosmic timeline

More details with respect to the evolution of the universe are given by the following list of important timescales, for which information from Ref. [101] is used:

- $t \sim 10^{-43}$, $T \sim 10^{19}$ GeV: GR is not valid at this scale and must be replaced by some quantum theory of gravity, maybe string theory. The particles or field content of the universe is unknown.
- $t \sim (10^{-43} - 10^{-14})$ s, $T \sim (10^{19} - 10^4)$ GeV: GR might be used below the Planck scale. The particle content is possibly very different than at energies accessible to accelerators. Maybe there is a supersymmetric phase. This is also the energy scale, where “Grand Unification” of strong and electroweak interactions is assumed. Probably, baryon asymmetry is produced and inflation takes place.

⁷Curvature is set to zero in the calculations.

- $t \sim (10^{-14} - 10^{-10})$ s, $T \sim (10^4 - 10^2)$ GeV: All gauge bosons of the electroweak interaction, Z , W^\pm , and γ , are massless. Electroweak symmetry is broken at the end of this period and the Z and W^\pm become massive.
- $t \sim 10^{-5}$ s, $T \sim 200$ MeV: This is the scale of the strong interaction. Scale symmetry and chiral symmetry of QCD are broken. The quarks and gluons of the quark–gluon plasma are confined into hadrons.
- $t \sim 0.2$ s, $T \sim (1 - 2)$ MeV: Weak interactions become inefficient. Hence, the ratio of neutrons to protons stays constant and neutrinos decouple from the cosmic medium.
- $t \sim 1$ s, $T \sim 0.5$ MeV: The typical photon energy drops below the electron mass. Electron–positron pairs annihilate and are not produced anymore. A few electrons are left over. The annihilation increases the photon temperature with respect to the neutrino temperature because the neutrino interaction with the medium has already come to an end.
- $t \sim (200 - 300)$ s, $T \sim 0.05$ MeV: Epoch of Big Bang Nucleosynthesis (BBN). Helium and traces of other light elements form. Observations of the helium abundance in the universe confirm the BBN scenario at thermal equilibrium. Therefore, inflaton decay and thermalization have to be finished.
- $t \sim 10^{11}$ s, $T \sim 1$ eV: Matter–radiation equality. Up to now, the contribution of radiation to the energy content has surmounted the matter part. Because energy density of radiation decays faster with a than that of matter, the radiative contribution becomes more and more negligible.
- $t \sim (10^{12} - 10^{13})$ s: Recombination of electrons and protons to hydrogen atoms leaves freely streaming photons. They form the CMB today, the observation of which allows a conclusion to be drawn about the state of the universe at decoupling. CMB measurements also yield important information about inflation, see Chapter 5.
- $t \sim (10^{16} - 10^{17})$ s: Age of structure formation. Gravitational instabilities of overdense regions leads to collapse resulting in galaxies and galaxy clusters, filaments, and voids in between.

4.3. Problems of pure Big Bang

Besides its great successes, the cosmological hot Big Bang theory leaves some open questions concerning the initial conditions of the scenario. They are described in the following sections and the mechanism of inflation as a possible solution will be presented in the next chapter.

4.3.1. Horizon problem

The Big Bang theory without an initial period of inflation fails to explain why the CMB is isotropic to a very high degree. Within this theory the photons of the CMB originate from regions of space that have never been in causal contact, which suggests that there should be no correlations between them. Correlations and even isotropy seem plausible only for radiation that is detected within small angles around a given direction. To see this, the size of a patch of sky, for which causal contact at decoupling of the CMB photons is expected, can be estimated by calculating the particle horizon of that time. This is the distance a photon may have travelled since the Big Bang. First, note that a light-like geodesic is characterized by $ds^2 = 0$, which gives

$$|d\mathbf{x}| = d\eta \quad (4.4)$$

in a comoving coordinate system. Then the comoving particle horizon at time t is

$$l_{\text{p.h.}}(t) = \eta(t) = \int_0^t \frac{dt'}{a(t')}. \quad (4.5)$$

The ratio of this quantity at different times is estimated as in Eq. (4.6). Being a ratio of two lengths both measured at the same time, it makes no difference whether they are taken as comoving or physical:

$$\frac{l_{\text{p.h.}}(t_0)}{l_{\text{p.h.}}(t_1)} = \frac{\int_0^{t_0} dt'/a(t')}{\int_0^{t_1} dt'/a(t')} = \frac{\int_0^{a_0} da/Ha^2}{\int_0^{a_1} da/Ha^2} \approx \frac{a_1 H(a_1)}{a_0 H(a_0)}. \quad (4.6)$$

For the second equality dt is replaced by da/Ha . The approximation is exact under the assumption $a(t) \propto t^\alpha$, $\alpha < 1$ because then

$$H \propto t^{-1} \propto a^{-1/\alpha} \quad (4.7)$$

and therefore

$$l_{\text{p.h.}}(t_0) \propto \int_0^{a_0} \frac{da}{a^{2-1/\alpha}} = a_0^{1/\alpha-1} \propto \frac{1}{a_0 H(a_0)}. \quad (4.8)$$

Apart from the power law $a(t) \propto t^\alpha$ with constant α , the calculation relies on a second simplification: The lower boundary of the integrals is taken as zero although the laws of physics are unknown at least until the Planck time t_{Pl} . So nothing can be said about the evolution of the particle horizon before that time. However, it seems plausible that at t_{Pl} the particle horizon is of the order of the Planck scale, too. It could be taken as a lower value for the integrals in Eq. (4.5) and (4.6) but it is neglected in comparison to the much larger upper values. This is done by taking the initial time as zero because within radiation (or matter) domination the lower value of the integral vanishes.

Now the redshift at photon decoupling $z \approx 1100$ is inserted in Eq. (4.6). This yields an angle of order $1/30$ within which causal connection can be assumed. So the number of patches of the sky which seem to be causally distinct is of order 1000. Therefore within a pure hot Big Bang scenario very homogeneous initial conditions have to be assumed without motivation.

4.3.2. Flatness problem

The horizon problem arises because the Planck length l_{Pl} seems to be a natural guess for the horizon size at Planck time t_{Pl} . A similar guess for the scale of the spatial curvature can be made from the structure of the Friedmann equation (2.39): Written as

$$H^2 = \frac{8\pi}{3m_{\text{Pl}}^2}(\rho_{\text{m}} + \rho_{\text{r}} + \rho_{\Lambda} + \rho_{\text{c}}), \quad (4.9)$$

the curvature term is interpreted as a contribution to the energy content as well. Normalization of the four energy densities by H^2 and appropriate definition of Ω for each contribution leaves

$$1 = \Omega_{\text{m}} + \Omega_{\text{r}} + \Omega_{\Lambda} + \Omega_{\text{c}}, \quad (4.10)$$

the most natural initial contributions to the Hubble parameter coming from matter (ρ_{m}), radiation (ρ_{r}), the cosmological constant (ρ_{Λ}), and curvature (ρ_{c}) are suggested to be of the same order for all sources. Comparison with Eq. (2.39) gives

$$\frac{\Omega_{\text{c}}(t_0)}{\Omega_{\text{c}}(t_1)} = \left(\frac{a(t_1)H(t_1)}{a(t_0)H(t_0)} \right)^2, \quad (4.11)$$

similarly to Eq. (4.8). If the two moments of time are chosen as t_{Pl} and today, one estimates $a(t_{\text{Pl}})/a(t_0) \sim T_0/m_{\text{Pl}}$ and $H(t_{\text{Pl}})/H(t_0) \sim m_{\text{Pl}}/H_0$. So Eq. (4.11) gives the value

$$|\Omega_{\text{c}}(t_{\text{Pl}})| \sim |\Omega_{\text{c}}(t_0)| \frac{H_0^2}{T_0^2} \sim 10^{-60}. \quad (4.12)$$

for the contribution of curvature to the energy content at the Planck epoch. This is many orders of magnitude smaller than what should be assumed from Eq. (4.10).

In other words the flatness problem is the following: For any cosmological evolution with $\ddot{a} < 0$, Eq. (4.11) shows that Ω_{c} grows with time. Why then is it still so small?

4.3.3. Monopole problem

The monopole problem is not concerned with the initial conditions of Big Bang cosmology. However, it is included here because it can be solved by inflation. At very high energies magnetic monopoles or topological defects may be produced as predicted by theories beyond the Standard Model of particle physics. Possible monopoles from a GUT phase transition played an important role in motivating early models of inflation [64]. This problem is different from the ones mentioned before because it stems from particle physics and not from Big Bang cosmology itself. Nevertheless, if such relics are to be expected from the very early mechanism and if they contradict observation there should be a mechanism which dilute them down to a tolerable concentration.

4.3.4. Primordial perturbations

The horizon problem discussed above raises the question whether the observed homogeneity and isotropy of the universe seem natural or not. But in addition to the homogeneity on large scales, the sky shows obvious perturbations like planets, stars and galaxy clusters. Cosmology can explain their formation from small initial perturbations upon a homogeneous background. However, in order to understand the creation of these initial perturbations, an additional mechanism is needed: inflation.

5. Inflation

This section presents the basics of the theory of cosmological inflation. It is based on the introductions in [59,94,95]. Assuming an inflationary epoch before the hot Big Bang scenario is a possible solution to several problems cosmology, which are discussed at the end of the preceding chapter. By definition, a period of time in the early universe is called inflation when the scale parameter $a(t)$ is accelerating. With the Hubble parameter $H = \dot{a}/a$ the following equivalent defining conditions for inflation are found:

$$\ddot{a} > 0 \quad \Leftrightarrow \quad \frac{d}{dt} \frac{1}{Ha} < 0 \quad \Leftrightarrow \quad -\frac{\dot{H}}{H^2} < 1 \quad (5.1)$$

The second one stresses the fact that the comoving Hubble length $1/Ha$ becomes smaller during inflation. The third inequality in Eq. (5.1) sets a limit on the change of the Hubble parameter with time. The decrease of H has to be small within one Hubble time $1/H$. In Chapter 4 it was found that the Hubble length is a measure for the observable part of the cosmos, which is now seen to shrink in an accelerating universe. On the other hand, the comoving wavelength of a fluctuation is constant during any cosmological epoch. Then it should be expected that there are fluctuations whose wavelengths grow with respect to the Hubble scale and finally exceed it. Then they are said to leave the Hubble horizon. Such a horizon crossing changes the character of the time evolution of the mode and prevents it from extinction.

Independently from the mechanism and the dynamics of inflation, these two aspects of accelerated expansion, namely decrease of the observable part of the universe and freezing of oscillations during horizon crossing, solve problems posed by standard hot Big Bang cosmology.

The second section of this chapter discusses the solutions to some of these open questions more thoroughly. Before that, however, we should make a short detour to take a glimpse on the historic evolution of the inflationary theory:

5.1. Short history of cosmological inflation

In the 1970s the cosmological role of phase transitions in gauge theories was examined. As discussed by Andrei Linde in Ref. [88], the hot stage of the universe could be preceded by an era with the dominating part of energy and momentum coming from a metastable vacuum state of gauge theories. Within this scenario the cold era ends with the decay

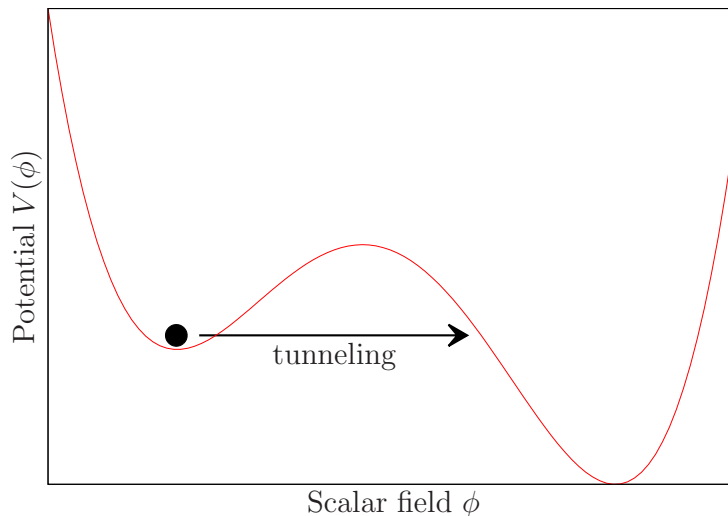


Figure 5.1.: Sketch of the potential in “old inflation.” The exponential expansion is driven by the potential energy of the false vacuum state. The scalar field during inflation is illustrated with the black dot. Inflation ends when ϕ tunnels through the potential barrier and decays while oscillating around the absolute minimum.

of this “false vacuum” into the true one. This phase transition is accompanied with a strong rise of entropy. However, the universe after such a scenario was found to be too inhomogeneous to match with observations.

An approach within quantum gravity was followed by Alexei Starobinsky [121] who obtained a spectrum of primordial gravitational waves that are produced before the classical Friedmann expansion starts. Also the presence of scalar perturbations can be explained within this model as was found later in Ref. [102]. Here the perturbations were viewed as possible seeds for structure formation.

In 1981, Alan Guth suggested a scenario which was based on a phase transition again. He called it the “inflationary universe” and showed that it could solve the three major problems concerning flatness, the horizon size, and the amount of entropy within the observable universe [64]. He also pointed out what was later called the “graceful exit problem”: The exponential expansion in this model is driven by the potential energy of a field trapped in a false vacuum state, see also Fig. 5.1. The phase transition takes place when bubbles of the new phase, the true vacuum, form. Bubble nucleation occurs through a tunneling process. If the state of acceleration is to last long enough to solve the cosmological puzzles, the maximal nucleation rate is determined by the Hubble expansion. Nucleation rates that are allowed by this condition entail too strong inhomogeneities to be acceptable. This is because there are too few bubble collisions to thermalize the medium before nucleosynthesis [70]. The assumption that the observable universe today has emerged from a single bubble was considered in Ref. [65]. It had to be discarded because the entropy in such a bubble would be much lower than observed.

5.2. Inflation as a solution to cosmological problems

Later this scenario was called “old inflation.”

At the end of the year 1981, Linde suggested an improved inflationary model in [89], which was based on spontaneous symmetry breaking induced by thermal corrections (Coleman–Weinberg mechanism [38]). A few months later, a similar way of solving the cosmological problems was examined in [10]. The graceful exit problem of old inflation is not encountered here because the barrier between the false and the true vacuum vanishes when the temperature decreases. The scenario is now called “new inflation” and belongs to the category of hilltop inflation considered in Sect. 5.3.3. An important difference to old inflation is the non-zero $\dot{\phi}$ of the inflaton field, which can make the spectrum of generated perturbations slightly tilted. However, just as old inflation this scenario relies on the thermodynamics of phase transitions. This is problematic since observations demand a very small coupling constant for which thermal equilibrium cannot be taken as given.

In 1983 Linde proposed a scenario that he called “chaotic inflation” [90]. It is based on the observation that for a large class of potentials $V(\phi)$ an inflationary period occurs if the initial field values are chaotically distributed. The most important condition is that there are field values for which the potential is flat enough. For sufficiently large ϕ this is for example the case in a quadratic or quartic potential. Then an inflationary solution is obtained. Within a chaotic field distribution it is natural to assume the existence of regions where inflation takes place. Such a region could evolve into the observable universe today.

From then on a multitude of potentials and scenarios have been considered which include periods of accelerated expansion of the early universe. There are many scalar fields that can be motivated from string theory and supergravity and used for driving inflation. In models of multifield inflation, various fields can contribute to acceleration and production of fluctuations.

In 1991 a new version of chaotic inflation was proposed by Linde who called it hybrid inflation [92]. Hybrid inflation is a multifield model but there is only one inflaton field that evolves during inflation. A second one, the “waterfall field” ends inflation by rolling down into its vacuum state.

Some details on how the inflationary universe can reconcile observations with the hot Big Bang theory and on important examples for potentials leading to inflation will be provided in the next sections.

5.2. Inflation as a solution to cosmological problems

In Sec. 4.3 some problems are described which cannot be overcome within the standard hot Big Bang scenario of cosmology. However, if a period of inflation takes place during the very early universe all of these problems are solved at once. There are arguments that inflation should start very early within the nascent spacetime because it needs sufficient homogeneity within the Hubble horizon. This quantity increases with time

and fulfillment of the condition of homogeneity seems to become less probable. In addition, if $\Omega \equiv 1 - \Omega_c > 1$ the universe is expected to recollapse soon after its creation unless there is a mechanism that drives this value very close to unity. Inflation has this effect as can be seen from Eqs. (5.1) and (4.11): The first equation shows that during inflation the combination $H(t)a(t)$ grows with time. Then Eq. (4.11) gives the corresponding decrease of Ω_c .

A small value of Ω_c after inflation resolves the flatness problem of cosmology. Assuming the Hubble parameter to be constant, Eq. (4.12) gives the necessary growth of the scale parameter from a_i at the beginning of accelerated expansion to its end at a_f :

$$N_e \equiv \ln \left(\frac{a_f}{a_i} \right) \approx 70. \quad (5.2)$$

In this equation N_e is called the total number of e-foldings of inflation. This value corresponds to a vast expansion of the universe, but, as will be seen below, it is easily obtained in simple models of inflation.

The number of e-foldings required to solve the horizon problem is much smaller: A short calculation of the comoving particle horizon Eq. (4.5) within de Sitter spacetime ($a(t) \propto \exp(Ht)$) shows that it stays constant while the comoving Hubble horizon decreases as $1/a(t)$. Because the former is a measure for the volume that has been in causal contact and the latter is a measure for the observable universe, the part of the CMB sky for which isotropy seems plausible is enlarged by a factor $\exp(N_e)$. So only a few e-foldings are enough to cover the full sky instead of an angle $\sim 1/30$ and to explain observations.

The exponential dilution of any structures that may have existed before inflation solves the problem of missing magnetic monopoles described in Sec. 4.3.3. After phase transitions with spontaneous symmetry breaking topological defects such as domain walls or cosmic strings may occur. They are likewise attenuated if they are produced before inflation. However, especially if the preheating temperature after inflaton decay is high, production of such unwanted relics after inflation can arise and may pose a problem.

The last and for this work the most important effect of inflation is the production of small density perturbations as seeds for structure formation. As will be demonstrated later, they are generated from quantum fluctuations in one or more scalar fields on each scale at the time of its horizon exit. Direct observation of these fluctuations today is possible for a spectral range from 10^{-3} Mpc to 10^4 Mpc, where the latter is the length scale of the observable universe $1/H_0$. Most probably they require a period of about 16 e-folds of almost exponential inflation. The total amount of inflation must be larger because the largest observable scale had to be driven out far enough as to reenter the horizon not earlier than now. The corresponding value of N_e is estimated as in Eq. (5.124). The value $q_0 = 0.002 \text{ Mpc}^{-1}$ should only be replaced by the current Hubble scale $H_0 \sim 10^{-4} \text{ Mpc}^{-1}$, which makes a difference of 3 in the value N_e . So the necessary inflationary expansion is in the range $N_e \in [50, 65]$, mainly depending on the models of

inflation and preheating.

Put together, the total number of e-folds necessary to solve the presented problems is around 70. Generically inflation leads to an expansion much larger than this, as will be seen in Sec. 5.3.

5.3. Inflation driven by a homogeneous scalar field

If the energy density of the universe is dominated by vacuum energy, the scale parameter $a(t)$ will accelerate. This is seen in the following way:

Because of coordinate invariance, the energy–momentum tensor of vacuum has the form

$$T_{\mu\nu} = \rho_{\text{vac}} g_{\mu\nu} \quad (5.3)$$

with a constant energy density ρ_{vac} . Comparison with the energy–momentum tensor of an ideal fluid in the local rest frame,

$$T_{\mu\nu} = \text{diag}(\rho, p, p, p), \quad (5.4)$$

reveals that the pressure is negative and has the same absolute value as the energy density. This gives the equation of state

$$p_{\text{vac}} = -\rho_{\text{vac}}. \quad (5.5)$$

Since $\rho + 3p < 0$, the positive acceleration of a is seen from the second Friedmann equation Eq. (2.41). The Hubble parameter has the constant value

$$H_{\text{vac}} = \sqrt{\frac{8\pi}{3} \frac{\rho_{\text{vac}}}{m_{\text{Pl}}^2}}, \quad (5.6)$$

yielding the exponential growth of the scale parameter

$$a(t) \propto e^{H_{\text{vac}} t}. \quad (5.7)$$

This is a de Sitter solution. Of course, it does not constitute a viable model for inflation because there is no mechanism of a transition to a radiation dominated universe. An evolution into the universe today seems more plausible for an inflation driven by dynamical fields. If there are suitable interactions, a decay into the observed particle content is conceivable.

In this section the simplest case of a single, homogeneous scalar “inflaton” field is presented. The potentials discussed in the following correspond to the scenarios for which the historic evolution has been outlined in Sec. 5.2. But first let us collect the basic equations for the description of a simplified setting: Inflation driven by a slowly rolling scalar field.

5.3.1. Slow-roll inflation

The evolution of a homogeneous scalar field $\phi(t)$ within a spatially flat FRW universe obeys the equation of motion (3.2) and the Friedmann equation (3.5). Pressure and energy density can be read off from the energy momentum tensor and are given by Eq. (3.4). This equation for ρ and p yields a vacuum-like equation of state if the kinetic energy is negligible compared to the potential energy,

$$\frac{\dot{\phi}^2}{2V(\phi)} \ll 1. \quad (5.8)$$

To ensure that this situation continues for some time, the acceleration $\ddot{\phi}$ should be small, too. As for a classical particle moving in a potential, this means that it is negligible compared to the friction term:

$$\left| \frac{\ddot{\phi}}{3H\dot{\phi}} \right| \ll 1. \quad (5.9)$$

The last two equations constitute a possible definition for slow-roll evolution of a scalar field. If they are satisfied, Eqs. (3.2) and (3.5) can be approximated as

$$\dot{\phi} = -\frac{1}{3H}V'(\phi) \quad (5.10)$$

and

$$H = \frac{1}{m_{\text{Pl}}} \left(\frac{8\pi V}{3} \right)^{1/2}. \quad (5.11)$$

The two conditions (5.8) and (5.9) also prevent the Hubble parameter from rapid relative changes within the scale of a Hubble time $1/H$:

$$\left| \frac{\dot{H}}{H^2} \right| \ll 1. \quad (5.12)$$

This inequality shows that $a(t)$ grows almost exponentially, as could be expected from the similarity of the equation of state to that of vacuum. Equation (5.12) is obtained from the time derivative of Eq. (5.11): After replacing V' with the help of Eq. (5.10) one has

$$\frac{\dot{H}}{H} = -\frac{3}{2} \frac{\dot{\phi}^2}{V} H \quad (5.13)$$

and (5.12) follows from the slow-roll condition (5.8).

Now that a slowly evolving field has been shown to entail an accelerated expansion, the question arises, in what kind of potential slow roll occurs. Using the conditions (5.8) and (5.9) and the slow-roll versions of the equations of motion, Eqs. (5.10) and (5.11), the following requirements can be deduced:

$$\epsilon \ll 1, \quad \eta \ll 1, \quad (5.14)$$

5.3. Inflation driven by a homogeneous scalar field

where the two slow-roll parameters are defined as

$$\epsilon = \frac{m_{\text{Pl}}^2}{16\pi} \left(\frac{V'}{V} \right)^2 \quad \text{and} \quad \eta = \frac{m_{\text{Pl}}^2}{8\pi} \left(\frac{V''}{V} \right). \quad (5.15)$$

A potential with small slow-roll parameters is called flat. The two inequalities (5.14) were obtained under the assumption of slow roll and quasi-exponential expansion. However, inflation as defined in Eq. (5.1) poses a weaker requirement. So there can be accelerated expansion without slow roll. Scenarios of fast-roll inflation before and after a slow-roll stage are considered for example in [93] and [41], respectively. On the other hand, also a flat part of a potential can fail to sustain inflation if the initial field velocity $\dot{\phi}$ is too large.

For slow-roll inflation the expansion taking place between two given field values can be calculated as in Eq. (5.16). The function $N_e(\phi_0)$ denotes the number of e-foldings from the time when the field takes on the value $\phi_0 = \phi(t_0)$ to the end of inflation at $\phi_f = \phi(t_f)$. It is calculated as

$$\begin{aligned} N_e(\phi_0) &= \ln \left(\frac{a_f}{a(\phi_0)} \right) = \int_{t_0}^{t_f} H(t) dt = \int_{\phi_0}^{\phi_f} \frac{H(\phi)}{\dot{\phi}} d\phi \\ &= \int_{\phi_f}^{\phi_0} \frac{3H^2}{V'} d\phi = \frac{8\pi}{m_{\text{Pl}}^2} \int_{\phi_f}^{\phi_0} \frac{V}{V'} d\phi. \end{aligned} \quad (5.16)$$

Through Eqs. (5.10) and (5.11) the slow-roll assumption enters in the second line. The same two equations are used for calculating the time a slowly rolling field needs to evolve from ϕ_0 to ϕ_f :

$$\Delta t = \int_{t_0}^{t_f} dt = \int_{\phi_0}^{\phi_f} \frac{d\phi}{\dot{\phi}} = \int_{\phi_f}^{\phi_0} \frac{3H}{V'} d\phi \quad (5.17)$$

$$= \frac{\sqrt{24\pi}}{m_{\text{Pl}}} \int_{\phi_f}^{\phi_0} \frac{\sqrt{V}}{V'} d\phi. \quad (5.18)$$

In the sections to follow examples for slow-roll inflation are discussed.

5.3.2. Large-field inflation

In this section some properties of inflation within the potentials

$$V = \frac{1}{n} g_n \phi^n \quad (5.19)$$

are presented. In the following, the coupling g_n is also written as λ and m^2 in the cases $n = 2$ and $n = 4$, respectively. For these potentials inflation is usually assumed to start from chaotic initial conditions. This was suggested in Ref. [90] where the scenario was named chaotic inflation. When the initial field values are randomly distributed, there

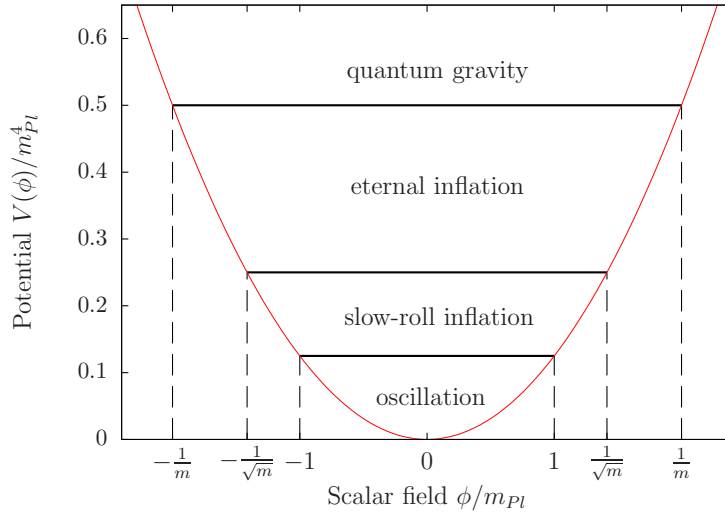


Figure 5.2.: Sketch of the quadratic potential $m^2\phi^2/2$ for large-field inflation. Above $\phi \sim 1/m$ the description within classical general relativity breaks down. Eternal inflation occurs when quantum fluctuations dominate over the slow-roll evolution of the field. If ϕ starts in this regime, then in the greatest part of the universe inflation continues forever. Standard slow-roll inflation takes place at lower energies. After inflation a period of field oscillations is expected, which lead to the decay of the homogeneous mode. The situation is similar for other large-field models.

should be regions of space where the system is in the slow-roll regime but below energies where quantum gravity effects become important:

$$\frac{n}{4\sqrt{\pi}}m_{\text{Pl}} \ll \phi \ll \left(\frac{m_{\text{Pl}}^4}{g_n}\right)^{1/n}. \quad (5.20)$$

The first inequality is the slow-roll condition. It requires ϕ to be super-Planckian, $\phi > m_{\text{Pl}}$. At the upper boundary also the energy density is of order the Planck scale m_{Pl}^4 . The inequalities in Eq. (5.20) can be fulfilled for small coupling g_n . This is consistent with the requirement for small couplings from observation.

In this context one should also mention the possibility of “eternal inflation” [58, 91]. This concept is based on the fact that for very high field values in chaotic inflation the quantum fluctuations in ϕ can be larger than the classical evolution of the homogeneous part. Then the field can also move upwards with time. The accelerated expansion gives rise to more and more regions within the universe which are not interacting anymore since they are outside of each other’s horizon. So the quantum fluctuations of ϕ lead to strong inhomogeneities on large scales. In fact it should be expected that large parts of the universe remain in the inflationary state.⁸ A similar mechanism exists for hilltop inflation, see [124].

⁸ In connection with string theory this might alleviate problems with the anthropic principle: Eternal inflation gives birth to ever new universes and to infinitely many of them with possibly different

5.3. Inflation driven by a homogeneous scalar field

Let us now continue with the amount and the duration of large-field inflation: Equation (5.16) leads in this case to

$$N_e(\phi_0) = \frac{4\pi}{n} \frac{\phi_0^2}{m_{\text{Pl}}^2} \quad (5.21)$$

if ϕ_0 is taken as the value at begin of inflation and the field value at the end is assumed to be much smaller. Similarly, Eq. (5.18) gives

$$\Delta t \sim \begin{cases} \frac{\phi_0}{m \cdot m_{\text{Pl}}} & \text{for } V = m^2 \phi^2 / 2 \\ \frac{1}{\sqrt{\lambda} \cdot m_{\text{Pl}}} \ln \frac{\phi_0}{\phi_r} & \text{for } V = \lambda \phi^4 / 4. \end{cases} \quad (5.22)$$

For a universe starting to inflate at

$$V \sim m_{\text{Pl}}^4 \Leftrightarrow \phi_0 \sim g_n^{-1/n} m_{\text{Pl}}^{4/n} \quad (5.23)$$

and for coupling constants $m = 10^{-6}$ and $\lambda = 10^{-13}$ one gets

$$N_e^{\text{tot}} \sim 10^{13}, \quad \Delta t^{\text{tot}} \sim 10^{-31} \text{s} \quad \text{for } V = m^2 \phi^2 / 2 \quad (5.24)$$

$$N_e^{\text{tot}} \sim 10^7, \quad \Delta t^{\text{tot}} \sim 10^{-35} \text{s} \quad \text{for } V = \lambda \phi^4 / 4. \quad (5.25)$$

for the total number of e-foldings and the total duration of inflation, respectively. When eternal inflation is taken into account these numbers corresponding to standard inflation will be smaller. But in either case the required number of e-foldings is surpassed by a large amount.

5.3.3. Hilltop inflation

The slow-roll conditions can also be fulfilled around a flat maximum of a potential. An example that was discussed early in this context is “new inflation” within the Coleman–Weinberg potential [38],

$$V(\phi) = V_0 + \frac{1}{4} \lambda \phi^4 \left(\ln \left| \frac{\phi}{v} \right| - \frac{1}{4} \right) \quad (5.26)$$

with

$$V_0 = \frac{1}{16} \lambda v^4, \quad (5.27)$$

where v is the symmetry-breaking scale. This potential complies with the slow-roll condition not only for large field values but also around $\phi = 0$. The beginning of inflation in this region can be motivated by assuming symmetry restoration for high temperature and a symmetry breaking phase transition when the medium cools. Breaking the

compactification of extra-dimensions and different vacuum state. So the existence of a (region of the) universe with life-sustaining conditions could be seen as less improbable.

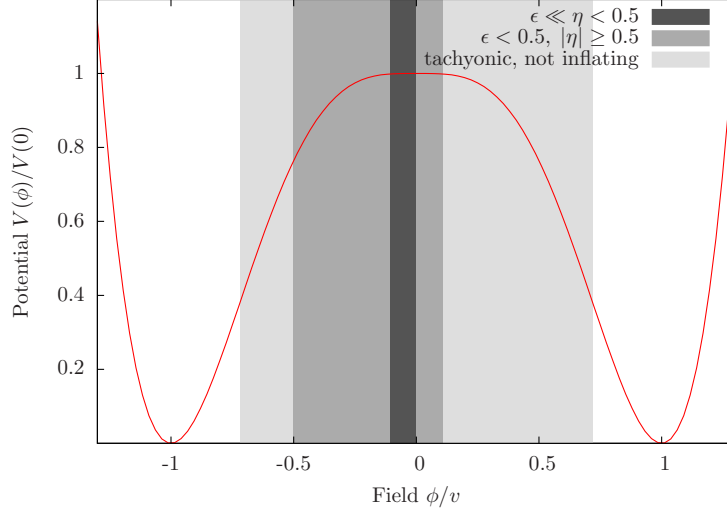


Figure 5.3.: The logarithmic potential Eq. (5.26) for new inflation. The tachyonic region is shaded in light grey. The field values where the universe is inflating but already preheating (fixed at $\epsilon < 0.5 < \eta$) are marked with darker grey. The strip with the darkest shading tags the range of slow-roll inflation ($\epsilon < \eta < 0.5$). The shadings at negative field values correspond to the case $v = 10^{-1}m_{\text{Pl}}$ and the ones on the right to $v = 10^{-3}m_{\text{Pl}}$.

symmetry the field evolves slowly down into a minimum at $\phi = \pm v$. During small-field inflation the potential can be simplified to

$$V(\phi) = V_0 - \frac{1}{16}\lambda\phi^4. \quad (5.28)$$

Then the slow-roll parameters are

$$\epsilon = \frac{1}{\pi} \left(\frac{m_{\text{Pl}}}{16} \frac{\lambda\phi^3}{V_0} \right)^2 \quad (5.29)$$

and

$$\eta = -\frac{m_{\text{Pl}}^2}{32\pi} \frac{3\lambda\phi^2}{V_0}, \quad (5.30)$$

Having the larger absolute value, slow roll is broken by η first. Then the energy density is typically still approximately V_0 . This value, however, can be considerably smaller than the Planck scale. Then also for rapid decay of the homogeneous mode after inflation the reheating temperature is many orders of magnitude below T_{Pl} . So the hot Big Bang evolution might start with energy densities for which physics is well known. A problem might rather arise from thermalization taking place below the temperature of Big Bang Nucleosynthesis, see Sec. 4.1.

The total amount of accelerated expansion is calculated as in Eq. (5.16): For this purpose inflation is taken to start at

$$\phi_0 = H \quad (5.31)$$

5.3. Inflation driven by a homogeneous scalar field

because this is the value expected from quantum fluctuations around $\phi = 0$. The contribution from the upper boundary ϕ_f of the integral for N_e can be neglected because of $\phi_0 \ll \phi_f$. So the computation is

$$N_e^{\text{tot}} = \int_{\phi_f}^{\phi_0} \frac{3H^2}{V'} d\phi \quad (5.32)$$

$$\approx \frac{6H^2}{\phi_0^2} \frac{1}{\lambda} \sim \frac{1}{\lambda} \gg 1. \quad (5.33)$$

Also in this case the number of e-foldings is far beyond the necessary amount. The duration of inflation is

$$\Delta t^{\text{tot}} \int_{\phi_f}^{\phi_0} \frac{3H}{V'} d\phi \sim \frac{1}{\lambda} \frac{1}{H}. \quad (5.34)$$

In the small-field case the Hubble parameter does not decrease substantially during slow roll. So one can read off from this result that inflation lasts much more than one Hubble time.

5.3.4. Hybrid inflation

There are many inflationary models with more complicated potentials. A broad class is hybrid or multifield inflation. In this section the first model of this kind is presented, see [59, 92]. The corresponding potential,

$$V(\phi, \chi) = V_0 + \frac{1}{2} (g^2 \phi^2 - \mu^2) \chi^2 + \frac{\lambda}{4} \chi^4 + U(\phi), \quad (5.35)$$

with inflaton potential

$$U(\phi) = \frac{1}{2} m^2 \phi^2 \quad (5.36)$$

and offset

$$V_0 = \frac{\mu^4}{4\lambda} \quad (5.37)$$

is shown in Fig. 5.4. The parameters in [92],

$$g^2 = \lambda = 0.1, \quad m = 10^2 \text{ GeV}, \quad \mu = 1.3 \cdot 10^{11} \text{ GeV}, \quad (5.38)$$

are used. The evolution of the fields is taken to start at large ϕ and small or zero χ . The initial stage resembles large field inflation with chaotic spatial distribution of ϕ . When the critical value

$$\phi_c = \frac{\mu}{g} \quad (5.39)$$

is reached the waterfall field χ breaks slow roll and terminates inflation. During the subsequent reheating the fields oscillate around a minimum at $\phi = 0$ and $\chi = \pm v$ with the symmetry breaking scale

$$v = \frac{\mu}{\sqrt{\lambda}}. \quad (5.40)$$

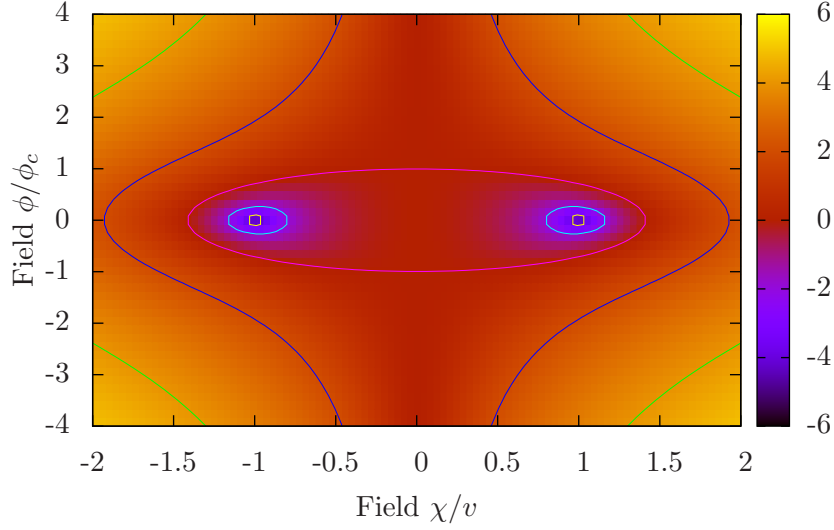


Figure 5.4.: Potential for hybrid inflation Eq. (??). The universe is inflating when ϕ is in one of the valleys at $\chi = 0$ and $|\phi| > \phi_c$. When ϕ reaches the critical value $\pm\phi_c$ inflation ends and the system reheats during field oscillations around one of the minima. The parameters v for this figure were taken from Ref. [92].

The end of the accelerating period in hybrid inflation bears more analogy with the hilltop case. If the offset V_0 dominates over the inflaton potential at ϕ_c during inflation, the mechanism leading to acceleration is different from the large field case. The additional potential energy extends slow roll down to field values well below the Planck scale.

Assuming a quick drop of the waterfall field into the minimum, the number of e-foldings before the end of inflation can be calculated as

$$N_e(\phi) \approx \frac{8\pi}{m_{\text{Pl}}^2} \int_{\phi_c}^{\phi} \frac{V_0}{U'} \cdot \quad (5.41)$$

The contribution of U to the numerator has been neglected. For a quadratic and a quartic inflaton potential, integration gives

$$N_e(\phi) \approx \frac{8\pi V_0}{m_{\text{Pl}}^2 m^2} \ln \frac{\phi_0}{\phi_c} \quad (5.42)$$

and

$$N_e(\phi) \approx \frac{4\pi V_0}{m_{\text{Pl}}^2 \lambda} \left(\frac{1}{\phi_0^2} - \frac{1}{\phi_i^2} \right) \quad (5.43)$$

respectively.

For large ϕ the offset V_0 is negligible compared to $U(\phi)$. So the total amount of inflation is again beyond the required $N_e \approx 70$, as obtained from the computation within large-field inflation.

5.4. Inflation and the origin of fluctuations

In the early 1970's Edward R. Harrison and Yakov B. Zeldovich proposed an initial flat spectrum of scalar metric fluctuations to explain the origin of structure in the universe [68,127]. Ten years later the production of these primordial inhomogeneities was attributed to an inflationary period [69,102]. As already mentioned, tensor perturbations from inflation were considered already very early [121]. Later their possible traces in the CMB were studied [3,48,117]. Up to now tensor perturbations from inflation could not be detected [5–7]. The topic of this section is the theory of fluctuations produced in slow-roll inflation. The presentation follows [59], see also [95] and [103].

5.4.1. Scalar perturbations

This section concentrates on scalar perturbations during inflation. More precisely the goal is to obtain the equation of motion for fluctuations of a scalar field and for the scalar perturbations in the metric. The latter are characterized by \mathcal{R} , which quantifies the curvature of 3-dimensional equal-time hypersurfaces in the comoving reference frame, see Section 2.2.4. The velocity v , which is zero by definition in this coordinate system, will be found shortly. From \mathcal{R} the curvature scalar $R^{(3)}$ is calculated as

$$R^{(3)} = -\frac{4}{a^2}\Delta\mathcal{R}. \quad (5.44)$$

Metric and energy–momentum tensor. The system is described using a metric with scalar perturbations in conformal Newtonian gauge,

$$ds^2 = a^2(\eta) \left((1 + 2\Phi)d\eta^2 - (1 - 2\Phi)d\mathbf{x}^2 \right), \quad (5.45)$$

see Section A.4. The field ϕ is separated into a homogeneous, classical part and fluctuations,

$$\phi(\mathbf{x}, t) = \phi_c(t) + \varphi(\mathbf{x}, t). \quad (5.46)$$

Then the energy–momentum tensor,

$$T_\nu^\mu = g^{\mu\rho}\partial_\nu\phi\partial_\rho\phi - \delta_\nu^\mu \left(\frac{1}{2}g^{\rho\sigma}\partial_\rho\phi\partial_\sigma\phi - V(\phi) \right), \quad (5.47)$$

allows to read off the energy density

$$\rho = T_0^0 = \frac{1}{2a^2} \frac{1}{1 + 2\Phi} \phi'^2 + \frac{1}{2a^2} \frac{1}{1 - 2\Phi} \partial_i\phi\partial_i\phi + V(\phi). \quad (5.48)$$

Primes denote a derivative with respect to conformal time. The first order in the small fluctuations Φ and φ is

$$\delta\rho = \frac{1}{a^2} (\varphi'\phi'_c - \Phi\phi_c'^2) + \frac{dV}{d\phi_c}\varphi \quad (5.49)$$

and using the equation of motion (3.2) results in

$$\delta\rho = \frac{1}{a^2} \left\{ \varphi' \phi'_c - \Phi \phi_c'^2 - \left(\phi_c'' + 2 \frac{a'}{a} \phi_c' \right) \varphi \right\}. \quad (5.50)$$

The $(0, i)$ -component of the perturbation is

$$\delta T_i^0 = g^{00} \partial_i \phi \partial_0 \phi = \frac{1}{a^2} \partial_i \varphi \phi_c' \quad (5.51)$$

to first order. For the following the velocity potential defined in Eq. (2.72) is needed. Comparing this equation,

$$\delta T_i^0 = -(p + \rho) \partial_i v, \quad (5.52)$$

with Eq. (5.51) gives

$$v = -\frac{1}{a^2} \frac{\phi_c'}{\rho + p} \varphi = -\frac{\varphi}{\phi_c'}, \quad (5.53)$$

where the zero mode of both v and φ are taken to vanish and the second equality uses Eq. (3.4). The field is unperturbed in the comoving reference frame defined by $v = 0$. Note that Eq. (5.53) gives also

$$\rho + p = \frac{\phi_c'^2}{a^2}. \quad (5.54)$$

Equations of motion. The following two equations are components of the perturbed Einstein equation obtained from Eqs. (2.75) and (2.76). The contributions from the energy momentum tensor on the right hand sides stem from the corresponding expressions in Eqs. (5.50) and (5.51):

$$\Delta \Phi - 3 \frac{a'}{a} \Phi' - 3 \frac{a'^2}{a^2} \Phi = \frac{4\pi}{m_{\text{Pl}}^2} \left\{ -\phi_c'^2 \Phi + \phi_c' \varphi' - \left(\phi_c'' + 2 \frac{a'}{a} \phi_c' \right) \varphi \right\}, \quad (5.55)$$

$$\Phi' + \frac{a'}{a} \Phi = \frac{4\pi}{m_{\text{Pl}}^2} \phi_c' \varphi. \quad (5.56)$$

These equations are now transformed into the wave equation (5.63): Using the Friedmann equations (2.42) and (2.43) one rewrites the term proportional Φ in Eq. (5.55) with the result

$$\Delta \Phi - 3 \frac{a'}{a} \Phi' - \left(\frac{a''}{a} + \frac{a'^2}{a^2} \right) \Phi = \frac{4\pi}{m_{\text{Pl}}^2} \left\{ \phi_c' \varphi' - \left(\phi_c'' + 2 \frac{a'}{a} \phi_c' \right) \varphi \right\}. \quad (5.57)$$

This can be simplified by replacing the second Φ on the left by the corresponding expression obtained from (5.56). Then one arrives at the more convenient equation

$$\Delta \Phi = \frac{4\pi}{m_{\text{Pl}}^2} \frac{a}{a'} \phi_c'^2 \frac{d}{d\eta} \left(\Phi + \frac{a' \varphi}{a \phi_c'} \right). \quad (5.58)$$

With the additional definitions

$$u = \varphi a + \Phi \frac{\phi_c' a^2}{a'} \quad (5.59)$$

5.4. Inflation and the origin of fluctuations

and

$$z = \frac{\phi'_c a^2}{a'} \quad (5.60)$$

it is further abbreviated to

$$\Delta\Phi = \frac{4\pi}{m_{\text{Pl}}^2} \phi'_c \frac{z}{a} \frac{d}{d\eta} \left(\frac{u}{z} \right). \quad (5.61)$$

Using the definition (5.59) in Eq. (5.56) yields

$$\frac{a'}{a^2} \frac{d}{d\eta} \left(\frac{a^3}{a'} \Phi \right) = \frac{4\pi}{m_{\text{Pl}}^2} \phi'_c u. \quad (5.62)$$

From the system (5.61) and (5.62) all variables but u and z can be eliminated: After sorting the derivatives one arrives at a wave equation for $u(\mathbf{x}, \eta)$,

$$u'' - \frac{z''}{z} u - \Delta u = 0. \quad (5.63)$$

This equation governs the behavior of the scalar field and of the metric. The oscillation of fluctuations stops in the superhorizon regime because then the spatial derivative of u is negligible in the last equation. In this regime there is a decaying and a growing solution. The former is not important for cosmology and the latter is

$$u(\mathbf{x}, \eta) \propto z, \quad (5.64)$$

which will be referred to later. During slow roll (5.63) is simplified to

$$u'' - \frac{a''}{a} u - \Delta u = 0 \quad (5.65)$$

with

$$a = -\frac{1}{\eta H} \quad (5.66)$$

because then H and $\dot{\phi}_c$ vary only slowly with time and so

$$z = \frac{\phi'_c a^2}{a'} = \frac{\dot{\phi}_c}{H} a \propto a. \quad (5.67)$$

Spatial curvature outside the Hubble horizon. Up to now the behavior of small scalar fluctuations during inflation has been studied. The following concentrates on the resulting spectrum of fluctuations of \mathcal{R} . From Eq. (2.100) it is

$$\mathcal{R} = \frac{a'}{a} v - \Phi. \quad (5.68)$$

Taking the velocity potential v from Eq. (5.53) and remembering the definitions of u , (5.59), and z , (5.60), the curvature \mathcal{R} is seen to be proportional to u ,

$$\mathcal{R}(\mathbf{x}, \eta) = -\frac{u(\mathbf{x}, \eta)}{z(\eta)}, \quad (5.69)$$

where the dependence on the spacetime coordinates has been restored. With Eq. (5.64) it is now seen that for modes larger than the Hubble horizon the curvature \mathcal{R} stays constant in time.

For slow-roll inflation the following simplifications can be made: When definition (5.59) is written for cosmic time t ,

$$u = \left(\varphi + \Phi \frac{\dot{\phi}_c}{H} \right) a, \quad (5.70)$$

the metric perturbation is seen to be negligible because $\dot{\phi}_c \ll H$. Then the curvature is

$$\mathcal{R} = -\frac{\varphi a}{z} = -\frac{H\varphi}{\dot{\phi}_c} \quad (5.71)$$

where the last equality makes use of Eq. (5.67).

Scalar field perturbations on unperturbed background. Equation (5.71) relates the curvature perturbations to field fluctuations φ . These are created by the spacetime curvature arising from accelerated expansion. They are calculated without considering inhomogeneities of the metric. The derivation is presented in the following: The action S of a scalar field within a curved background is given in Eq. (3.1). The action of a small perturbation φ , defined by

$$\phi(\mathbf{x}, \eta) = \phi_c(\eta) + \varphi(\mathbf{x}, \eta), \quad (5.72)$$

then reads

$$S_\varphi = \frac{1}{2} \int d^4x \sqrt{-g} (g^{\mu\nu} \partial_\mu \varphi \partial_\nu \varphi - V''(\phi_c) \varphi^2), \quad (5.73)$$

where the prime indicates a derivative with respect to the classical field ϕ_c . The action is taken to second order in φ because the aim is a linear equation of motion. For subhorizon modes during slow roll the second term is small as is shown by

$$V'' \approx \frac{8\pi}{m_{\text{Pl}}^2} V \eta \approx 3H^2 \eta \ll H^2 \ll \left(\frac{k}{a} \right)^2, \quad (5.74)$$

where η is the slow-roll parameter. The following equations will use η as letter for conformal time again. The dominant part of the action is conveniently written using this coordinate:

$$S_\varphi = \frac{1}{2} \int d^4x a^2(\eta) ((\partial_\eta \varphi)^2 - (\partial_i \varphi)^2). \quad (5.75)$$

The equation of motion is noted for later reference:

$$\varphi'' + 2\frac{a'}{a}\varphi' - \Delta\varphi = 0. \quad (5.76)$$

The expansion of the universe is better accounted for when the field

$$\chi(\mathbf{x}, \eta) = a(\eta)\varphi(\mathbf{x}, \eta) \quad (5.77)$$

5.4. Inflation and the origin of fluctuations

is taken as variable. The corresponding replacement in Eq. (5.75) is done in

$$S_\chi = \frac{1}{2} \int d^4x \left(\chi'^2 + \chi^2 \frac{a'^2}{a^2} - (\chi^2)' \frac{a'}{a} - (\partial_i \chi)^2 \right) \quad (5.78)$$

$$= \frac{1}{2} \int d^4x \left(\chi'^2 + \chi^2 \frac{a''}{a} - (\partial_i \chi)^2 \right), \quad (5.79)$$

where partial integration of the third term leads to the second line. Variation with respect to χ gives

$$\chi_k'' - \frac{a''}{a} \chi_k + k^2 \chi_k = 0 \quad (5.80)$$

for a mode χ_k . From Eq. (5.66) the second term in this equation is seen to be small for large negative η , i.e. at early times. So it is concluded that the action and the equation of motion are those of a massless, non-interacting field in flat spacetime. The regime described above coincides with the sub-horizon condition $k > 1/aH$ for a mode of momentum k . The corresponding field operator is written as

$$\chi(\mathbf{x}, \eta) = \int \frac{d^3k}{(2\pi)^{3/2} \sqrt{2k}} \left(e^{ik\eta - i\mathbf{k}\mathbf{x}} A_{\mathbf{k}}^\dagger + e^{-ik\eta + i\mathbf{k}\mathbf{x}} A_{\mathbf{k}} \right). \quad (5.81)$$

Inside the horizon the modes of χ oscillate freely. This means that the oscillation of the physical field φ encounters a damping proportional to $1/a$. Later the second term in Eq. (5.80) becomes more important until the third one can be neglected. Apart from a possible decaying contribution, the solution of χ_k is then proportional to a . So we are left with constant modes φ_k outside the horizon.

In order to calculate the constant result outside the horizon, it has to be matched with the oscillating solution inside the horizon. For this purpose the solution around horizon crossing has to be obtained: The equation of motion Eq. (5.80) can be simplified under the assumption $a = -1/\eta H$. This is a good approximation also if the accelerated expansion is not exactly exponential because the time span in question is not much larger than a Hubble time. Thus, Eq. (5.80) is written as

$$\chi_k'' - \frac{2}{\eta^2} \chi_k + k^2 \chi_k = 0 \quad (5.82)$$

being solved by

$$\chi_k^\pm = \frac{1}{\sqrt{2k}} e^{\pm ik\eta} \left(1 \pm \frac{i}{k\eta} \right). \quad (5.83)$$

Here the upper (lower) signs refer to a solution with positive (negative) frequency. Well inside the horizon the solutions correspond to a non-interacting field because then the second term in brackets is small. So the field operator χ_k evolves from the non-interacting oscillatory form to a growing one. The mode function of the inflaton operator is then

$$\varphi_k^\pm = -\frac{1}{\sqrt{2k}} e^{\pm ik\eta} H \left(\eta \pm \frac{i}{k} \right). \quad (5.84)$$

Late times correspond to η approaching zero from below. According to Eq. (5.84) the oscillation stops in this case and a constant solution develops. With some time-independent phase shift α_k the field operator then reads

$$\varphi(\mathbf{x}, \eta) = \int \frac{d^3k}{(2\pi)^{3/2}\sqrt{2k}} \frac{H}{k} \left(e^{-i\mathbf{k}\mathbf{x} + i\alpha_k} A_{\mathbf{k}}^\dagger + e^{i\mathbf{k}\mathbf{x} - i\alpha_k} A_{\mathbf{k}} \right). \quad (5.85)$$

The last equation is only valid for modes that have left the horizon.

The final goal of this section is to arrive at the formula for the power spectrum $\mathcal{P}_{\mathcal{R}}(k)$ of \mathcal{R} after inflation. The connection between \mathcal{R} and φ has been obtained in Eq. (5.71). So the next step is the power spectrum of scalar field fluctuations φ_k after inflation. The power spectrum of a field φ quantifies the strength of its fluctuations, as will be seen in the following: First it is assumed that they are Gaussian random fluctuations, such that they are fully characterized by their two-point correlation function. This statement is also valid the Fourier transformed quantities. The calculation is done for homogeneous and isotropic space. From the two-point function in real space, $\langle \varphi(\mathbf{x})\varphi(\mathbf{y}) \rangle$, the two-point function in Fourier space is obtained as

$$\langle \varphi(\mathbf{k})\varphi(\mathbf{k}') \rangle = \int \frac{d^3x d^3y}{(2\pi)^6} e^{-i\mathbf{k}\mathbf{x} - \mathbf{k}'\mathbf{y}} \langle \varphi(\mathbf{x})\varphi(\mathbf{y}) \rangle \quad (5.86)$$

$$= \int \frac{d^3z d^3y}{(2\pi)^6} e^{-i(\mathbf{k} + \mathbf{k}')\mathbf{y}} e^{-i\mathbf{z}\mathbf{k}} \langle \varphi(\mathbf{x})\varphi(\mathbf{y}) \rangle \quad (5.87)$$

$$= \frac{P_\varphi(\mathbf{k})}{(2\pi)^3} \delta(\mathbf{k}, \mathbf{k}'), \quad (5.88)$$

where for the second line the variable $\mathbf{z} = \mathbf{x} - \mathbf{y}$ is introduced. The function $P_\varphi(\mathbf{k})$ in the third line is defined as correlation function in Fourier space. In the homogeneous and isotropic case, the correlator can be written as a function of $|\mathbf{z}| = |\mathbf{x} - \mathbf{y}|$: $D(|\mathbf{z}|) = \langle \varphi(\mathbf{x})\varphi(\mathbf{y}) \rangle$. Then the Fourier transformation is

$$P_\varphi(k) = \int d^3z e^{-i\mathbf{z}\mathbf{k}} D(|\mathbf{z}|), \quad (5.89)$$

which has been used in Eq. (5.88). Later on, an alternative definition of the power spectrum will be used,

$$\mathcal{P}(k) = \frac{k^3}{2\pi^2} P(k). \quad (5.90)$$

In either case, the fluctuations are quantified as

$$\langle \varphi^2(\mathbf{x}) \rangle = \int d^3k d^3k' e^{i(\mathbf{k} + \mathbf{k}')\mathbf{x}} \langle \varphi(\mathbf{k})\varphi(\mathbf{k}') \rangle \quad (5.91)$$

$$= \int d^3k \frac{P_\varphi(k)}{(2\pi)^3} = \int \frac{dk}{k} \mathcal{P}_\varphi(k). \quad (5.92)$$

It can be calculated using Eq. (5.85) and the commutation relation

$$[A_{\mathbf{k}}, A_{\mathbf{k}'}^\dagger] = \delta(\mathbf{k} - \mathbf{k}'). \quad (5.93)$$

5.4. Inflation and the origin of fluctuations

As a result the power spectrum of scalar field fluctuations after horizon exit in slow-roll inflation is obtained:

$$\mathcal{P}_\varphi = \left(\frac{H_k}{2\pi} \right)^2. \quad (5.94)$$

H_k denotes the Hubble parameter during horizon exit of the mode k :

$$H_k = \frac{a}{k}. \quad (5.95)$$

Curvature power spectrum. Equation (5.94) and the connection to spatial curvature in Eq. (5.71) result in the formula for the curvature on equal-time hypersurfaces within the comoving reference frame:

$$\mathcal{P}_{\mathcal{R}}(k) = \left(\frac{H^2}{2\pi\dot{\phi}_c} \right)_{t_k}^2 \quad (5.96)$$

As indicated by t_k the Hubble parameter and the velocity of the classical field are evaluated at horizon crossing. The spectrum is also characterized by the square root of the power spectrum,

$$\Delta_{\mathcal{R}}(k) = \sqrt{\mathcal{P}_{\mathcal{R}}(k)} = \left(\frac{H^2}{2\pi|\dot{\phi}_c|} \right)_{t_k}, \quad (5.97)$$

which is a direct measure for the amplitude of the fluctuations.

5.4.2. Tensor perturbations

In this section the production of gravitational waves during inflation is examined. From comparison of the action of a scalar field (5.75) to the action of tensor perturbations (2.88) it is seen that the fluctuations behave identically when the factor $m_{\text{Pl}}^2/32\pi$ is taken into account: The action of one degree of freedom of GWs, $h^{(A)} = h^{(+)}$ or $h^{(\times)}$, is equal to the action for φ times this factor. A redefinition

$$\tilde{h}^{(A)} = \frac{m_{\text{Pl}}}{\sqrt{32\pi}} h^{(A)} \quad (5.98)$$

allows for a literal repetition of the scalar field case. Then the power spectrum for each $\tilde{h}^{(A)}$ is given by Eq. (5.94). Restoring the factor in Eq. (5.98) and summing over both polarizations gives the power spectrum of gravitational waves outside the horizon:

$$\mathcal{P}_T(k) = \frac{16}{\pi} \frac{H_k^2}{m_{\text{Pl}}^2}. \quad (5.99)$$

5.4.3. The spectra of fluctuations after slow-roll inflation

This section contains a discussion of the spectra of scalar and tensor metric fluctuations after slow-roll inflation. The link between properties of the inflaton potential and of the resulting spectra is established. The equations derived in this section are valid for both large-field and small-field potentials. Specific examples are worked out in Section 5.5.

Chapter 5. Inflation

Using Eqs. (5.10) and (5.97) the amplitude of scalar perturbations is seen to be

$$\Delta_{\mathcal{R}}(k) = \frac{3H_k^3}{2\pi V'} = 4\sqrt{\frac{8\pi}{3}} \frac{V^{3/2}}{m_{\text{Pl}}^3 V'}, \quad (5.100)$$

where in the last step the potential is evaluated at the time of horizon exit of the mode k . The tensor power spectrum is connected to the potential by

$$\mathcal{P}_T = \frac{128}{3} \frac{V}{m_{\text{Pl}}^4}, \quad (5.101)$$

see Eq. (5.99). With Eqs. (5.100) and (5.101) the scalar-to-tensor ratio r in the slow-roll regime can be calculated as

$$r = \frac{\mathcal{P}_T}{\mathcal{P}_{\mathcal{R}}} = \frac{m_{\text{Pl}}^2}{\pi} \left(\frac{V'}{V} \right)^2, \quad (5.102)$$

where also Eqs. (5.10) and (5.11) have been used. The spectral scalar and tensor indices are defined as

$$n_s = \frac{d \ln \mathcal{P}_{\mathcal{R}}(k)}{d \ln k} + 1 \quad \text{and} \quad n_T = \frac{d \ln \mathcal{P}_T(k)}{d \ln k}. \quad (5.103)$$

If they are constant, this is equivalent to

$$\mathcal{P}_{\mathcal{R}}(k) \propto k^{n_s-1} \quad \text{and} \quad \mathcal{P}_T(k) \propto k^{n_T}. \quad (5.104)$$

Both spectral indices are connected to the parameters defined so far: It is

$$n_s - 1 = 2\eta - 6\epsilon \quad (5.105)$$

and

$$n_T = -\frac{r}{8}. \quad (5.106)$$

To derive these equations the power spectra are expanded around arbitrary k_0 in the following way:

$$\mathcal{P}_{\mathcal{R}}(k) = \mathcal{P}_{\mathcal{R}}(k_0) \left\{ 1 + \frac{d \ln \mathcal{P}_{\mathcal{R}}}{d\phi} (\phi(t_k) - \phi(t_{k_0})) \right\} \quad (5.107)$$

$$= \mathcal{P}_{\mathcal{R}}(k_0) \left\{ 1 + \left(3\frac{V'}{V} - 2\frac{V''}{V'} \right) (\phi(t_k) - \phi(t_{k_0})) \right\} \quad (5.108)$$

and

$$\mathcal{P}_T(k) = \mathcal{P}_T(k_0) \left\{ 1 + \frac{d \ln \mathcal{P}_T}{d\phi} (\phi(t_k) - \phi(t_{k_0})) \right\} \quad (5.109)$$

$$= \mathcal{P}_T(k_0) \left\{ 1 + \frac{V'}{V} (\phi(t_k) - \phi(t_{k_0})) \right\}. \quad (5.110)$$

Both results depend on field values fixed by the horizon exit of the arbitrary modes k and k_0 . The slow-roll approximation allows for a formula connecting k with $\phi(t_k)$: First remember Eq. (5.16) and use it in the Taylor expansion

$$N_e(\phi(t_k)) - N_e(\phi(t_{k_0})) = \frac{dN_e}{d\phi}(\phi(t_k) - \phi(t_{k_0})) \quad (5.111)$$

$$= \frac{8\pi}{m_{\text{Pl}}^2} \frac{V}{V'}(\phi(t_k) - \phi(t_{k_0})) \quad (5.112)$$

to obtain the second line. Then it is observed that the left hand side of Eq. (5.111) can also be written in terms of the wavenumbers in question:

$$N_e(\phi(t_k)) - N_e(\phi(t_{k_0})) = \ln\left(\frac{k_0}{k}\right). \quad (5.113)$$

The combination of both results,

$$\phi(t_k) - \phi(t_{k_0}) = \frac{m_{\text{Pl}}^2}{8\pi} \frac{V'}{V} \ln\left(\frac{k_0}{k}\right), \quad (5.114)$$

is now used in the expansions of the power spectra above. The resulting combinations of the potential and its derivative match the slow-roll parameters defined in Eq. (5.14). More precisely, it is

$$\mathcal{P}_{\mathcal{R}}(k) = \mathcal{P}_{\mathcal{R}}(k_0) \left\{ 1 + (2\eta - \epsilon) \ln \frac{k}{k_0} \right\} \quad (5.115)$$

and

$$\mathcal{P}_T(k) = \mathcal{P}_T(k_0) \left\{ 1 - 2\epsilon \ln \frac{k}{k_0} \right\}. \quad (5.116)$$

Equations (5.105) and (5.106) follow from comparison with the definitions in (5.103). Only relying on slow roll, Eq. (5.106) connects the two observables r and n_T . This offers a verification of inflation that is independent of specific models. However, measurements of n_T are not possible in the foreseeable future.

5.5. Examples and observations

Let us now turn to the behavior of the homogeneous field and the fluctuations in specific examples of slow-roll inflation. The large-field models discussed here have a potential of the form

$$V(\phi) = \frac{1}{n} g \phi^n. \quad (5.117)$$

The time evolution of a free massive scalar field rolling down from a large value is displayed in Fig. 5.5. The two slow-roll parameters ϵ and η (defined in Eq. (5.15)) are equal for $V = m^2 \phi^2/2$ and well below one down to $\phi = 1m_{\text{Pl}}$. Assuming Eqs. (5.10) and (5.11) to be valid in this regime, a constant velocity of the field is expected. This is displayed in Fig. 5.5, as well as the corresponding decay of the Hubble parameter H

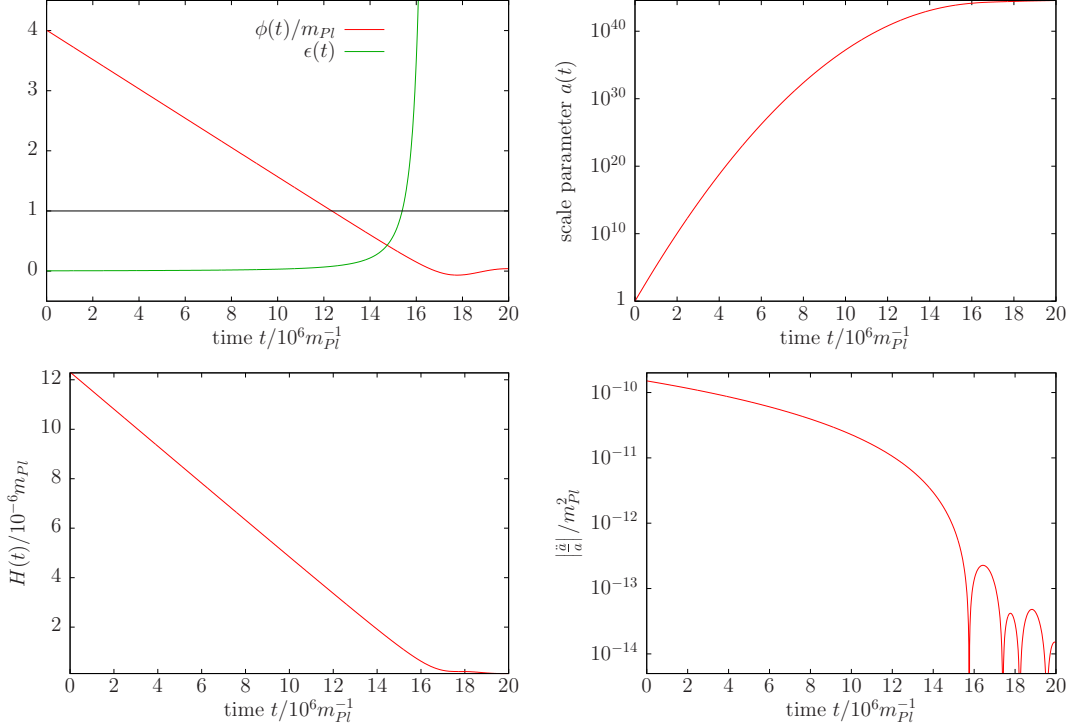


Figure 5.5.: Time evolution of the scalar field ϕ , the slow-roll parameter ϵ , and of the scale parameter and its derivatives during inflation within the potential $V = m^2\phi^2/2$, $m = 1.5 \cdot 10^{-6}$. Hubble damping leads to a linear decrease of $\phi(t)$ and of the Hubble parameter $H(t)$. Accelerating expansion ends when the slow-roll parameter ϵ becomes bigger than one (top left and bottom right panels).

(left panels). The latter is linear too, because the kinetic term in Eq. (3.5) is negligible. The right panels illustrate the strong, almost exponential growth of the scale parameter $a(t)$ and its acceleration, which ends shortly after ϵ and η acquire values greater than one.

The evolution of these quantities in $\lambda\phi^4/4$ is similar and is therefore not displayed here. Let us instead go on to the fluctuations within the scalar field, which are produced at the horizon exit of each mode. In order to compare theoretical predictions with observation, it is necessary to connect the length scales during inflation with corresponding ones today. The calculations in this thesis will be compared with WMAP and Planck data obtained for modes with wavenumber $q_0 = 0.002 \text{ Mpc}^{-1}$ today. For example, this will be done for the power spectrum $\mathcal{P}_{\mathcal{R}}$ and its spectral index n_s .

During inflation a comoving length scale $\lambda = 2\pi/k$ can be identified by the number of e-foldings N_e that follow after its horizon crossing but before the end of inflation. This is defined by

$$\exp(N_e(k)) = \frac{a_{\text{end}}}{a(t_k)}. \quad (5.118)$$

5.5. Examples and observations

Here and in the following the label “end” is used for quantities evaluated at the end of inflation. $a(t_k)$ is the scale parameter at the time when a wave with comoving wavenumber k crosses the Hubble horizon: The time t_k is fixed by

$$k = H(t_k)a(t_k). \quad (5.119)$$

So for a present-day wavenumber $q_0 = k/a_0$, the exponent in Eq. (5.118) can be calculated as (see the following text for explanations or Ref. [59]):

$$N_e(k) = \ln \left(\frac{a_{\text{end}} H(t_k)}{k} \right) = \ln \left(\frac{a_{\text{end}} a_{\text{reh}} H(t_k)}{a_{\text{reh}} a_0 q_0} \right) \quad (5.120)$$

$$\approx \ln \left(\frac{\rho_{\text{reh}}^{1/\beta} T_0 H(t_k)}{\rho_{\text{end}}^{1/\beta} T_{\text{reh}} q_0} \right) \quad (5.121)$$

$$\approx \ln \left(\frac{T_0 T_{\text{reh}}^{4/\beta-1} H_{\text{end}}^{1-2/\beta} H(t_k)}{q_0 m_{\text{Pl}}^{2/\beta} H_{\text{end}}} \right), \quad (5.122)$$

where the following considerations are used: For the second line the energy density during the reheating epoch is assumed to decay like $a^{-\beta}$ (with, for example, $\beta = 4$ for radiation and $\beta = 3$ for matter) with a constant β . The ensuing radiation dominated era is taken to last until today without changes of the degrees of freedom: So the present scale factor is written as

$$a_0 = a_{\text{reh}} \frac{T_{\text{reh}}}{T_0}. \quad (5.123)$$

The third line uses the simplifications $\rho_{\text{reh}} \approx T_{\text{reh}}^4$ and $\rho_{\text{end}} \approx H_{\text{end}}^2 m_{\text{Pl}}^2$. The final form is obtained after approximating $H_{\text{end}} \approx T_{\text{end}}^2/m_{\text{Pl}}$ (where T_{end} is the temperature that would result after instantaneous reheating) and splitting the logarithm:

$$N_e(k) \approx \ln \frac{T_0}{q_0} - \left(\frac{4}{\beta} - 1 \right) \ln \frac{T_{\text{end}}}{T_{\text{reh}}} - \frac{1}{2} \ln \frac{m_{\text{Pl}}}{H_{\text{end}}} + \ln \frac{H(t_k)}{H_{\text{end}}}. \quad (5.124)$$

The largest contribution to $N_e(k)$ comes from the first term: $\ln(T_0/q_0) \approx 65$ for $T_0 = 2.7\text{K}$ and $q_0 = 0.002 \text{Mpc}^{-1}$. The subsequent terms are smaller and model dependent: The second term is determined by the mechanisms of preheating and reheating after inflation: The prefactor lies between 0 and 1/3; the temperature T_{end} in the logarithm can be estimated as

$$T_{\text{end}} \approx \sqrt{H_{\text{end}} m_{\text{Pl}}} \approx \begin{cases} \sqrt{m\phi_{\text{end}}} \approx 10^{-3} m_{\text{Pl}} & \text{for } V = m^2 \phi^2/2 \\ \lambda^{1/4} \phi \approx 10^{-3} m_{\text{Pl}} & \text{for } V = \lambda \phi^4/4 \\ (\lambda v^4/16)^{1/4} \approx 10^{-4} v & \text{for small-field inflation, Eq. (5.26).} \end{cases} \quad (5.125)$$

The range of $N_e(k)$ is now computed with $T_{\text{reh}} \in (10^8 \text{GeV}, T_{\text{end}})$ and, for the case of small-field inflation, with $v \in (10^{-3}, 10) m_{\text{Pl}}$. The last term in Eq. (5.26) is neglected. So for each inflationary scenario, any q_0 today is to be connected with this range in $N_e(k)$, stemming from our ignorance about the history of the universe after inflation. For the

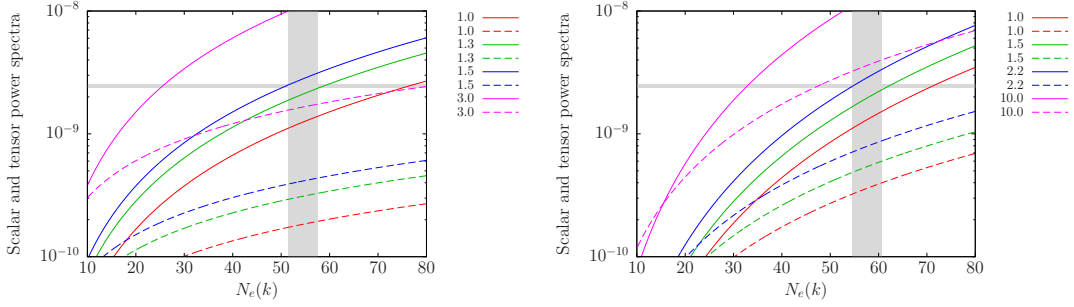


Figure 5.6.: Scalar (solid lines) and tensor (dashed lines) power spectra after inflation within the potentials $m^2\phi^2/2$ (left panel) and $\lambda\phi^4/4$ (right panel). The couplings m and λ are given in units of $10^{-6}m_{\text{Pl}}$ and 10^{-13} , respectively. The grey vertical band between $N_e = 50$ and 60 corresponds to the wavenumber $q_0 = 0.002 \text{ Mpc}^{-1}$ today. The horizontal band indicates the measurements of WMAP [71] in this region, which fix the couplings to $m^2 \approx (1.4 \pm 0.1) \cdot 10^{-6}m_{\text{Pl}}$ for the quadratic potential and to $\lambda \approx (1.8 \pm 0.4) \cdot 10^{-13}$ in the ϕ^4 case.

choice of parameters in the potentials this leaves a greater freedom that is illustrated by the grey vertical band in the figures to follow. Some effort has been made to match the borders of this band to the potential and its parameters but the uncertainty of these values should be kept in mind.

In Fig. 5.6 the scalar and tensor power spectra are shown for the quadratic and the quartic inflaton potentials with various values of the couplings. The reasoning and the calculations are based on Ref. [59]: The function $N_e(\phi)$ is special to each model but in the present cases it is independent of the coupling. This can be read from the result of the calculation (5.16). For $V = g_n\phi^n/n$ one gets

$$N_e(\phi_0) = \frac{4\pi}{n} \frac{\phi_0^2}{m_{\text{Pl}}^2}. \quad (5.126)$$

Then the sole dependence of the tensor power spectrum on ϕ in Eq. (5.101) explains, why for different couplings the dashed lines in Fig. 5.6 are simply shifted in the y-direction. As already discussed, the mode with wavenumber $q_0 = 0.002 \text{ Mpc}^{-1}$, for which the WMAP measurements obtained the value

$$\mathcal{P}_{\mathcal{R}}(k) = \Delta_{\mathcal{R}}^2(k) = (2.46 \pm 0.09) \cdot 10^{-9} \quad (5.127)$$

can correspond to a range of values of $N_e(k)$ or $\phi(t_k)$. This results in the uncertainty in the couplings $m^2 \approx (1.4 \pm 0.1) \cdot 10^{-6}m_{\text{Pl}}$ and $\lambda \approx (1.8 \pm 0.4) \cdot 10^{-13}$, as suggested by the results displayed in Fig. 5.6. The dependence of the scalar power spectrum on the coupling constant is calculated from the square of Eq. (5.100). With

$$\frac{V^{3/2}}{V'} = \frac{\sqrt{g_n}}{n} \phi^{n/2+1} \quad (5.128)$$

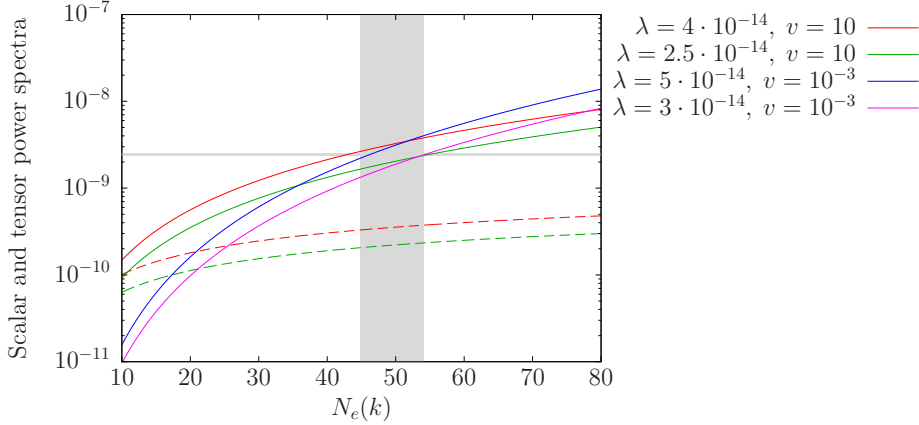


Figure 5.7.: Scalar (solid lines) and tensor (dashed lines) power spectra after inflation within the small-field model Eq. (5.26). For two values of v , which is given in units of the Planck mass, the allowed range for the coupling λ is found. The shaded regions again mark the part of the spectrum corresponding to $q_0 = 0.002 \text{ Mpc}^{-1}$ and the measurement of WMAP at this wavenumber [71].

and Eq. (5.126) the result is

$$\mathcal{P}_{\mathcal{R}}(k) = \frac{16}{n^2} \frac{8\pi}{3} \left(\frac{nN_e}{4\pi} \right)^{(n+2)/2} \frac{g_n}{m_{\text{Pl}}^{4-n}} \quad (5.129)$$

giving the order of magnitude of the estimations noted above.

Fig. 5.7 shows the scalar power spectra after inflation in this potential for several parameter sets. For a wide range of the energy scale v the coupling λ has to be of the order 10^{-14} . As in the cases above, the power spectrum decays with smaller N_e because this corresponds to later times leading to smaller amounts of energy in the potential and larger field velocities. For equal symmetry breaking scale v , a similar argument as the one after Eq. (5.16) predicts the simple proportionality between spectra with different coupling λ . This is verified by the two pairs of solid lines in Fig. 5.7. From Eq. (5.101) a very small tensor perturbation in the low- v case is expected. The result is many orders of magnitude below the range of this figure.

The tensor-to-scalar ratio calculated in Eq. (5.102),

$$r = \frac{m_{\text{Pl}}^2}{\pi} \left(\frac{V'}{V} \right)^2 = 16\epsilon, \quad (5.130)$$

is displayed in Fig. 5.8. As expected, when plotted against N_e or ϕ , it is independent of the coupling in the case of quartic and of quadratic potentials. The same is true for the hilltop potential if v is not varied. The analytic estimate for slow roll in $V = \lambda\phi^n/n$ is

$$r(N_e) = \frac{m_{\text{Pl}}^2}{\pi} \left(\frac{n}{\phi} \right)^2 = \frac{4n}{N_e}, \quad (5.131)$$

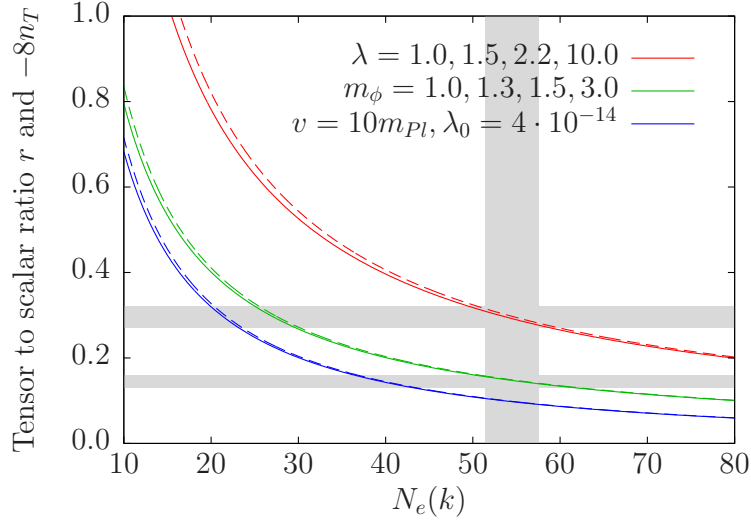


Figure 5.8.: Tensor-to-scalar ratio resulting from inflation within a quartic, a quadratic, and a hilltop potential illustrated by the red, green, and blue lines, respectively. Shaded horizontal regions correspond to the analytic estimation (5.132) based on the corresponding potential. The units of the couplings in the two former cases are chosen as in Fig. 5.6. The tensor spectral index n_T is plotted in the form $-8n_T$ in dashed lines. Within the slow-roll approximation this expression is predicted to be equal to r .

where Eq. (5.16) is used for the second equality. Inserting $N_e = 50 - 60$ gives

$$\begin{aligned} r &= 0.13 - 0.16, & n &= 2, \\ r &= 0.27 - 0.32, & n &= 4. \end{aligned} \quad (5.132)$$

This is not within the region allowed by Planck measurements [113] which give $r(q_0 = 0.002 \text{ Mpc}^{-1}) < 0.12$ at 95% confidence level. In contrast, the results for r in the hilltop model are compatible with this bound. The second quantity displayed in Fig. 5.8 is the tensor spectral index defined in Eq. (5.103). Assuming slow roll the proportionality

$$n_T = -\frac{r}{8} \quad (5.133)$$

has been shown in Eq. (5.106). In Fig. 5.8 the quantity $-8n_T$ is indicated in dashed lines. The agreement with the solid lines confirms the slow roll prediction for large enough N_e .

The scalar spectral index n_s as a function of N_e is displayed in Fig. 5.9. As with r and n_T , the function $n_s(N_e)$ does not change when the potential is multiplied by an overall factor. So for the simple quadratic and quartic potentials the outcome is independent of the coupling. The numerical result for $V = m^2\phi^2/2$ and $\lambda\phi^4/4$ closely follows the analytical formula Eq. (5.134)

$$n_s - 1 = -\frac{n+2}{2N_e} \quad (5.134)$$

which is derived from Eq. (5.105) ($n_s - 1 = 2\eta - 6\epsilon$) and using Eq. (5.16) for potentials of the form $V = \lambda\phi^n/n$. Inflation with a massive free scalar inflaton field yields results within the range allowed by Planck measurements and so does hilltop inflation with a large enough energy scale.

In the above discussion the example for a potential leading to hilltop inflation was (5.26). It has been argued that during slow roll the simplified form

$$V(\phi) = V_0 - \frac{\lambda}{16}\phi^4 \quad (5.135)$$

can be used. The coupling, for which the power spectrum (5.127) is obtained, is calculated as follows: Using Eq. (5.16) gives

$$N_e(\phi_0) = -\frac{32\pi}{m_{\text{Pl}}^2} \int_{\phi_f}^{\phi_0} \left(\frac{V_0}{\lambda\phi^3} - \frac{\phi}{16} \right) d\phi \quad (5.136)$$

The second term and the term proportional to ϕ_f^{-2} are neglected. Then one has

$$\phi^2 = \frac{16\pi V_0}{m_{\text{Pl}}^2} \frac{1}{\lambda N_e(\phi)}. \quad (5.137)$$

On the other hand, evaluating Eq. (5.100) for the present case leads to

$$\mathcal{P}_{\mathcal{R}} = \Delta_{\mathcal{R}}^2 = \frac{8\pi}{3} \left(\frac{16}{\lambda\phi^3 m_{\text{Pl}}^3} \right)^2 V_0^3. \quad (5.138)$$

So the formula connecting the fluctuations with the coupling is

$$\lambda = 6\pi^2 \frac{\mathcal{P}_{\mathcal{R}}}{N_e^3}. \quad (5.139)$$

Inserting the required value for the spectrum at $N_e = 60$ gives $\lambda \approx 7 \cdot 10^{-13}$. In accordance with the different prefactors in Eq. (5.117) and (5.135) this value is somewhat larger than the one found in Eq. (5.129). In hilltop and hybrid inflation the slow-roll parameter ϵ is generically very small, $\epsilon \ll |\eta| \ll 1$. Therefore, by virtue of Eq. (5.130), a small tensor-to-scalar ratio is expected.

In the hybrid inflation scenario Eq. (5.35) the inhomogeneities are produced during slow roll of ϕ within the potential

$$U(\phi) = V_0 + \frac{1}{2}m^2\phi^2. \quad (5.140)$$

A significant difference to inflation driven by a free massive field requires the offset V_0 to be the dominant contribution. Approximating $\phi \approx \phi_c$ at $N_e = 60$ and using the slow-roll parameter

$$\eta = \frac{m_{\text{Pl}}^2 m^2}{8\pi V_0} \quad (5.141)$$

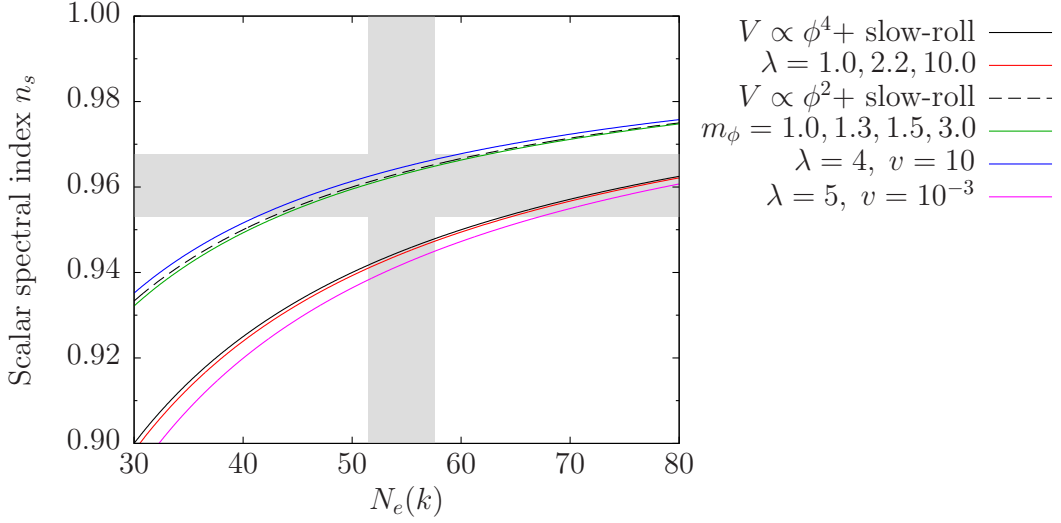


Figure 5.9.: The scalar spectral index n_s as a function of N_e . The black lines illustrate the slow-roll formula Eq. (5.134) for the quartic (solid line) and quadratic (dashed line) potentials. The numerical results in the large-field models only slightly deviate from the corresponding part of Eq. (5.134) and coincide for different values of the couplings, which are given in units of 10^{-14} (λ) and $10^{-6}m_{\text{Pl}}$ (m_ϕ). The units within the small-field examples (blue and magenta) are 10^{-14} (λ) and m_{Pl} (v).

gives

$$\frac{V^{3/2}}{V'} \approx \frac{V_0^{3/2}}{m^2\phi} \quad (5.142)$$

and, with Eq. (5.100),

$$\mathcal{P}_{\mathcal{R}} = \frac{m^2}{12\pi^2\phi_c^2\eta^3}. \quad (5.143)$$

Within this model the appropriate coupling m depends on the critical field and η . The former is expected to be below the Planck scale and the latter should be much smaller than one. Therefore also for this potential measurements require $m \sim 10^{-6}$ or smaller. A similar model will be discussed in greater detail in Chapter 6.

To assess the viability of an inflationary potential it is convenient to plot the resulting tensor-to-scalar ratios r and scalar spectral indices n_s for the values of N_e that are accessible to measurements. This is done for several models in Figs. 6.10, 6.11, and 6.12.

5.6. A universe without inflation?

Of course, neither is inflation a scenario without conceptual problems nor is it the only theory trying to solve the open questions which are posed by hot Big Bang cosmology. In this Section some alternative scenarios are mentioned. The presentation relies on Ref. [24, 26].

Inflation renders the initial conditions of cosmological evolution more plausible. The strong requirements arising from the spatial flatness and the homogeneity of the universe can be reduced to the less restrictive necessary conditions for a successful inflationary stage.

However, the latter makes its claims too. For inflation driven by scalar fields the initial cosmological medium needs to be dominated by flat potentials. The initial condition for the fields must allow for the necessary amount of accelerated inflation. In addition, the field content of the inflationary system must be appropriately coupled to the fields of the known subsequent evolution, see Chapter 7.

Then it has been shown that for scalar field inflation there is still the unsolved problem of the initial singularity [23]. Inflation relies on the vast dilatation of very small scales. Since physics at scales smaller than the Planck length l_{Pl} is not known, it is not clear if the predictions for cosmological scales can be trusted. Reference [75] presents conditions under which this is the case, while Ref. [96] shows deviating results when the assumptions about high energy physics are varied. This is called the trans-Planckian problem of inflation. It can be concluded that it is reasonable to look for alternative scenarios and to check how promising they are.

One such a scenario is called the matter bounce where the initial singularity is removed and time extends to the infinite past [25, 81]. The observable universe is causally connected because the Big Bang scenario is assumed to be preceded by a period of contraction that is symmetric to later expansion. The trans-Planckian problem does not arise if the bounce is slowed down before the energy density penetrates the realm of unknown physics. Matter domination during the contraction leads to a scale-invariant spectrum [112]. On the other hand one should mention as a severe drawback that the flatness problem is not solved in this scenario. Another problem is that during the bounce strongly growing anisotropy may spoil a smooth transition to the expanding phase. A non-singular bounce within General Relativity is only possible when fields with exotic properties are introduced [14].

For example this is done in the scenario of the ekpyrotic⁹ universe [31, 78], which solves the horizon and flatness problems and can provide a slightly tilted spectrum. The scenario of a bouncing universe can be extended to a cyclic history of cosmic crunches and bangs [122].

A spectrum of scalar perturbations can also be produced during a period of constant scale-factor. This scenario is called the “emergent universe” [46, 47]. It solves the horizon problem and can provide a flat spectrum of perturbations. An important difference to standard inflation is that the emergent universe avoids the initial singularity. A possible realization is string gas cosmology [105].

Many scenarios and theories were proposed as an alternative to cosmological inflation. However, it seems that in spite of the open questions of inflation, up to now there is no strong competitor to the elegance of inflationary theory.

⁹The greek word ἐκπύρωσις (ekpyrosis) has been used by ancient philosophers and denotes the cyclic destruction of the world by fire.

6. Fluctuations after two periods of inflation

6.1. The potential and its simplification

In this section the results of calculations within the potential

$$V(\phi) = V_0 + \frac{1}{4}\lambda_0\chi^4 \left(\ln \left| \frac{\chi}{v} \right| - \frac{1}{4} \right) + \frac{1}{4}\lambda_1\phi^4 - \frac{1}{4}\lambda_2\chi^2\phi^2 \quad (6.1)$$

with

$$V_0 = \frac{1}{16}\lambda_0v^4 \exp(\lambda_2^2/\lambda_0\lambda_1) \quad (6.2)$$

are presented. The potential Eq. (6.1) is displayed in Fig. 6.1 along with a possible path $(\chi(t), \phi(t))$ during and after inflation. The color code reflects the value of the potential $V(\chi, \phi)$ in units of V_0 . The constants are chosen as $\lambda_0 = \lambda_1 = \lambda_2 = 10^{-14}$ and $v = 0.1m_{\text{Pl}}$ and the calculation of the path is done without consideration of field inhomogeneities. The starting point of the fields is at large ϕ and small positive χ with zero initial field velocities. Then $\phi(t)$ starts to evolve down the quartic potential while the value of χ is still close to zero, i.e. much smaller than the symmetry breaking scale v . During this period of time the evolution can be described as large field inflation with an offset V_0 in the potential. After one and a half oscillations the field ϕ stays close to zero due to Hubble damping. Now the main evolution in field space is a slow roll along the χ direction. Accordingly, this period of time can be characterized as a small-field hilltop inflation. Between these two inflationary stages the universe undergoes a short phase of decelerated expansion.

This model is related to the standard potential for hybrid inflation discussed in Section 5.3.4. One difference is that in the potential Eq. (6.1) there is no channel the field χ could be confined to during the first inflationary period. In order not to terminate inflation too early, the initial values of χ and $\dot{\chi}$ therefore have to be very close to zero, as mentioned above. Then the field χ does not act as a waterfall field that rapidly rolls down to the minimum of the potential after a critical value of ϕ has been passed. Instead, it could lead to the second period of inflation mentioned in the last paragraph.

This second inflation is due to the symmetry breaking logarithmic term in the potential. If $\lambda_2 \neq 0$, there is a second symmetry breaking term in the potential Eq. (6.1). Because it can considerably enlarge the offset V_0 in Eq. (6.2), the inflationary range in

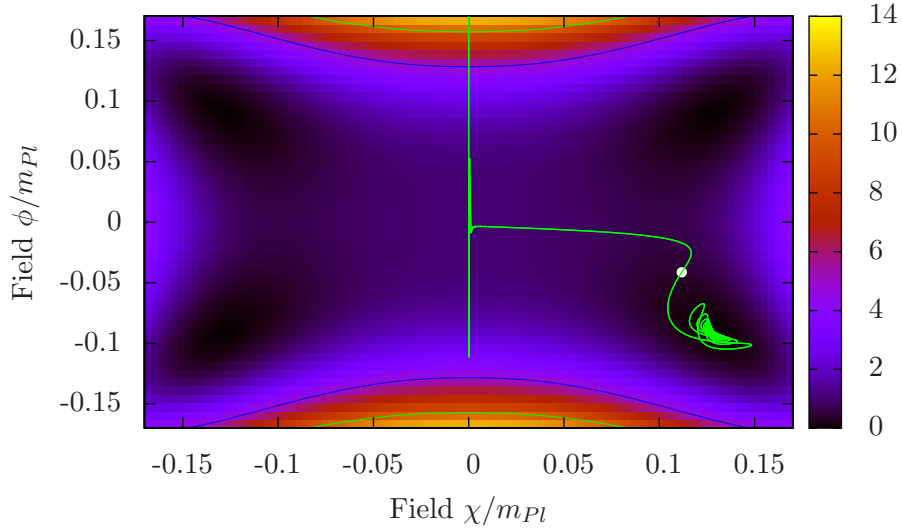


Figure 6.1.: Possible way of the fields ϕ and χ through the potential Eq. (6.1). In this case the energy scale and the couplings are chosen as $v = 0.1m_{Pl}$, $\lambda_0 = \lambda_1 = \lambda_2 = 10^{-12}$. The white dot marks the end of accelerated expansion. The color of the background encodes the value of the potential, $V(\phi, \chi)/V_0$.

field space is extended to $\chi \approx v$ for large enough λ_2 . The scenario ends with oscillations of the scalar fields around one of the minima in Fig. 6.1. The particle production that accompanies the oscillations reheats the universe and the standard hot Big Bang history sets in.

The potential discussed above includes two scalar fields both acting as inflaton fields which by definition drive the inflation. This means that the resulting fluctuations should in general be calculated within the framework of multifield inflation [61, 73, 125]. Then one has to care for adiabatic modes which correspond to fluctuations along the inflaton field and for entropy modes which describe fluctuations between the energy contributions of different fields without changing the total energy density ρ . Even after horizon exit, entropy modes can source adiabatic fluctuations with corresponding wavelengths. As discussed in Ref. [61] however, entropy fluctuations are only produced when the background fields follow a curved trajectory in field space. Thus, only during the time when the main field evolution changes its direction from $\pm\phi$ to χ , the development of entropy fluctuations is expected. But since at this stage the field ϕ is not evolving slowly anymore and no accelerated expansion takes place, there will be no production of non-adiabatic fluctuations even in this moment. So within this scenario no complication due to multifield dynamics will occur. Therefore, in this work the calculations are done within a simplified setting with single field inflation. The two inflationary epochs are both ascribed to the same scalar field ϕ evolving within an adapted potential. More

6.2. Evolution of the homogeneous mode

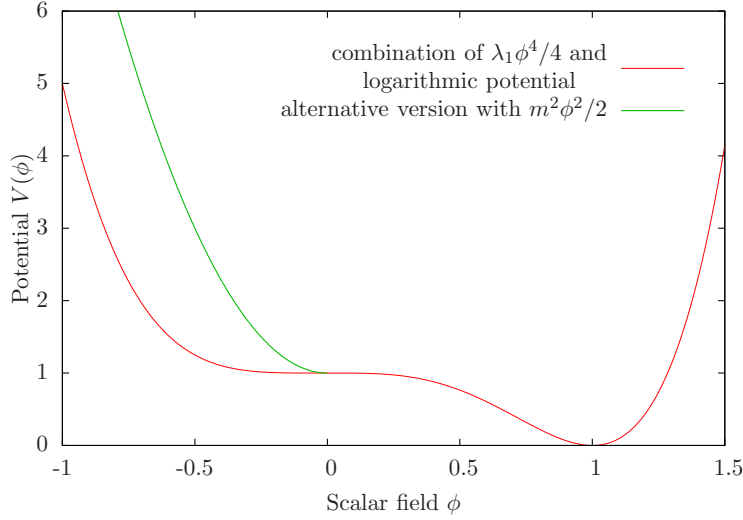


Figure 6.2.: The two potentials Eqs. (6.3) and (6.4) that are used in the following calculations of fluctuations produced during inflation.

precisely the computation of fluctuations is done using the two alternative potentials

$$V_4(\phi) = \begin{cases} V_0 + \frac{1}{4}\lambda_1\phi^4 & \phi < 0 \\ V_0 + \frac{1}{4}\lambda_0\phi^4 \left(\ln\left|\frac{\phi}{v}\right| - \frac{1}{4}\right) & \phi \geq 0 \end{cases} \quad (6.3)$$

and

$$V_2(\phi) = \begin{cases} V_0 + \frac{1}{2}m^2\phi^2 & \phi < 0 \\ V_0 + \frac{1}{4}\lambda_0\phi^4 \left(\ln\left|\frac{\phi}{v}\right| - \frac{1}{4}\right) & \phi \geq 0, \end{cases} \quad (6.4)$$

see Fig. 6.2. In both cases V_0 is given by Eq. (6.2).

6.2. Evolution of the homogeneous mode

Within the simplified scenario described in the last section, the field starts at a super-Planckian negative value and moves slowly down to the flat region around $\phi = 0$. In spite of vanishing potential gradient, for small field values slow roll ends for a short time within many parameter sets. The second part of the evolution uses the same hilltop potential for both variants. The solution $\phi(t)$ is sketched in Fig. 6.3 for three different sets of couplings and the same symmetry breaking scale $v = 1m_{\text{Pl}}$ in each case. For most of the evolution of the homogeneous mode down to $\phi = 0$, the contribution of the offset V_0 is negligible. So Eq. (5.18) yields the proportionality

$$\frac{\Delta t^{(1)}}{\Delta t^{(2)}} = \frac{m^{(2)}}{m^{(1)}} \quad (6.5)$$

for the time the field ϕ needs to evolve down a fixed interval $\Delta\phi$ within different parameter sets 1 and 2. The delay of the blue and green curves when arriving at $\phi = 0$ is a

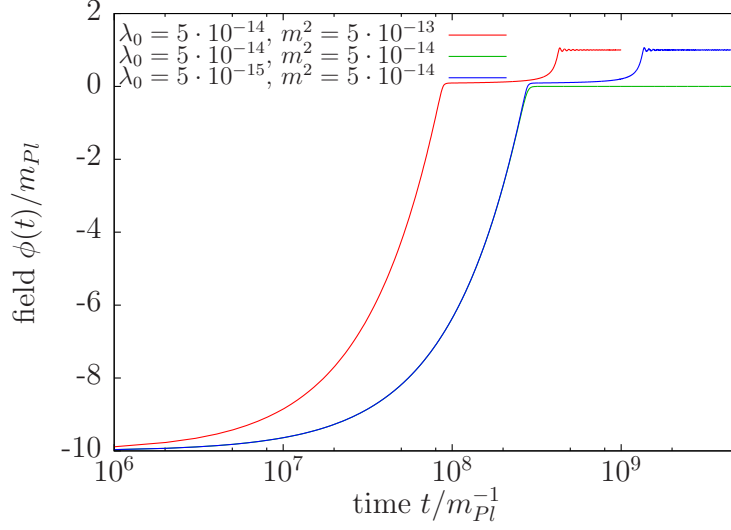


Figure 6.3.: The scalar field ϕ rolling down the potential Eq. (6.4) for three different parameter sets with $v = 1m_{Pl}$ in each case. Too large λ_0/m^2 retains the field for a very long time at values around $\phi = 0$ (green curve).

consequence of this result. Also the duration of the second inflation can be estimated with Eq. (5.18) to be

$$\frac{\Delta t^{(1)}}{\Delta t^{(2)}} = \sqrt{\frac{\lambda_0^{(2)}}{\lambda_0^{(1)}}}, \quad (6.6)$$

which matches the numerical result. The latter can be read from the duration of the almost flat regions of the red and blue curves in Fig. 6.3: Being delayed by a factor $\sqrt{10}$, the second inflation appears to have the same length in the third (“blue”) parameter set because it lasts longer by a factor of $\sqrt{10}$. For the parameter set $\lambda_0 = 5 \cdot 10^{-14}$, $m^2 = 5 \cdot 10^{-14}m_{Pl}^2$, the evolution of $\phi(t)$ is stopped at $\phi = 0$. This happens when the inflaton is slowly rolling until it reaches this value. Due to the negligible kinetic energy, ϕ is stopped by the Hubble drag and does not overcome the region with $V' \approx 0$.

Corresponding phenomena are found in the field motion within the potential Eq. (6.3), and are not displayed here. This is also the case with the content of the following figures. For the same parameter sets as in the previous figure, in Fig. 6.4 the Hubble parameter is plotted as a function of time. As for the evolution of the field $\phi(t)$, also here the successive cosmological periods can be observed. Reflecting the energy content of the field, $H(t)$ starts from a large value and evolves downward, and for fixed ϕ the coupling $m^2 \hat{=} \lambda_1$ determines the energy density. As expected, the value of H during the second inflation is the same for equal λ_0 because v is left unchanged and the kinetic energy of the field is negligible again. Fig. 6.5 shows the absolute value of the acceleration parameter \ddot{a}/a for the previous cases as a function of time. Knowing that the evolution starts with a period of inflation, time intervals of decelerated expansion can be identified from this plot. They correspond to sign changes in \ddot{a} which appear as steep dips. There

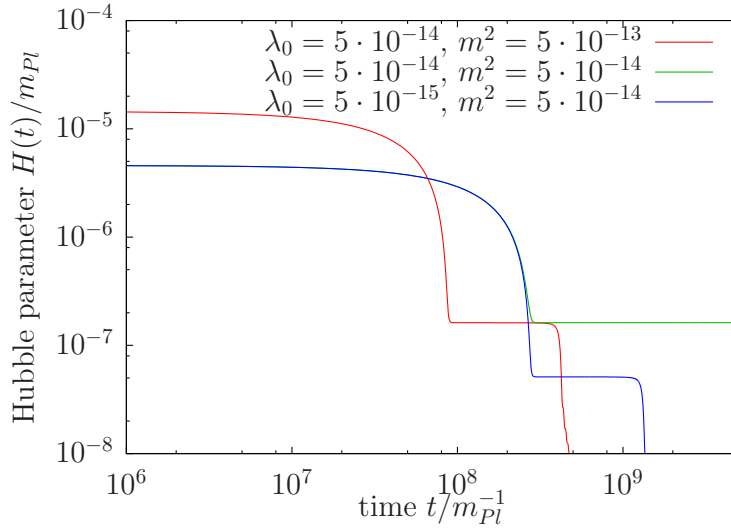


Figure 6.4.: Evolution of the Hubble parameter $H(t)$ in the same three cases as in Fig. 6.3. Periods of inflation correspond to (almost) constant H . The different potential energies determined by the couplings can be clearly distinguished.

is no interruption of accelerated expansion in the second case. As already mentioned, this is the reason for the field to be trapped at $\phi \approx 0$ entailing a sustained accelerated expansion.

6.3. Scalar and tensor perturbations

The spectra being produced in this scenario are displayed in the left panel of Fig. 6.6. The parameter sets one and three lead to potentials that are proportional to each other, which is the reason why the function $N_e(\phi)$ is identical in both cases as long as the slow-roll assumption is valid, see Eq. (5.16). So the transition from the first to the second period of inflation takes place at the same value of $N_e \approx 50$. Even for larger N_e this proportionality holds, which suggests that the short time interval of slow-roll breaking is not important here. Then it follows from Eq. (5.100) that also the two scalar power spectra should be proportional to each other. The same equation explains the diverging behavior of the scalar power spectrum in the second case, where $\dot{\phi}$ vanishes at the transition to the second inflation. The green curve is given an arbitrary offset in $N_e(k)$ -direction. Because there is no end of inflation, it cannot be uniquely fixed in this case.

The right panel of Fig. 6.6 shows the corresponding tensor power spectra. Being proportional to the Hubble parameter at horizon exit of the mode in question, the curves just illustrate the loss of (mostly) potential energy of the field. The scalar and the tensor power spectra arising from the potential V_4 , Eq. (6.3), are displayed in Fig. 6.7. As far as the period of inflation is concerned, the non-zero coupling λ_2 used for this figure

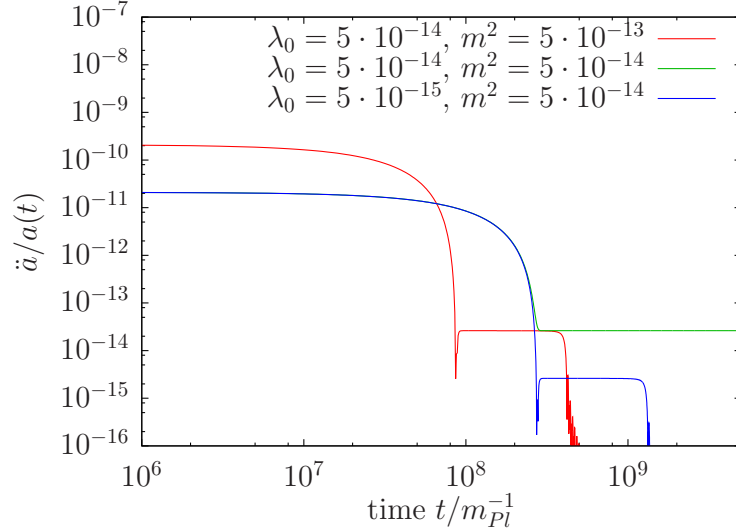


Figure 6.5.: Absolute value of the acceleration of the scale parameter $a(t)$ for the same three parameter sets as in Fig. 6.3. During the steep dips in the cases one and three, \ddot{a} changes its sign twice. During these short intervals, inflation stops and the expansion of the universe is decelerated. The green line shows no dip, which corresponds to a single, uninterrupted inflation.

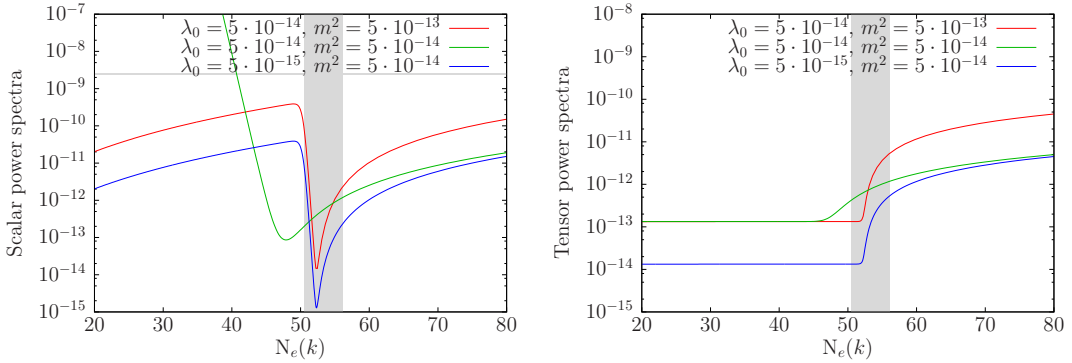


Figure 6.6.: Resulting scalar and tensor power spectra $\mathcal{P}_{\mathcal{R}}(k)$ and $\mathcal{P}_{\mathcal{T}}(k)$ in the same three cases as in Figs. 6.3 and 6.4. As can be seen from the cases one and three, shifting the potential by a constant factor leads to the same shift in the spectra. In the right panel, the green line interpolates between the two other cases because the respective potentials are (almost) the same at the relevant instances of time.

6.3. Scalar and tensor perturbations

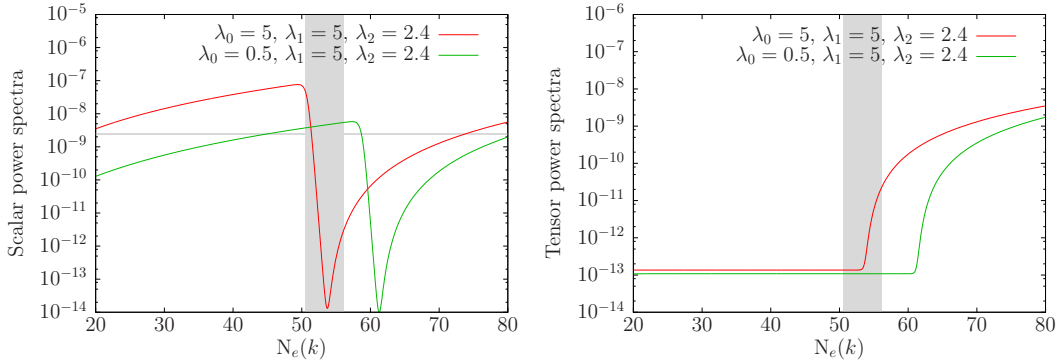


Figure 6.7.: Results of a similar calculation as in Fig. 6.6 but within the model Eq. (6.3). The couplings are given in units of 10^{-12} . As seen in the text, a larger coupling λ_0 entails less e-foldings of the second inflation and thus shifts the spectra of this figure to the left.

just means an additional offset of the potential and the new offset is not proportional to λ_0 , see Eq. (6.2). Then the potentials corresponding to the two parameter sets are not proportional to each other anymore and also a shift of the spectra in $N_e(k)$ -direction is possible. This shift can be seen in Fig. 6.7. It is reproduced analytically with the help of Eq. (5.16). The parameters for Figs. 6.3 to 6.9 are chosen such that the wavenumber q_0 today corresponds to a mode that exits the Hubble horizon around the transition between the two inflationary periods. As already stated, the correspondence to q_0 cannot be narrowed down to a single value of N_e or k because the physics of the inflaton decay is not settled yet. Altogether, CMB measurements cover an N_e -range of roughly ten [29]. For these scales the primordial fluctuations have been obtained to high accuracy. So, for the presented scenarios to be viable, there should be a range of at least ten e-foldings in which the computational results match with observation. This range should overlap with the grey band in Figs. 6.6 and 6.7. The observational result¹⁰ is represented by the narrow horizontal stripe at $2.4 \cdot 10^{-9}$. While it is possible to tune the parameters such that the results match for a fixed wavelength, the strong variation of $\mathcal{P}_{\mathcal{R}}(k)$ on the scale of a few $N_e(k)$ renders it impossible to fit the curves to the measurements over the whole interval. This leads to the conclusion that the transition between large-field and small-field inflation should occur when the Hubble parameter is either much smaller or much larger than the wavenumber q_0 today. This problem will be discussed further in the following.

The tensor-to-scalar ratio resulting from the previously discussed parameter sets within the potentials V_2 and V_4 is depicted in Fig. 6.8. During the transition to small-field inflation, r drops by several orders of magnitude. This reflects the drop of the field velocity $\dot{\phi}$. It occurs because the Hubble drag is the only force acting on the field in an almost flat region of the potential. The cases one and three in Fig. 6.6 yield the same

¹⁰While observation does not yield exactly the same value for the whole interval, compared to the large gradients of the calculated curves it can be regarded as constant.

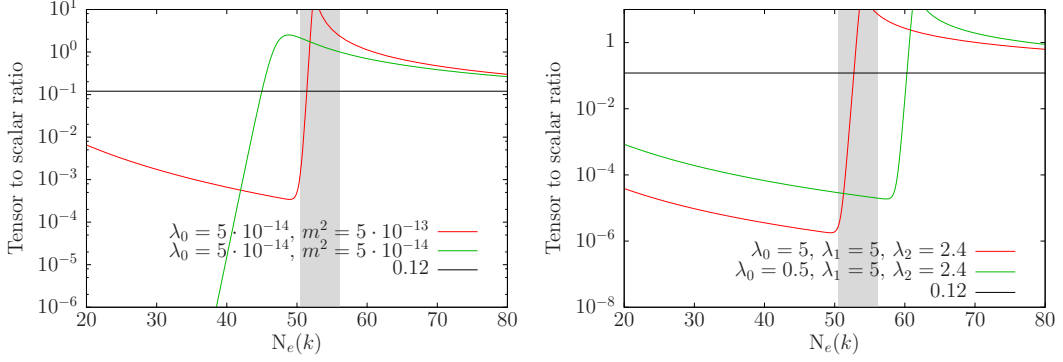


Figure 6.8.: The tensor-to-scalar ratio strongly drops down at the transition to small-field inflation. If $\dot{\phi}$ becomes very small, also r vanishes at corresponding values of $N_e(k)$ (left panel, green curve).

(red) curve here. The green curve drops to very small numbers when ϕ is practically fixed at a constant value. Also for r , the maximally allowed value of $r = 0.12$, shows that compatibility is only possible when $\dot{\phi} = 0$ is reached outside the range observable in the CMB. The same is true for the allowed range of the scalar spectral index n_s , which can be seen in Fig. 6.9. During the transition it takes on values far away from the ones being measured. It is clear from the definition of n_s in Eq. (5.103) that multiplying the scalar spectrum with a constant factor does not alter the value of the spectral index. So parameter set three yields the same result as set one and is not displayed in the left panel of the figure. The right panel shows a similar behavior of n_s within the potential V_4 .

6.4. Compatibility with measurements

Figures 6.10 to 6.12 summarize the results for the tensor-to-scalar ratio and for the scalar spectral index within the models considered so far. As noted in the keys of these figures, the black dashed lines sketch the dependence of r on n_s as obtained from an analytical estimation for the two potentials $m^2\phi^2/2$ and $\lambda\phi^4/4$. The result varies along these lines when different values of N_e are chosen. Including the possibility of an offset V_0 , the slow-roll equations Eq. (5.102) for the tensor-to-scalar ratio and Eq. (5.105) for the scalar spectral index combine to

$$r_2 = 4 \frac{n_s - 1}{V_0/m^2\phi^2 - 1}, \quad (6.7)$$

and

$$r_4 = \frac{16}{3} \frac{n_s - 1}{4V_0/\lambda\phi^4 - 1}, \quad (6.8)$$

where r_2 and r_4 are the tensor-to-scalar ratio in the squared and the quartic case, respectively. The black dashed lines give the results of Eqs. (6.7) and (6.8) with V_0

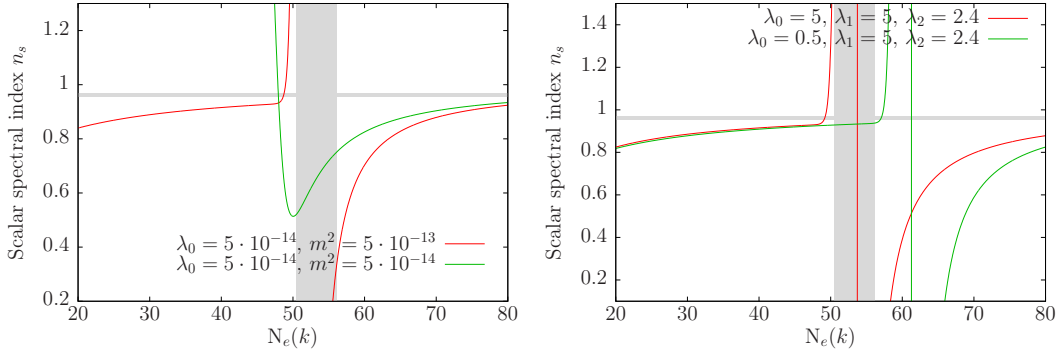


Figure 6.9.: Evolution of the scalar spectral index for the previously discussed cases.

The transition region between the two periods of inflation should be far outside the sensitivity range of the Planck measurements. The scalar spectrum within the third case in Fig. 6.6 was just shifted by a factor with respect to the first one. As expected, the logarithmic derivative of these functions is the same, and therefore omitted in this figure. By choosing a suitable offset in N_e , the result of the analytic formula Eq. (5.134) can be matched to the red curve.

set to zero. Numerical calculations within the same cases are represented by the five large dots which are obtained at three different stages of inflation. These are labelled by the number N_e which is large ($N_e = 50$ and 60) for early production well within the slow-roll regime and small ($N_e = 10$) for late production, i.e. for fluctuations in modes crossing the horizon shortly before the end of inflation. Then the slow-roll approximation is expected to lose its validity. So, the deviation of the large dot in dark red from the long-dashed black line is no surprise since also the dots are calculated assuming slow roll. The position of the large dots is independent from the coupling when values $\lambda \in [10^{-15}, 10^{-11}]$ and $m^2 \in [10^{-15}, 10^{-11}]$ are chosen. The small dots represent results computed within the combined potentials V_2 and V_4 . They arrange along curves starting on the corresponding straight line (for the monomic quadratic and quartic potential, respectively) and more and more deviate when evolving to larger r and smaller n_s . Since this deviation also occurs for the monomic potential, it is attributed to the breaking of slow roll. Corrections due to V_0 seem to be small in comparison. They tend to enlarge the value of r at given n_s .¹¹

The color of the small dots encodes the number of e-foldings of the second inflation, which varies according to different parameter choices. It is clearly visible that this number $N_e^{(2)}$ grows monotonically when following the dots from the lower right to the upper left. This suggests the following interpretation: The fluctuations being measured within the present scenario at $N_e = 60$ resemble those that would be produced in the quartic and quadratic potentials at later times. The main effect of the second period of inflation is a shift of the remaining e-foldings connected to the fluctuations.

¹¹Note that both the numerator and the denominator in Eqs. (6.7) and (6.8) are negative.

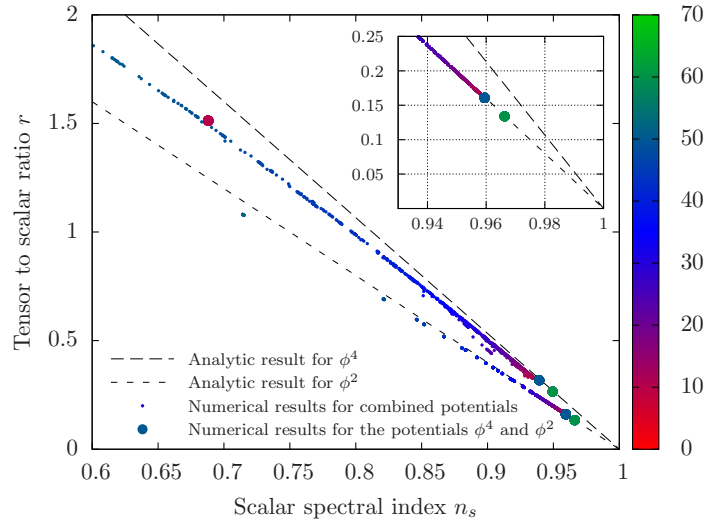


Figure 6.10.: This figure shows the result of different calculations of the tensor-to-scalar ratio r and the scalar spectral index n_s . These quantities are computed for modes leaving the horizon a fixed number of e-foldings before inflation ends. The two dashed lines follow the analytic formulae (6.7) and (6.8) for slow-roll inflation within the potentials $m^2\phi^2/2$ and $\lambda\phi^4/4$, respectively. The large dots mark the results of numerical calculations within the same two potentials. The number of e-foldings N_e before the end of inflation are 60, 50, and 10, respectively. Along the dashed lines (and more and more departing from them) the small dots represent results from the combined potentials V_2 and V_4 described in the main text. The color code shows the number of e-foldings of the second inflation, whereas the total N_e is 60 for each of the small dots. All results were obtained within slow-roll approximation.

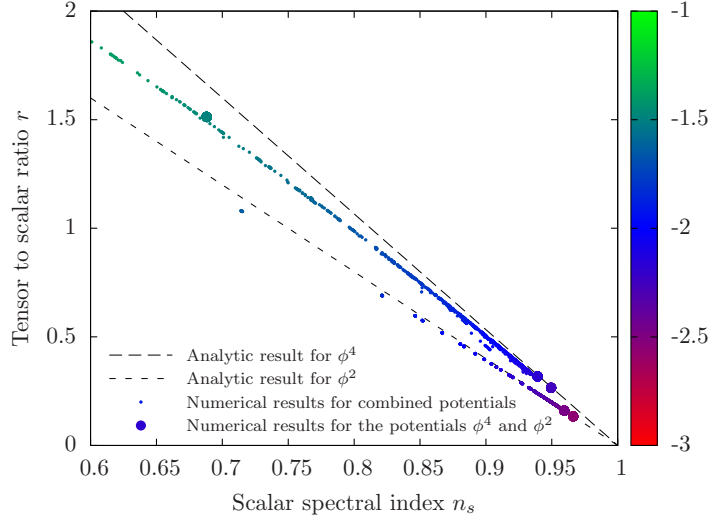


Figure 6.11.: The same as in Fig. 6.10 but with the colors representing the decimal logarithm of the slow-roll condition $\dot{\phi}^2/2V(\phi)$. This figure shows that the deviation of the points from the dashed lines can be explained from the lack of slow roll.

The small figure in Fig. 6.10 is a detail of the lower right region of the large one. This is the interesting range as CMB measurements are concerned. The values allowed by Planck lie below 0.15 for r and between 0.94 and 0.98 for n_s . So one can see that the second inflation drives the computed values of r and n_s further away from the ones measured in the CMB. The more effective it is in terms of e-foldings the more severe it renders the discrepancy.

Figs. 6.11 and 6.12 show the same results as Fig. 6.10 but with a different choice of the color code. This is used to illustrate the reason why the lines formed by the small dots deviate from the analytic estimate (dashed lines). In Fig. 6.11 the colors reflect the value of $\log_{10}(\dot{\phi}^2/2V(\phi))$ which is a measure for slow roll, see Eq. (5.8). The largest deviations are observed where the kinetic energy amounts to a few percent of the potential and the results agree better for a lower proportion.

The values of $V_0/m^2\phi^2$ and $4V_0/\lambda_1\phi^4$ are encoded in the colors of the dots in Fig. 6.12. These quantities are proportional to the ratio of the offset to the field dependent part of the potential, and they are computed at the time the mode of interest leaves the horizon. They also occur in Eqs. (6.7) and (6.8). As stated above, they are expected to give corrections enlarging r for given n_s . So it can be concluded that their influence on the result is less important than that of missing slow roll. This is confirmed by the fact that the deviations are considerably smaller for the massive field, where $V/m^2\phi^2$ is largest and slow-roll violation is quite small. For the pure squared and quartic potentials the quantity reflected by the color code is zero and they are plotted in black.

The parameter sets that yield the small dots are chosen in the following way: First a sweep over the parameter range $v \in [0.01, 1] \cdot m_{\text{Pl}}$, $\lambda_0 \in [10^{-15}, 10^{-12}]$, $\lambda_1 \in [10^{-15}, 10^{-12}]$

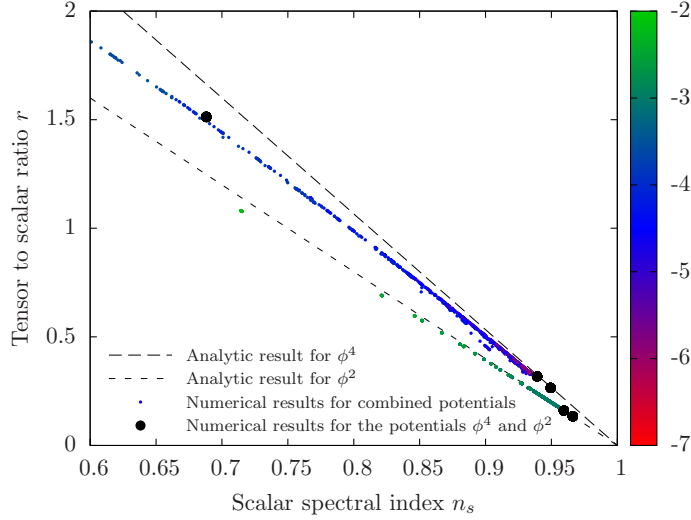


Figure 6.12.: The same as in Figs. 6.10 and 6.11 but with the colors representing the decimal logarithm of the quantities $V_0/m^2\phi^2$ and $4V_0/\lambda_1\phi^4$ for the combined potentials with $m^2\phi^2/2$ and with $\lambda_1\phi^4/4$, respectively. In combination with Fig. 6.10 this figure suggests that the deviation of the numerical calculation from the analytic result stems from the violation of slow roll rather than from the offset V_0 in the potential $V(\phi)$.

is done. The parameter λ_2 is restricted to $\lambda_2 = 0$ and the interval $\lambda_2 \in [10^{-15}, 10^{-14}]$. Stronger couplings are not computed with because they lead to larger values of V_0 which stop the evolution of ϕ before reaching the minimum.

For each parameter set the e-foldings of the first and the second inflation, $N_e^{(1)}$ and $N_e^{(2)}$, are determined. The interesting cases are those with enough $N_e^{(2)}$, such that the expected spectra are discernible from standard large field inflation. On the other hand the value should not exceed $N_e^{(2)} = 60$ because then only the second, small-field inflation is visible today. As exemplified in Figs. 6.6 to 6.9 the spectra produced near the transition between the two inflationary periods deviate strongly from the CMB measurements which set tight bounds on the magnitude of fluctuations. These arguments lead to the approach that parameter sets entailing $N_e^{(2)} \in [10, 60]$ are selected and the fluctuations are calculated for modes leaving the horizon at $N_e = 60$ e-foldings before the end of the second inflation.

7. Fluctuations produced after inflation: Preheating

At the end of inflation, the universe is assumed to be cold and empty, with the exception of the inflaton field. The inflaton pervades space almost homogeneously before it decays into its excitations and other particles. The first, rapid decay is characterized by non-perturbative effects. It is crucial for accomplishing thermal equilibrium at the temperature, where Big Bang nucleosynthesis takes place. This is decisive for a scenario to be viable. This work follows the convention to give the name “preheating” to the early non-perturbative stage, while “reheating” is reserved for the subsequent period of perturbative evolution. The following will only be concerned with preheating.

7.1. Initial vacuum fluctuations

A typical calculation of preheating after cosmological inflation starts when all particles that might have filled the universe before are extremely dilute. During preheating, the fluctuations discussed in the last section have wavelengths much larger than the Hubble horizon. Therefore, interactions with the fluctuations and particles produced during the preheating epoch are neglected. So, a vacuum state is assumed as initial condition for the computations. In this section the spectrum of vacuum fluctuations for a non-interacting massless scalar field in a spatially flat FRW universe is derived. The presentation follows Refs. [51, 77, 114]. The evolution of the field ϕ is governed by the action S and the Lagrange density \mathcal{L} ,

$$S = \frac{1}{2} \int d^4x \sqrt{-g} \partial^\mu \phi \partial_\mu \phi = \int d^4x \sqrt{-g} \mathcal{L}, \quad (7.1)$$

in conformal coordinates. It is $g_{\mu\nu} = a^2 \eta_{\mu\nu}$ and $\sqrt{-g} = a^4$. The definition $\varphi := a\phi$, and the prime as shorthand for ∂_0 simplify the Lagrange density, the field momentum, and the Hamiltonian density to

$$\mathcal{L} = \frac{1}{2} \sqrt{-g} \partial^\mu \phi \partial_\mu \phi = \frac{1}{2} \left(\varphi' - \varphi \frac{a'}{a} \right)^2 + \frac{1}{2} (\nabla \varphi)^2, \quad (7.2)$$

$$\pi = \frac{\partial \mathcal{L}(\varphi, \varphi')}{\partial \varphi'} = \varphi' - \varphi \frac{a'}{a}, \quad \text{and} \quad (7.3)$$

$$\mathcal{H} = \pi \varphi' - \mathcal{L} = \frac{1}{2} \left\{ \varphi'^2 - (\nabla \varphi)^2 - \left(\frac{a'}{a} \varphi \right)^2 \right\}, \quad (7.4)$$

Chapter 7. Fluctuations produced after inflation: Preheating

respectively. Normalizing the Fourier transform of any function $f(\mathbf{r})$ as

$$f_{\mathbf{k}} = \frac{1}{(2\pi)^{3/2}} \int d^3k \exp(-i\mathbf{k}\mathbf{r}) f(\mathbf{r}) \quad (7.5)$$

and using the shorthand $k^2 := |\mathbf{k}|^2$, the Hamiltonian reads

$$H = \frac{1}{2} \int d\eta d^3k \left\{ \varphi'_{\mathbf{k}} \varphi'_{-\mathbf{k}} + k^2 \varphi_{\mathbf{k}} \varphi_{-\mathbf{k}} - \left(\frac{a'}{a} \right)^2 \varphi_{\mathbf{k}} \varphi_{-\mathbf{k}} \right\}, \quad (7.6)$$

where for the second term the collection of one minus sign from Eq. (7.4), one of an i^2 , one from the opposite directions of $\pm\mathbf{k}$, and one from the metric ends up with a plus. Assuming that $\varphi(\mathbf{x}, \eta)$ vanishes for large η , the Lagrange density Eq. (7.2) can also be written as

$$\mathcal{L} = \frac{1}{2} \left(\varphi'^2 + \varphi^2 \frac{a''}{a} \right) + \frac{1}{2} (\nabla \varphi)^2 \quad (7.7)$$

$$\Rightarrow H = \frac{1}{2} \int d\eta d^3k \left\{ \varphi'_{\mathbf{k}} \varphi'_{-\mathbf{k}} + k^2 \varphi_{\mathbf{k}} \varphi_{-\mathbf{k}} - \left(\frac{a''}{a} \right) \varphi_{\mathbf{k}} \varphi_{-\mathbf{k}} \right\}. \quad (7.8)$$

When quantizing the system, creation and annihilation operators, $\hat{a}^+(\mathbf{k}), \hat{a}^-(\mathbf{k})$, are introduced, in terms of which the field and momentum operators are

$$\hat{\varphi}(\mathbf{k}) = \frac{1}{\sqrt{2k}} \{ \hat{a}^-(\mathbf{k}) + \hat{a}^+(-\mathbf{k}) \} \quad \text{and} \quad \hat{\pi}(\mathbf{k}) = -i\sqrt{\frac{k}{2}} \{ \hat{a}^-(\mathbf{k}) - \hat{a}^+(-\mathbf{k}) \}, \quad (7.9)$$

respectively. The vacuum state at conformal time η_0 , $|0, \eta_0\rangle$, for every \mathbf{k} fulfills

$$\hat{a}^-(\mathbf{k}) |0, \eta_0\rangle = 0. \quad (7.10)$$

From this condition one can deduce the coordinate representation of this state: It is

$$\hat{a}^-(\mathbf{k}) = \hat{\varphi}(\mathbf{k}) + \frac{i}{k} \hat{\pi}(\mathbf{k}), \quad (7.11)$$

and in the coordinate representation one gets

$$\hat{\pi}(\mathbf{x}) = -i \frac{\delta}{\delta \varphi(\mathbf{x})} \quad \text{and} \quad \hat{\pi}(\mathbf{k}) = -i \frac{\delta}{\delta \varphi(-\mathbf{k})}. \quad (7.12)$$

So the wave functional of the vacuum state must be a product of

$$\Psi [\varphi(\mathbf{k}, \eta_0), \varphi(-\mathbf{k}, \eta_0)] \propto \exp \{ -k \varphi(\mathbf{k}, \eta_0) \varphi(-\mathbf{k}, \eta_0) \}. \quad (7.13)$$

The corresponding probability distribution for the Fourier modes of the real field φ is

$$\mathcal{P} [\varphi(\mathbf{k}, \eta_0)] \propto \exp \{ -2k |\varphi(\mathbf{k}, \eta_0)|^2 \}, \quad (7.14)$$

out of which the initial conditions after inflation are generated. They are used for the lattice calculations of preheating being presented in the following. Further issues of implementing the initial conditions will be dealt with in Appendix B.2.

7.2. Periodically changing mass and the Mathieu equation

As the first example for particle production during preheating, the setup of a scalar field ϕ with mass m coupled to a massless second scalar X is chosen. This mimics the situation after chaotic single-field inflation with a massive inflaton ϕ , see Section 5.5. The potential is taken to be

$$V = \frac{1}{2}m^2\phi^2 + \frac{1}{2}g^2\phi^2 X^2. \quad (7.15)$$

In a first attempt, $\phi(\mathbf{x}, t) = \phi_0 \sin(mt)$ is assumed and a possible expansion of the background is neglected. Within a simulation of a preheating universe this will be included later. The simplifications lead to a periodically changing mass term of X : The equation of motion for a mode X_k is

$$\ddot{X}_k + (k^2 + g^2\phi_0^2 \sin^2(mt)) X_k = 0. \quad (7.16)$$

Since the potential (7.15) is only quadratic in the field X , the evolution of any mode $X_{\mathbf{k}}$ does not depend on the other modes. Equation (7.16) is usually written as a Mathieu equation [84],

$$X_k'' + (A_k - 2q \cos(2z)) X_k = 0, \quad (7.17)$$

where the quantities

$$A_k = \frac{k^2}{m^2} + 2q, \quad q = \frac{g^2\phi_0^2}{4m^2}, \quad \text{and} \quad z = mt \quad (7.18)$$

are introduced. Equation (7.17) was first analyzed in [97] in the context of vibrating membranes. The features of its solutions are well-known. Their stability properties can be read from Fig. 1 in Ref. [11], which is also used for this presentation. Unstable solutions are characterized by their Floquet exponent μ_k which determines the exponential growth of a mode through

$$n_k = \frac{1}{2} \left(\omega_k |X_{\mathbf{k}}(z)|^2 + \frac{1}{2\omega_k} |X'_{\mathbf{k}}(z)|^2 \right) \sim |X_k|^2 \propto e^{2\mu_k z}. \quad (7.19)$$

A derivation of the Floquet exponent for Minkowski and FRW background is presented below. Interactions between different modes X_k are not accounted for in this model and, for now, backreaction of the modes onto the homogeneous field ϕ is neglected. Therefore, one can solve the problem numerically mode by mode and obtain the results shown in Figs. 7.1 and 7.2.

7.2.1. Broad and narrow parametric resonance

There are two regimes in parameter space where the modes X_k behave differently from each other: One is the regime of narrow resonance where only a few separate modes show

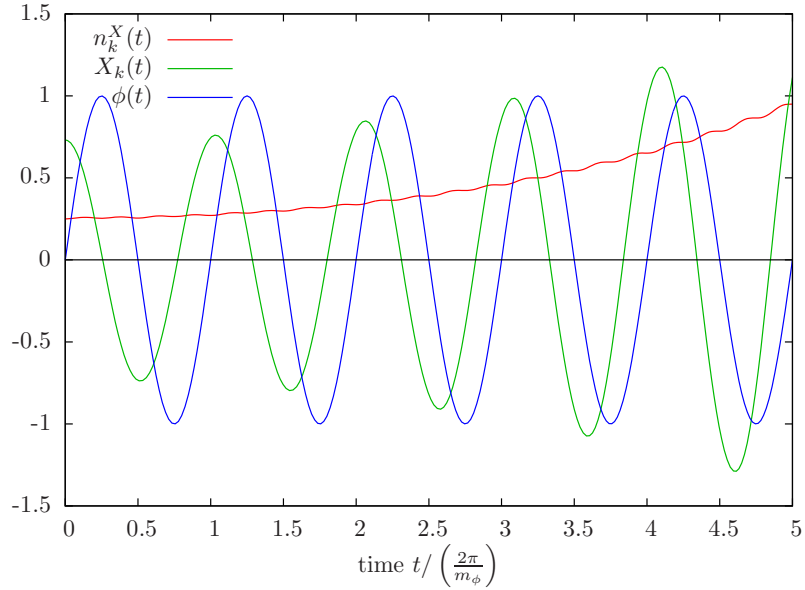


Figure 7.1.: The mode function X_k starting with a small amplitude $1/\sqrt{2\omega_k}$. $\phi(t)$ is displayed in units of $10^{-3}m_{\text{Pl}}$ and X_k in units of m_ϕ^{-1} . Its equation of motion is that of a harmonic oscillator with a small time-dependent perturbation which comes from the interaction with the inflaton $\phi(t)$. The additional restoring force exerted by $\phi(t)$ is proportional to $\phi^2(t)$. The mode $X_k(t)$ experiences a small amplification when returning from each maximal displacement because then ϕ^2 is slightly bigger as compared to moments of time when $X_k(t)$ is growing. The case shown in this figure is an example for narrow parametric resonance because if at all, neighboring modes are much less amplified. The parameters corresponding to Eq. (7.17) are chosen as $A_k = 1$ and $q = 1/16$ being consistent with $\Phi = 10^{-3}m_{\text{Pl}}$, $m_\phi = 10^{-6}m_{\text{Pl}}$, $g = 5 \cdot 10^{-4}$ and the wave number $k \approx 0.968m_\phi$. See also Fig. 7.2.

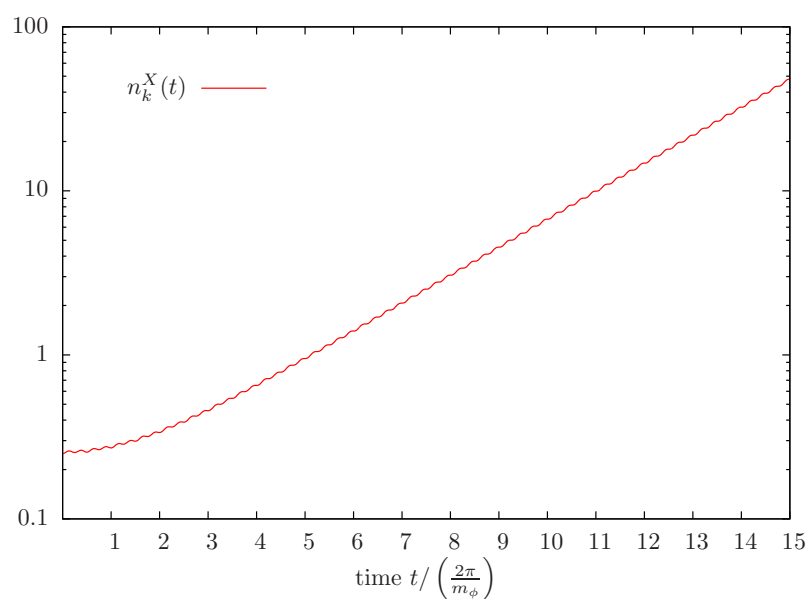


Figure 7.2.: The same setting as in Fig. 7.1 for a longer time period. As in Figure 7.1 and many others to come, time is given in units of an oscillation period of the inflaton. Up to $n_k^X \approx 1$ the classical formula Eq. (7.19), which is displayed here, should not be interpreted as a particle density. The small wiggles come from superposing the extrema of the mode function and its derivative.

unstable behavior. This entails a continuous exponential growth of the mode function and of the corresponding particle density. Both X_k and X'_k oscillate with the frequency of ϕ . In the time dependence of n_k this leaves a small oscillating structure, which, because of squaring and superimposing, shows four times the frequency of the ϕ oscillations. Within the more realistic setting of an FRW background, this regime could possibly occur at the end of preheating when the amplitude ϕ_0 has become small enough to give $q < 1$. However, for a successful preheating of the universe a non-negligible density of produced particles should be expected at this stage. So, the calculation within the regime of narrow resonance that is presented here is probably not directly applicable to the evolution of the early universe.

The other regime in parameter space of Eq. (7.17) is that of large q which corresponds to a broad resonance. This means that a broad range of modes undergoes exponential growth entailing very efficient particle production. A large parameter q is equivalent to $g\phi_0 \gg m$ and so the oscillation of ϕ is much slower than that of X_k . The sudden, stepwise growth of the X particle number occurs in moments of time when the inflaton field ϕ and therefore the oscillating X mass squared,

$$m_X^2 = g^2\phi_0^2\sin^2(mt) = g^2\phi(t)^2, \quad (7.20)$$

is close to zero. So, one observes

$$\text{change in } n_k \Rightarrow \phi(t) \ll \phi_0, \quad (7.21)$$

which is put into a more precise statement below. In these time intervals the frequency ω_k corresponding to the mode k changes non-adiabatically. This means that the adiabaticity condition,

$$\omega_k^2 \geq \dot{\omega}_k, \quad (7.22)$$

is violated, allowing the adiabatically invariant quantity n_k to change its value. As a simple rule one can state that this value grows if $|X_k|$ is growing while $\phi(t)$ is small. This happens for consecutive ϕ oscillations when X_k is in resonance with them. In contrast, when the evolution is adiabatic, n_X is constant while the frequency of the X -modes, ω_k , follows the sinusoidal oscillation of the field ϕ . From Eq. (7.19) it is clear that then the amplitude of the oscillating $X_k(z)$ has a minimum at each extremum of ϕ .

Again referring to [80], an estimation of the spectral range of produced X particles and of the corresponding time period is now presented: Being expected to occur at small $\phi \approx \phi_0 mt$, non-adiabaticity of

$$\omega \approx \sqrt{k^2 + (g\phi_0 mt)^2} \quad (7.23)$$

is present for momenta k with

$$k^2 + (g\phi)^2 \leq (g^2\phi m\phi_0)^{2/3}. \quad (7.24)$$

The corresponding function $k(\phi)$ assumes its maximal value

$$k_{\max} \approx \sqrt{gm\phi_0} \quad (7.25)$$

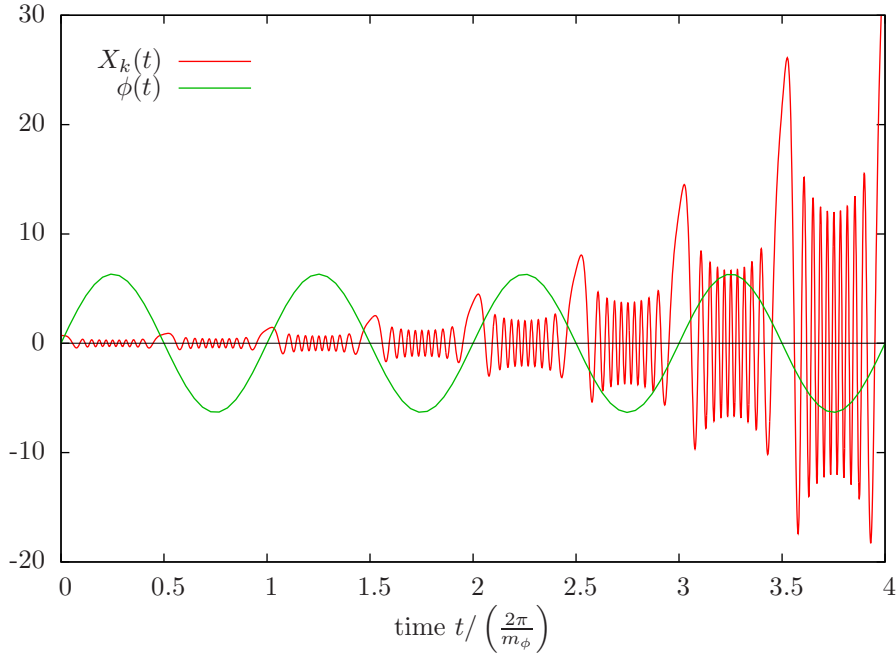


Figure 7.3.: Broad resonance regime of solutions to the Mathieu equation (7.17). The oscillatory inflaton field $\phi(t)$ couples to the mode function $X_k(t)$ as in the solution displayed in Figs. 7.1, 7.2. The parameters chosen for this figure are $q = 250$ and $A_k = 501$ corresponding to the coupling $g = 5 \cdot 10^{-4}$ and $m_\phi = 10^{-6} m_{\text{Pl}}$ as for Figs. 7.1, 7.2, and $k = m_\phi$ and $\phi_0 \approx 6.3 \cdot 10^{-2}$. The dips of the amplitude of $X_k(t)$ in the adiabatic regions around the extrema of $\phi(t)$ can be explained from Eq. (7.19) and the adiabatic invariance of n_k^X .

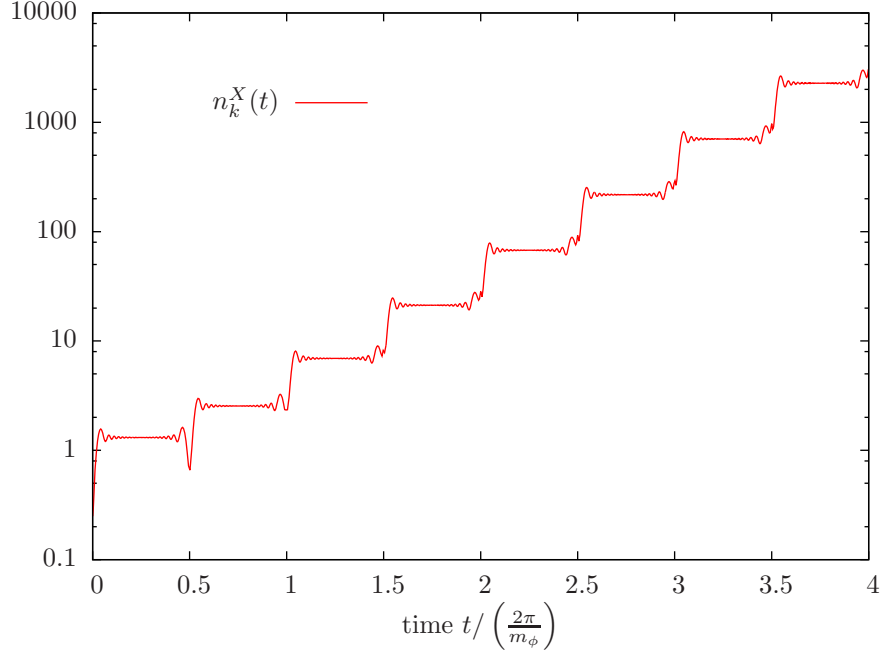


Figure 7.4.: The occupation number or particle density n_k^X in the same setting as in Fig. 7.3. Being adiabatically invariant, n_k^X changes only when $\phi^2(t) \propto m_X$ is close to zero because then $\dot{\omega}_k \leq \omega_k^2$ is not fulfilled.

at

$$\phi(k_{\max}) = \frac{1}{3^{0.75}} \sqrt{\frac{m\phi_0}{g}}, \quad (7.26)$$

which, in turn, corresponds to a time span of

$$T \sim \frac{2\phi(k_{\max})}{\dot{\phi}} \sim \frac{1}{\sqrt{gm\phi_0}} \sim \frac{1}{k_{\max}} \sim \frac{1}{\omega(k_{\max})}. \quad (7.27)$$

In this time interval particles with momenta up to the order of k_{\max} are produced. For the last step, $m_X(k_{\max}) \sim g\phi(k_{\max}) \sim k_{\max}$ has been used. It is included in order to show that the process respects the Heisenberg uncertainty principle.

Before discussing the specific effects of the FRW expansion let us review a more thorough theoretical treatment of broad parametric resonance. Only for later use the scale parameter $a(t)$ is already included. During most of the time, the evolution is adiabatic and the solution to Eq. (7.16) can be written in the WKB approximation,

$$\chi_k(t) := X_k(t)a^{3/2} \equiv \frac{\alpha_k(t)}{\sqrt{2\omega}} e^{-i \int_{t_0}^t \omega dt} + \frac{\beta_k(t)}{\sqrt{2\omega}} e^{+i \int_{t_0}^t \omega dt}. \quad (7.28)$$

Note that in this equation the comoving mode function χ_k has been defined with an additional factor \sqrt{a} with respect to Sec. 7.1 in order to keep the dependence of α_k and β_k on the scale factor as small as possible. (This dependence is not removed completely, however, because ω is not exactly proportional to $1/a$.)

7.2. Periodically changing mass and the Mathieu equation

In the non-adiabatic region the sine in the mass term of χ can be linearly approximated such that the equation of motion reads

$$\frac{d^2\chi_k}{dt^2} + \left(\frac{k^2}{a^2} + g^2 m^2 \phi_0^2 (t - t_j)^2 \right) \chi_k = 0. \quad (7.29)$$

After choosing convenient variables $\tau = k_{\max}(t - t_j)$ for time and $\kappa = k/(ak_{\max})$ for momentum, the mode equation can be written as

$$\frac{d^2\chi_k}{d\tau^2} + (\kappa^2 + \tau^2) \chi_k = 0. \quad (7.30)$$

Comparison with the time independent Schrödinger equation shows that Eq. (7.30) describes the behavior of a wave scattered on a parabolic potential barrier $V(\tau) = -\tau^2$. This is studied by various authors, for example in [18, 20, 52, 126]. In addition to [80], for this presentation especially [12] and the chapter on parabolic cylinder functions in [4] have been used.

7.2.2. Transmission and reflection coefficients

In order to find a formula for the growth of occupation number at each scattering off the parabolic potential Eq. (7.30) the starting point is to calculate the transmission and the reflection coefficients for the parabolic barrier. In doing so it is not important whether it is a space or a time coordinate along which the scattering takes place. So one can just as well think of the process in terms of an incoming and two outgoing solutions as in the most typical quantum mechanical scattering problems in one dimension. In order to set up a situation of scattering, solutions with definite flux direction are necessary. These are identified in the following. Solutions to Eq. (7.30) can be written as a superposition,

$$E\left(-\frac{\kappa^2}{2}, \sqrt{2}\tau\right) = \frac{1}{\xi} W\left(-\frac{\kappa^2}{2}, \sqrt{2}\tau\right) + i\xi W\left(-\frac{\kappa^2}{2}, -\sqrt{2}\tau\right), \quad (7.31)$$

with a real solution W and the constant $\xi > 0$ defined to fulfill

$$\xi^2 = \sqrt{1 + \exp(-\pi\kappa^2)} - \exp\left(-\pi\frac{\kappa^2}{2}\right) \quad (7.32)$$

and, consequently,

$$\frac{1}{\xi^2} = \sqrt{1 + \exp(-\pi\kappa^2)} + \exp\left(-\pi\frac{\kappa^2}{2}\right). \quad (7.33)$$

The validity of the last equation can be checked by multiplication with the preceding one. The functional form of W is only needed far away from the potential maximum ($\tau \gg \kappa^2$). There the following approximations are obtained [4]:

$$W\left(-\frac{\kappa^2}{2}, +\sqrt{2}\tau\right) = \frac{2^{1/4}\xi}{\sqrt{\tau}} \cos\left(\frac{\tau^2}{2} + \frac{\kappa^2}{2} \ln\sqrt{2}\tau - \frac{\Phi}{2} + \frac{\pi}{4}\right), \quad (7.34)$$

$$W\left(-\frac{\kappa^2}{2}, -\sqrt{2}\tau\right) = \frac{2^{1/4}}{\sqrt{\tau}\xi} \sin\left(\frac{\tau^2}{2} + \frac{\kappa^2}{2} \ln\sqrt{2}\tau - \frac{\Phi}{2} + \frac{\pi}{4}\right). \quad (7.35)$$

In order to save writing, for the rest of this paragraph the shorthand

$$\zeta := \frac{\tau^2}{2} + \frac{\kappa^2}{2} \ln \sqrt{2\tau} - \frac{\Phi}{2} + \frac{\pi}{4} \quad (7.36)$$

is defined. Put together, for the complex solution at $\tau \gg \kappa^2$ this gives:

$$E \left(-\frac{\kappa^2}{2}, \sqrt{2\tau} \right) = \frac{2^{1/4}}{\sqrt{\tau}} \exp i\zeta. \quad (7.37)$$

A more exact formula would include a power series in τ^{-2} which, in the limit $\tau \rightarrow \infty$, gives 1. The present calculation is done in this limit. The angle Φ is given by the complex gamma function as

$$\Phi = \arg \Gamma \left(\frac{1 + i\kappa^2}{2} \right). \quad (7.38)$$

The solution at negative times is obtained to be

$$\begin{aligned} E \left(-\frac{\kappa^2}{2}, -\sqrt{2\tau} \right) &= \frac{1}{\xi} W \left(-\frac{\kappa^2}{2}, -\sqrt{2\tau} \right) + i\xi W \left(-\frac{\kappa^2}{2}, +\sqrt{2\tau} \right) \\ &\xrightarrow{\tau \gg \kappa^2} \frac{2^{1/4}}{\sqrt{\tau} \xi^2} \sin \zeta + i \frac{2^{1/4} \xi^2}{\sqrt{\tau}} \cos \zeta \\ &= i \frac{2^{1/4}}{\sqrt{\tau}} \left(\sqrt{1 + e^{-\pi\kappa^2}} e^{-i\zeta} - e^{-\pi\kappa^2/2} e^{i\zeta} \right), \end{aligned} \quad (7.39)$$

where ζ is defined in Eq. (7.36). To identify the incoming, the reflected, and the transmitted part of the solution, which are named E_i , E_r , and E_t , respectively, one has to calculate the flux

$$j = -i \left(E^* \frac{\partial E}{\partial \tau} - \frac{\partial E^*}{\partial \tau} E \right) \quad (7.40)$$

of the three components in Eqs. (7.37) and (7.39). From the sign of this quantity the first component of Eq. (7.39) is identified as the incoming wave E_i , the second component of Eq. (7.39) as E_r , and Eq. (7.37) as E_t . The ratios of the respective solutions give the reflection coefficient

$$R_{\text{PCF}} = \frac{E_r}{E_i} = -e^{2\zeta i} \frac{e^{-\pi\kappa^2/2}}{\sqrt{1 + e^{-\pi\kappa^2}}} \quad (7.41)$$

and the transmission coefficient

$$T_{\text{PCF}} = \frac{E_t}{E_i} = -ie^{2\zeta i} \frac{1}{\sqrt{1 + e^{-\pi\kappa^2}}}. \quad (7.42)$$

The index is to reflect their origin from parabolic cylinder functions. Note that in this form the coefficients depend on the length of the interval that is considered, e.g. $2\tau_0$. This should be expected because, through the time dependent quantity ζ , they include the phase evolution of the oscillating solution E .

However, applied to the problem of particle production by an oscillating field, the solution to the equation of motion Eq. (7.16) is a parabolic cylinder function only in

7.2. Periodically changing mass and the Mathieu equation

the vicinity of the scattering times t_j . Elsewhere it is written within the WKB approximation. Therefore, the correct phase of R and T is obtained by subtracting the WKB phase shift from the phase shift of the parabolic cylinder functions. From Eq. (7.30) the first one is

$$\Phi_{\text{WKB}} = \int_{-\tau_0}^{\tau_0} d\tau \sqrt{\tau^2 + \kappa^2} = \kappa^2 \int_{-\tau_0/\kappa}^{\tau_0/\kappa} d\tau \sqrt{\tau^2 + 1} \quad (7.43)$$

$$= \frac{\kappa^2}{2} \left[\tau \sqrt{\tau^2 + 1} + \ln \left(\tau + \sqrt{\tau^2 + 1} \right) \right]_{-\tau_0/\kappa}^{\tau_0/\kappa} \quad (7.44)$$

$$\approx \frac{\kappa^2}{2} \left[\tau |\tau| \left(1 + \frac{1}{2\tau^2} \right) + \ln \left(\tau + |\tau| \left(1 + \frac{1}{2\tau^2} \right) \right) \right]_{-\tau_0/\kappa}^{\tau_0/\kappa} \quad (7.45)$$

$$\approx \tau_0^2 + \frac{\kappa^2}{2} + \kappa^2 \ln \left(\frac{2\tau_0}{\kappa} \right), \quad (7.46)$$

in the limit $\tau_0 \gg \kappa^2$. This gives

$$\Delta\phi_k := 2\zeta - \Phi_{\text{WKB}} - \frac{\pi}{2} = -\arg\Gamma \left(\frac{1 + i\kappa^2}{2} \right) - \frac{\kappa^2}{2} \left(1 + \ln \frac{2}{\kappa^2} \right). \quad (7.47)$$

In this definition a phase $\pi/2$ is subtracted. It comes from the last term in the definition of ζ , Eq. (7.36), and changes factors of the imaginary unit i in the reflection and transmission coefficients. Then the result for the reflection and transmission coefficient based on incoming and outgoing waves within the WKB solution is

$$R = -ie^{i\Delta\phi_k} \frac{e^{-\pi\kappa^2/2}}{\sqrt{1 + e^{-\pi\kappa^2}}} \quad (7.48)$$

and

$$T = e^{i\Delta\phi_k} \frac{1}{\sqrt{1 + e^{-\pi\kappa^2}}}. \quad (7.49)$$

7.2.3. Evolution of the particle number

With the help of the reflection and the transmission coefficients, the transfer matrix of the quantities α_k and β_k in Eq. (7.28) for a single scattering off the inverse parabolic potential of Sec. 7.2.2 is written as

$$\begin{pmatrix} \alpha_k^{j+1} e^{-i\theta_k^j} \\ \beta_k^{j+1} e^{+i\theta_k^j} \end{pmatrix} = \begin{pmatrix} \frac{1}{T_k} & \frac{R_k^*}{T_k^*} \\ \frac{R_k}{T_k} & \frac{1}{T_k^*} \end{pmatrix} \begin{pmatrix} \alpha_k^j e^{-i\theta_k^j} \\ \beta_k^j e^{+i\theta_k^j} \end{pmatrix}. \quad (7.50)$$

This can be verified by checking the case of a single incoming wave and the complex conjugate solution. From now on, the notation accounts for the k -dependence of R and D . Following Ref. [80] the phase θ_k^j is defined similarly to the WKB phase as

$$\theta_k^j = \int_0^{t_j} dt \omega(t). \quad (7.51)$$

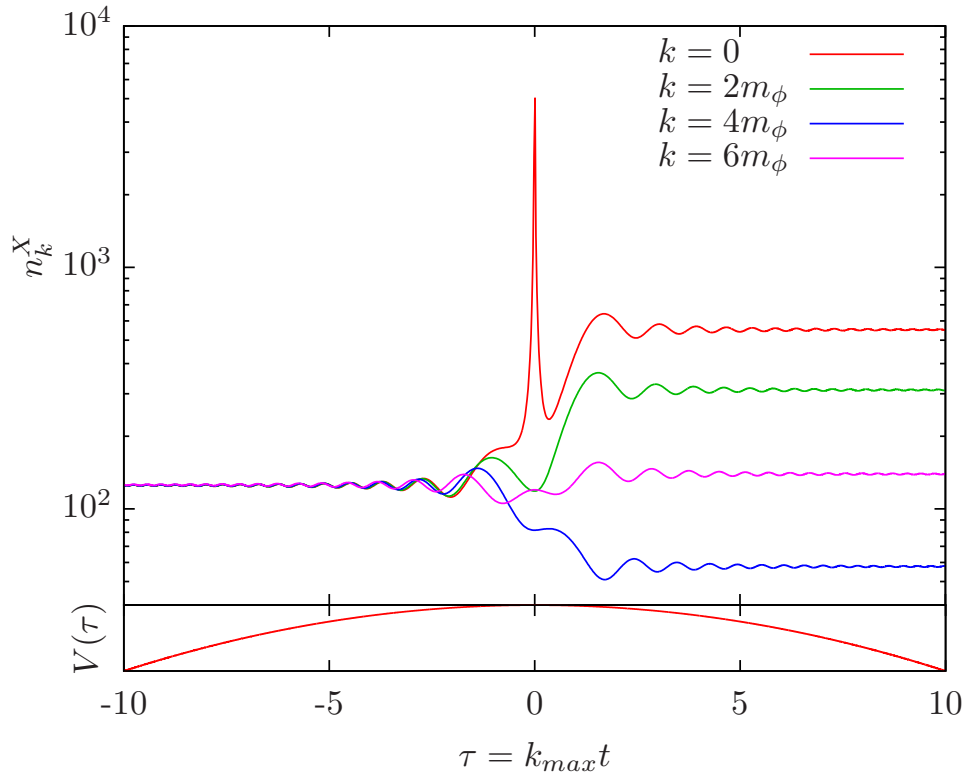


Figure 7.5.: Behavior of a wave scattered off a parabolic potential barrier. The upper panel shows the occupation number of some modes, n_k^X . Away from the maximum of the potential, which is sketched in the lower panel, the WKB solution is valid. The phase of the mode function decides whether the value of n_k^X belonging to this solution is bigger or smaller after the potential barrier.

7.2. Periodically changing mass and the Mathieu equation

Using Eqs. (7.48) and (7.49), each zero of the field ϕ is seen to have the following effect on the modes of field χ :

$$\begin{pmatrix} \alpha_k^{j+1} \\ \beta_k^{j+1} \end{pmatrix} = \begin{pmatrix} \sqrt{1 + e^{-\pi\kappa^2}} e^{-i\Delta\phi_k} & ie^{-\frac{\pi}{2}\kappa^2 + 2i\theta_k^j} \\ -ie^{-\frac{\pi}{2}\kappa^2 - 2i\theta_k^j} & \sqrt{1 + e^{-\pi\kappa^2}} e^{i\Delta\phi_k} \end{pmatrix} \begin{pmatrix} \alpha_k^j \\ \beta_k^j \end{pmatrix}. \quad (7.52)$$

Given the normalization $|\alpha_k|^2 - |\beta_k|^2 = 1$, the occupation number after the $(j+1)^{\text{th}}$ scattering is then calculated as

$$\begin{aligned} n_k^{j+1} &= \left| \beta_k^{j+1} \right|^2 \\ &= e^{-\pi\kappa^2} + \left(1 + 2e^{-\pi\kappa^2} \right) n_k^j - 2e^{-\frac{\pi}{2}\kappa^2} \sqrt{1 + e^{-\pi\kappa^2}} \sqrt{n_k^j (1 + n_k^j)} \sin \gamma_k^j, \end{aligned} \quad (7.53)$$

where growth or decay of particle number density is determined by k through the rescaled momentum κ and through the angle

$$\gamma = 2\theta_k^j - \Delta\phi_k + \arg\beta_k^j - \arg\alpha_k^j. \quad (7.54)$$

For large n_k Eq. (7.53) can be approximated as

$$n_k^{j+1} \approx \left(1 + 2e^{-\pi\kappa^2} - 2\sin \gamma_k^j e^{-\frac{\pi}{2}\kappa^2} \sqrt{1 + e^{-\pi\kappa^2}} \right) n_k^j, \quad (7.55)$$

which sets the growth parameter for the mode k in

$$n_k^{j+1} = n_k^j e^{2\pi\mu^j(k)} \quad (7.56)$$

to be

$$\mu^j(k) = \frac{1}{2\pi} \ln \left(1 + 2e^{-\pi\kappa^2} - 2e^{-\frac{\pi}{2}\kappa^2} \sqrt{1 + e^{-\pi\kappa^2}} \sin \gamma_k^j \right). \quad (7.57)$$

So, depending on γ_k^j , the occupation number can also decrease during the non-adiabatic evolution at small $\phi(t)$. Starting with a small number of particles $n_k(t_0)$ with momentum k , after N zeros of ϕ the order of magnitude of $n_k(t)$ is

$$\exp \left(2\pi \sum_{j=0}^N \mu^j(k) \right). \quad (7.58)$$

Assuming the case of a time-independent μ^j , the total number density in χ particles is then

$$n_\chi(t) = \frac{1}{(2\pi a)^3} \int d^3k n_k(t) = \frac{1}{4\pi^2 a^3} \int_{-\infty}^{\infty} dk k^2 e^{2m\mu(k)t}, \quad (7.59)$$

which gives

$$n_\chi(t) \approx \frac{1}{4\pi a^3} \frac{\tilde{k}^2 e^{2\mu(\tilde{k})mt}}{\sqrt{mt|\mu''(\tilde{k})|}} \quad (7.60)$$

when approximated within the saddle-point method. In the last formula \tilde{k} denotes the mode with the strongest growth and $\mu''(\tilde{k})$ stands for the second derivative of the

growth factor at this point. From comparison with a Gauss function, the curvature can be estimated as $|\mu''(\tilde{k})| \sim 2\mu(\tilde{k})/\Delta k^2$ as suggested by Ref. [80]. The authors of Ref. [80] estimate both the range of unstable modes in the first band (Δk) and the wavenumber \tilde{k} to be comparable to $k_{\max}/2$. Then one is led to the following formula predicting exponential growth of the number of χ particles,

$$n_\chi(t) \sim \frac{k_{\max}^3}{64\pi a^3} \sqrt{\frac{2}{\pi\mu(\tilde{k})mt}} e^{2\mu(\tilde{k})mt}. \quad (7.61)$$

7.2.4. Particle production in Minkowski spacetime

Before discussing the case of particle production within an expanding universe, in this section the scale factor is set to unity. Additionally, the formulae describing the mechanism of broad parametric resonance are derived assuming a constant amplitude ϕ_0 of the oscillating inflaton field $\phi(t)$. Then also the rescaled momentum κ in the last section is time-independent and the phase shift between two successive scattering events is always the same. This means that Eq. (7.51) simplifies to

$$\theta_k^j = j\theta_k = j \int_0^{\pi/m} dt \omega_k, \quad (7.62)$$

and θ_k , which is an important quantity for particle production, can be calculated as

$$\theta_k = \int_0^{\pi/m} dt t \sqrt{k^2 + g^2 \phi^2(t)} \quad (7.63)$$

$$\approx \frac{2g\phi_0}{m} + \frac{\kappa^2}{2} \left(\ln \frac{g\phi_0}{m\kappa^2} + 4\ln 2 + 1 \right) \quad (7.64)$$

$$= 4\sqrt{q} + \frac{k^2}{4\sqrt{q}m^2} \left(\ln \frac{4qm^2}{k^2} + 4\ln 2 + 1 \right), \quad (7.65)$$

if $k \ll g\phi_0$. The detailed steps from the first to the second line can be found in App. C, and the last line simply replaces the model quantities g, ϕ_0 , and κ by the resonance parameter q and k as defined above. The following paragraph will show the dependence of the growth index μ_k on the angles θ_k and ϕ_k : We know that for large n_k the absolute values of α_k and β_k have to be the same. Then from Eqs. (7.61) and (7.52) the ansatzes

$$\alpha_{k,\pm}^j = \frac{(\pm 1)^j}{\sqrt{2}} e^{(\pi\mu_k + i\theta_k)j}, \quad \beta_{k,\pm}^j = \frac{(\pm 1)^j}{\sqrt{2}} e^{i\vartheta_\pm e^{(\pi\mu_k + i\theta_k)j}} \quad (7.66)$$

seem reasonable. Here ϑ_\pm are two constant phases that will not be important in this context. Application in Eq. (7.52) leads to the equations

$$\pm e^{(\pi\mu_k + i\theta_k)} = \sqrt{1 + e^{-\pi\kappa^2}} e^{-i\Delta\phi_k} + ie^{-\frac{\pi}{2}\kappa^2 - i\vartheta_\pm}, \quad (7.67)$$

which determine the growth index: After isolating and removing ϑ_\pm , the solutions to a quadratic equation in $\exp(\pi\mu_k)$ suggest a distinction of the cases $\cos(\theta_k + \Delta\phi_k) \geq 0$

such that for both versions of Eq. (7.66) the stronger growth is given by

$$e^{\pi\mu_k} = |\cos(\theta_k + \Delta\phi_k)|\sqrt{1 + e^{-\pi\kappa^2}} + \sqrt{(1 + e^{-\pi\kappa^2})\cos^2(\theta_k + \Delta\phi_k) - 1}. \quad (7.68)$$

From this it is seen that real μ_k additionally requires

$$\left(1 + e^{-\pi\kappa^2}\right) \cos^2(\theta_k + \Delta\phi_k) \geq 1 \quad (7.69)$$

$$\Rightarrow |\tan(\theta_k + \Delta\phi_k)| \leq e^{-\frac{\pi}{2}\kappa^2}. \quad (7.70)$$

The last equation is the condition for a mode k to grow exponentially. The periodicity of the tangent leads to alternating regions of stability and instability. Equation (7.68) together with Eqs. (7.47) and (7.65) for $\Delta\phi_k$ and θ_k , respectively, then yields the growth parameter as a function of A_k and q . In order to calculate this it is convenient to follow an approximation suggested in [52] which amounts to

$$\arg\Gamma\left(\frac{1 + i\kappa^2}{2}\right) \approx -0.982\kappa^2, \quad (7.71)$$

yielding

$$\theta_k + \Delta\phi_k \approx 4\sqrt{q} + \frac{k^2}{8\sqrt{q}m^2}(\ln q + 9.474). \quad (7.72)$$

In Ref. [80] a comparison with numerical results shows good agreement up to the first two resonance bands.

7.3. Effects of the Hubble expansion

The Hubble expansion of an FRW universe leads to a redshift of momenta and a damping of the inflaton oscillation. So the resonance parameter $q = (g\phi_0/2m)^2$ decreases with time. The result is, that for an efficient decay of the inflaton field the initial value of q must be very large. Only then the system spends enough time in the parameter region of broad parametric resonance where strong particle production takes place. This also means that within a realistic setting, narrow parametric resonance with $q \sim 1$ occurs only when already a large number of particles has been produced. So in contrast to the approach presented in Sec. 7.2, interaction of these particles with the zero mode and other modes should then be taken into account. In this section the considerations in [80] concerning the model

$$V = \frac{1}{2}m^2\phi^2 + \frac{1}{2}g^2\phi^2X^2 \quad (7.73)$$

within an expanding background are reviewed. The results of some corresponding calculations are displayed. Following Ref. [101], the first step is to see how Hubble damping influences the oscillation of $\phi(t)$ without interaction with X : The Friedmann equation for $\phi(t)$,

$$H^2 = \frac{4\pi}{3m_{\text{Pl}}^2} \left(\dot{\phi}^2 + m^2\phi^2\right), \quad (7.74)$$

suggests a parameterization in H and in an angle α which is defined by

$$\dot{\phi} = \sqrt{\frac{3}{4\pi}} H m_{\text{Pl}} \cos \alpha, \quad m\phi = \sqrt{\frac{3}{4\pi}} H m_{\text{Pl}} \sin \alpha. \quad (7.75)$$

This together with the equation of motion,

$$\ddot{\phi} + 3H\dot{\phi} + m^2\phi = 0, \quad (7.76)$$

combines to

$$\dot{\alpha} = m + 3H \sin(\alpha) \cos(\alpha) \quad (7.77)$$

and then gives

$$\dot{H} = -3H^2 \cos^2(mt). \quad (7.78)$$

Solving for the Hubble parameter yields

$$H = \frac{2}{3t} \left(1 + \frac{\sin(2mt)}{2mt} \right)^{-1}, \quad (7.79)$$

which together with Eq. (7.75) also leaves

$$\phi(t) = \phi_0(t) \sin(mt) \left(1 + \frac{\sin(2mt)}{2mt} \right)^{-1} \approx \phi_0(t) \sin(mt), \quad (7.80)$$

where further terms are at least of order $(mt)^{-3}$ and the amplitude of the oscillating inflaton field, $\phi_0(t)$, decays with $1/t$ for large t ,

$$\phi_0(t) = \frac{m_{\text{Pl}}}{\sqrt{3\pi} mt}. \quad (7.81)$$

This result can be used for a computation that includes interaction with the second scalar X within an expanding background. Compared to the calculation presented in Sec. 7.2 the behavior of the inflaton field is now taken to follow a damped oscillation. The approximation is valid after a few oscillations of the inflaton field. The calculation starts at $t = \pi/2m$. The resulting behavior of χ modes is exemplified in Figs. 7.6 and 7.7. Another conclusion one can draw from Eq. (7.80) concerns the applicability of an analysis based on the stability/instability chart of parameter space: Applying the coupling constant $g = 5 \cdot 10^{-4}$ and the inflaton mass $m_\phi = 10^{-6} m_{\text{Pl}}$ as in the calculations above, the value of the parameter $A \approx 2q$ and its continuous decrease can be calculated. Furthermore, from the theory of Mathieu functions [84] it is known that for small q the instability bands are located at $A = n^2$ with n being a natural number. A short calculation shows that during a single oscillation of the inflaton the system sweeps over dozens of instability bands. This renders the Mathieu theory of separate instable modes inapplicable. Only later, when A has become small enough, the time a mode needs to cross a single instability band becomes longer. This enables resonant modes to grow continuously, see Fig. 7.7. Around $t/(2\pi/m_\phi) \sim 20$ the behavior lies between broad and

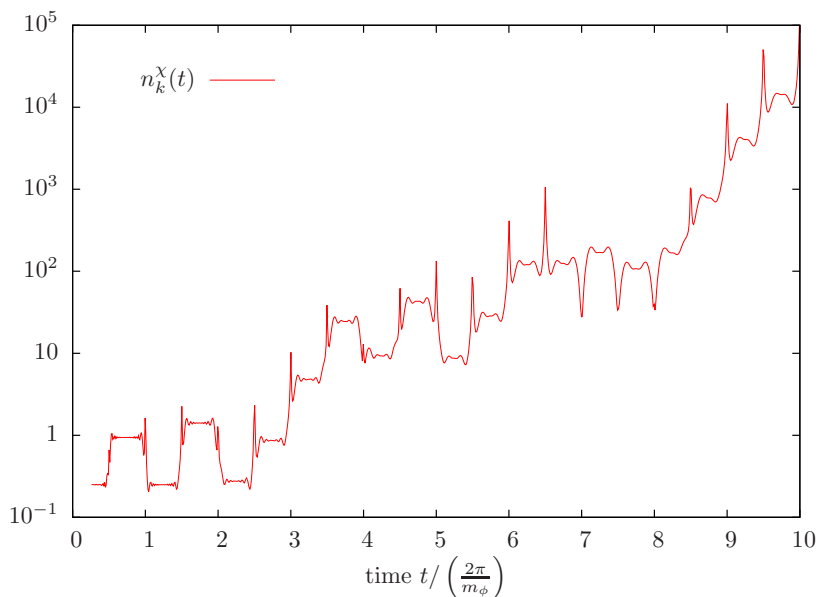


Figure 7.6.: Stochastic resonance in the model (7.73) for a comoving mode $\chi_k(t)$ within an expanding background. Equation (7.80) gives the time evolution of the inflaton $\phi(t)$ whose decreasing amplitude is reflected by the slowdown of the small oscillations in n_k^χ during the adiabatic intervals. Redshift prevents the mode from staying in the resonance band. Therefore, the growth parameter μ^j is different at each step and can also be negative.

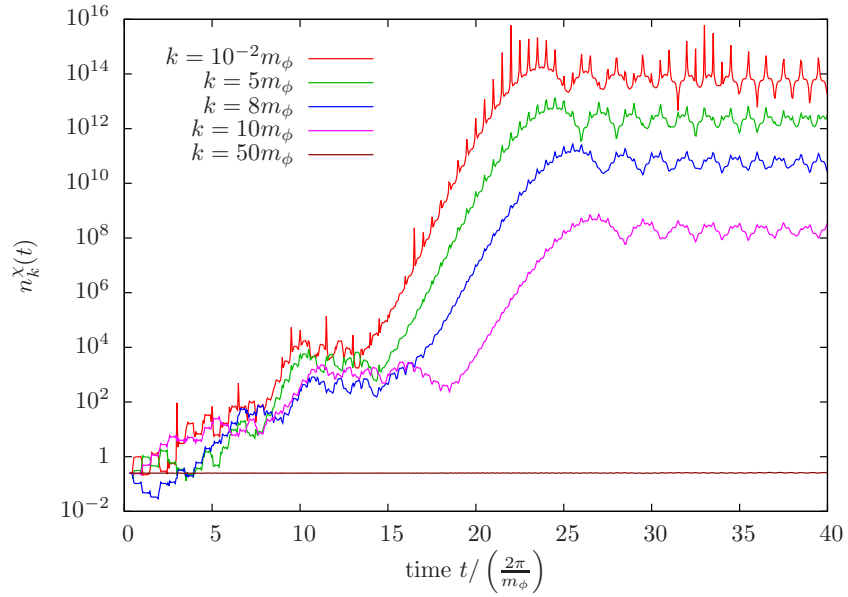


Figure 7.7.: The same setting as in Fig. 7.6 calculated for a longer time interval and for different modes. For large k the parameters do not stay in instability regions long enough for the occupation number to be considerably amplified. The strong growth of n_k which occurs for a broad region in parameter space around $t/(2\pi/m_\phi) \sim 20$ can be identified with the crossing of the last instability band. To the left of this ascent one observes a time interval of a few ϕ -oscillations with almost constant n_k . At this time the modes pass the stability region before the last instability band.

narrow resonance in Minkowski space. After $t/(2\pi/m_\phi) \sim 30$ the particle production has stopped and the stability region at small A and q is reached.

Since the parameter q is time dependent, this is also the case for the angles θ_k and $\Delta\phi_k$. Similarly to the case in Minkowski space one can calculate

$$\theta_k^j = \int_{t_j}^{t_{j+1}} dt \sqrt{\frac{k^2}{a} + g^2\phi^2(t)} \quad (7.82)$$

$$\approx \frac{2g\phi_0(t)}{m} + \frac{\kappa^2}{2} \left(\ln \frac{g\phi_0(t)}{m\kappa^2} + 4\ln 2 + 1 \right). \quad (7.83)$$

This equation shows that if q is large, θ_k^j can be treated as a random number: For a rough estimate it is enough to keep the first term. In Eq. (7.81) mt is replaced by $j\pi$ where j numbers the zeros of $\phi(t)$. Taking the derivative of

$$\theta_k^j \approx \frac{gm_{\text{Pl}}}{5mj} + O(\kappa^2) \quad (7.84)$$

gives an estimate for the variation of subsequent θ_k^j 's:

$$\delta\theta_k^j \sim \frac{gm_{\text{Pl}}}{5mj^2} \sim \frac{2\sqrt{q_0}}{j^2}, \quad (7.85)$$

where the value of the parameter q_0 after the end of inflation is estimated as

$$q_0 := \frac{\phi(t_0)}{2m} \sim \frac{gm_{\text{Pl}}}{10m} \quad (7.86)$$

when t_0 is chosen to be of order $1/m$. Therefore, $\delta\theta_k^j$ is bigger than π for the first

$$n_{\text{random}} \sim \frac{1}{2} \sqrt{\frac{5\pi m}{gm_{\text{Pl}}}} \approx \frac{q_0^{1/4}}{\sqrt{2\pi}} \quad (7.87)$$

inflaton oscillations. During this time the phase shifts θ_k for consecutive zeros of $\phi(t)$ can be treated as random. Because of Eq. (7.54) the same is done with γ . Then, from Eq. (7.55) it is seen that this renders the non-adiabatic particle number change a stochastic process. Depending on the value of γ the particle number can also decrease but the first two terms in Eq. (7.55) make this case less probable.

7.4. Preheating within $\lambda\phi^4$ theory

As a second example for preheating after inflation, a short section on $\lambda\phi^4$ theory is now included. A prominent feature of the evolution of particle number spectra immediately after inflation is a region in momentum space which shows strong particle production. In a numerical calculation this resonance peak is seen at $k \sim 1.27$, see Fig. 7.8. This result is analytically explained in the following way [63]: Transforming the equation of motion for the zero mode $\phi(t) = \langle \Phi(\mathbf{x}, t) \rangle$,

$$\ddot{\phi}(t) + 3H\dot{\phi} + \lambda\phi^3 = 0, \quad (7.88)$$

Chapter 7. Fluctuations produced after inflation: Preheating

from time t to conformal time $\eta = \int dt/a$ and defining $\varphi = a\phi$ one has

$$\varphi''(\eta) - \frac{a''}{a}\varphi(\eta) + \lambda\varphi(\eta)^3 = 0. \quad (7.89)$$

First, it is now shown that the second term is negligible in $\lambda\phi^4$ theory following the calculation in [123]: Let us assume that the field ϕ oscillates with frequency ω around the minimum of a potential $V(\phi)$ at $\phi = 0$. The timescale ω^{-1} of this oscillation is taken to be much smaller than the Hubble time, $\omega \gg H$, and so is the oscillation period of

$$\dot{\phi}^2 = \rho + p, \quad (7.90)$$

see Eq. (3.4). The slowly varying contribution to pressure and energy density is separated from the oscillating part,

$$\dot{\phi}^2 = (\gamma_s + \gamma_f)\rho. \quad (7.91)$$

The labels s and f stand for slow and fast, respectively. Energy–momentum conservation is then expressed as

$$\dot{\rho} = -3H(\rho + p) = -3H(\gamma_s + \gamma_f)\rho \quad (7.92)$$

and one finds

$$\ln\left(\frac{\rho}{\rho_0}\right) = -3 \int \gamma_s \frac{da}{a} - 3 \int H\gamma_f dt. \quad (7.93)$$

The last integral is negligible,

$$\int H\gamma_f dt = H \frac{\gamma_f}{\omega} \Big| - \int \frac{\gamma_f}{\omega} \dot{H} dt = \mathcal{O}\left(\frac{H}{\omega}\right) \ll 1, \quad (7.94)$$

allowing to write

$$\rho \propto a^{-3\gamma_s}. \quad (7.95)$$

Neglecting curvature, the Friedmann equation (2.39) gives

$$a \propto t^{2/(3\gamma_s)}. \quad (7.96)$$

The remaining step is to calculate γ_s for the potentials in question: Taking Δt as the oscillation period of ϕ one calculates

$$\gamma = \frac{1}{\Delta t} \int_0^{\Delta t} \frac{\dot{\phi}^2}{\rho} dt = \frac{\int_0^{\phi_{max}} (\dot{\phi}^2/\rho)^{1/2} d\phi}{\int_0^{\phi_{max}} (\rho/\dot{\phi}^2)^{1/2} d\phi} = 2 \frac{\int_0^{\phi_{max}} \left(1 - \frac{V}{V_{max}}\right)^{1/2} d\phi}{\int_0^{\phi_{max}} \left(1 - \frac{V}{V_{max}}\right)^{-1/2} d\phi}, \quad (7.97)$$

where the first equality follows from Eq. (7.91). The second equality relies on the fact that ρ is constant on this timescale. ϕ_{max} is the maximal displacement of the field

7.5. Preheating after hilltop inflation

and V_{max} is the corresponding potential. Concentrating on potentials $V(\phi) = \lambda\phi^n$ one computes the result [30, 62]

$$\gamma = \frac{2n}{n+2} \Rightarrow a(t) \propto t^{(n+2)/3n}, \quad (7.98)$$

which for $n = 2$ gives the expansion of a universe filled with massive particles and for $n = 4$ gives $a \propto \sqrt{t}$ as it is known from a radiation dominated universe. In this latter case Eq. (??) gives $a'' = 0$, and so (7.89) reads

$$\varphi'' + \lambda\varphi^3 = 0. \quad (7.99)$$

The solution will be an oscillating function f whose amplitude is for the moment taken to be normalized to one. f is written as a function of $x = \lambda\eta$. The stronger condition $2f'^2 = 1 - f^4$ is fulfilled by the elliptic cosine $\text{cn}(x, 1/\sqrt{2})$. The solution of the homogeneous case is now used to find the evolution of the modes φ_k which correspondingly to Eq. (7.99) follow the equation

$$\varphi_k'' + (k^2 + 3\lambda\varphi^2) \varphi_k = 0 \quad (7.100)$$

or, after inserting the homogeneous solution,

$$\varphi_k'' + \left(k^2 + 3\text{cn}^2\left(x, 1/\sqrt{2}\right)\right) \varphi_k = 0. \quad (7.101)$$

Note that in this equation the amplitude φ_{max} is not confined to unity anymore and time and momentum are measured in units of $(\sqrt{\lambda}\varphi_{max})^{\mp 1}$, respectively. Equation (7.101) is a Lamé equation having solutions with well-known stability properties, see [13]. The first resonance band at $1.22 \lesssim k \lesssim 1.32$ can be confirmed by a lattice computation. Figure 7.8 is obtained from calculations done with LATTICEEASY [50].

7.5. Preheating after hilltop inflation

In this section preheating after hilltop inflation within the potential Eq. (5.26) is discussed. Besides parametric resonance, within this potential a second mechanism of inflaton decay is observed. It stems from the negative curvature of the potential around small field values and is called tachyonic preheating. The curvature of the potential is negative during inflation and remains so also for a part of the subsequent evolution, see Fig. 5.3. The results presented in this section were obtained in [42] for the first time. The reasoning also relies on [28].

7.5.1. Slow roll and oscillations of the homogeneous field

Around the maximum of the potential at $\phi = 0$ the slow-roll parameters ϵ and η , which are defined in Eq. (5.15), are both much smaller than one. During inflation the potential Eq. (5.26) can be approximated by

$$V(\phi) = \frac{1}{16}\lambda(v^4 - \phi^4). \quad (7.102)$$

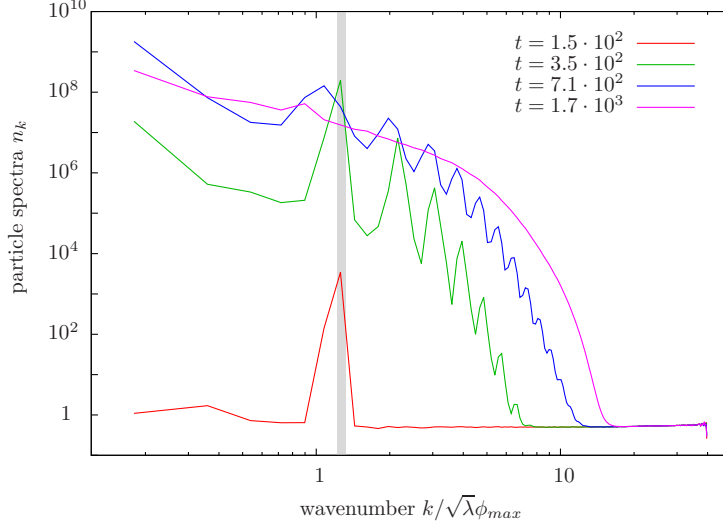


Figure 7.8.: Early evolution of the particle spectrum in $\lambda\phi^4$ theory. Correspondingly to the wavenumber, time is given in units of $(\sqrt{\lambda}\phi_{\max})^{-1}$, where ϕ_{\max} is the initial amplitude of inflaton oscillations. The shaded region around $k/\sqrt{\lambda}\phi_{\max} = 1.27$ indicates the (only) resonance band of the theory. Further peaks, which appear later, form due to scattering processes. Because the field amplitude decays with time, the peaks tend to move to the left.

Then the slow-roll parameters are

$$\epsilon \approx \frac{1}{\pi} \left(\frac{m_{\text{Pl}}}{v} \right)^2 \left(\frac{\phi}{v} \right)^6 \quad \text{and} \quad \eta = -\frac{3}{4\pi} \left(\frac{m_{\text{Pl}}}{v} \right)^2 \left(\frac{\phi}{v} \right)^2, \quad (7.103)$$

identifying η as the one which will break the slow-roll condition first. So, preheating starts around the field value $\phi_{\text{sp}} \sim v^2/m_{\text{Pl}}$, where here and in the following the label has the obvious meaning. The condensate $\langle \phi(t) \rangle$ continues rolling down the potential and starts a damped oscillation around the minimum at v . The decay of the amplitude can be estimated from energy conservation: During one oscillation period from t_j to t_{j+1} the Hubble damping amounts to

$$\Delta E = 3 \int_{t_j}^{t_{j+1}} dt H \dot{\phi}^2 = 3 \int_{\phi_j}^{\phi_{j+1}} d\phi H \dot{\phi}. \quad (7.104)$$

Approximating the Hubble parameter, the field velocity, and the distance covered by the field during one oscillation as

$$H^2 \approx H_{\text{sp}}^2 \approx \frac{V}{3m_{\text{Pl}}^2} \approx \frac{\lambda v^4}{48m_{\text{Pl}}^2}, \quad (7.105)$$

$$\dot{\phi}^2 \approx \frac{\lambda v^4}{16}, \quad \text{and} \quad (7.106)$$

$$\Delta\phi \approx 2v, \quad (7.107)$$

respectively, allows for an estimate of the integral. When the boundaries of the integrals in Eq. (7.104) are evaluated at minimal values of ϕ , only the potential contributes to ΔE . With Eq. (7.102), successive minima can be evaluated as

$$\left(\frac{\phi_n}{v}\right)^4 = \left(\frac{v}{m_{\text{Pl}}}\right)^4 + 2\sqrt{3}n\frac{v}{m_{\text{Pl}}} \approx n\frac{v}{m_{\text{Pl}}}, \quad (7.108)$$

where $n \in \mathbb{N}$ is introduced as a numeration of the minima. For small enough v the oscillatory motion of the field condensate partly goes through the tachyonic region of the potential, see Fig. 7.9. A higher energy scale v though, leads to stronger Hubble damping which prevents a recurrence to such small field values. The more important role of Hubble friction in this case is reflected in the broader regions of slow roll and inflation on the left-hand side of Fig. 5.3.

7.5.2. Tachyonic preheating

A negative curvature of the effective potential is reflected by a negative effective mass squared $m_{\text{eff}}^2 = d^2V/d\phi^2 < 0$ in the equation of motion for the modes,

$$\ddot{\phi}_k + (k^2 + m_{\text{eff}}^2)\phi_k = 0. \quad (7.109)$$

Here, interactions between the modes have been neglected. The solution for modes with small k is tachyonic. It does not oscillate but is an exponential function. To obtain an estimate of the fluctuations during preheating, their magnitude at the end of slow roll should be taken as an initial condition, see also Section 7.1. The modes with wavelengths around the Hubble scale will experience the strongest growth. This is because above the Hubble scale spacetime curvature prevents decay. So they have the smallest k for which particle production takes place. Because of the uncertainty principle their initial amplitude is expected to be $\delta\phi \sim 1/L \sim H$, where L is the wavelength of the modes. Hence, the Hubble parameter at the end of inflation can be taken as an initial condition for the fluctuations.

The growth of long wavelength inhomogeneities at the beginning of preheating can be estimated in the following way: Taking Hubble friction to be negligible, the equation of motion of the field condensate $\phi(t)$ is

$$\ddot{\phi} = -V' \quad (7.110)$$

with the time derivative

$$\ddot{\phi} = -V''\dot{\phi} \equiv -m_{\text{eff}}^2\dot{\phi}. \quad (7.111)$$

So, the derivative of the field follows the same equation of motion as the fluctuations with small k , see Eq. (7.109), yielding

$$\phi_k \propto \dot{\phi} \quad \text{and} \quad \dot{\phi}_k \propto \ddot{\phi} \propto V'. \quad (7.112)$$

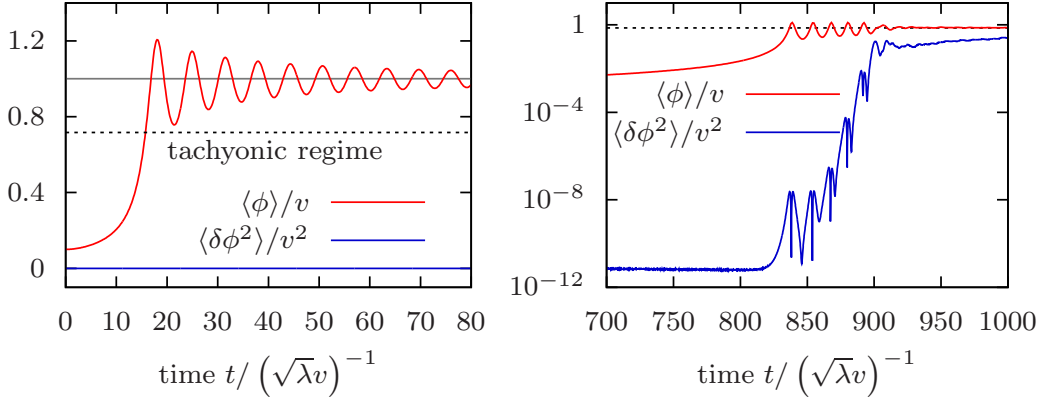


Figure 7.9.: This figure illustrates direct recalculations of Ref. [42]. The coupling constant is $\lambda = 10^{-12}$. The energy scale of the potential is $v = 0.1 m_{\text{Pl}}$ (left panel) and $v = 10^{-3} m_{\text{Pl}}$ (right panel). For high energies the inflaton field does not reenter the tachyonic regime below the dashed line and no particle production is observed. For lower energies a combination of tachyonic preheating and parametric resonance leads to a rapid decay of the zero mode.

On the other hand, in the potential Eq. (7.102) the field velocity $\dot{\phi}$ grows as ϕ^2 when rolling downhill. Therefore, also the long-wave fluctuations should show this proportionality. As mentioned above, most of the growth occurs for small k which justifies $\delta\phi \propto \dot{\phi} \propto \phi^2$. Put together, the fluctuation at the start of preheating is

$$\delta\phi_{\text{sp}} \sim H \sim \frac{\sqrt{V(\phi)}}{m_{\text{Pl}}} \sim \frac{\sqrt{\lambda} v^2}{m_{\text{Pl}}}, \quad (7.113)$$

and when $\phi = v$ for the first time, the fluctuation is

$$\delta\phi_v \sim \delta\phi_{\text{sp}} \frac{v^2}{\phi_{\text{sp}}^2} \sim \sqrt{\lambda} m_{\text{Pl}}. \quad (7.114)$$

If this fluctuation fulfills $\delta\phi_v \geq v \approx \langle \phi \rangle$, then preheating can be considered as finished already at this stage. If it is still smaller than the condensate, then the latter starts an oscillation around the potential minimum v . Of course, this goes with temporarily negative $\dot{\phi}$ and also a sign change in the mode functions ϕ_k for small k . In the upper right panel of Fig. 7.10 this is reflected by the sudden downward jumps of $|\phi_k|^2$. The asymmetry of the potential around v leads to a more rapid change of the low k mode functions when ϕ is on the right-hand side of the minimum and a slower change when ϕ is on the left-hand side. This is also the reason for the oscillations in n_k for early times and small k and in the variance of ϕ , see Fig. 7.9: When the field condensate is at the steeper (right-hand) side of the minimum, $\ddot{\phi}$ and $\dot{\phi}_k$ are large for small k , whereas on the flat (left-hand) side $\ddot{\phi}$ and $\dot{\phi}_k$ are small. The mode ϕ_k is small at both the maximal and the minimal value of $\phi(t)$. Having this in mind, a look at the equation for the number

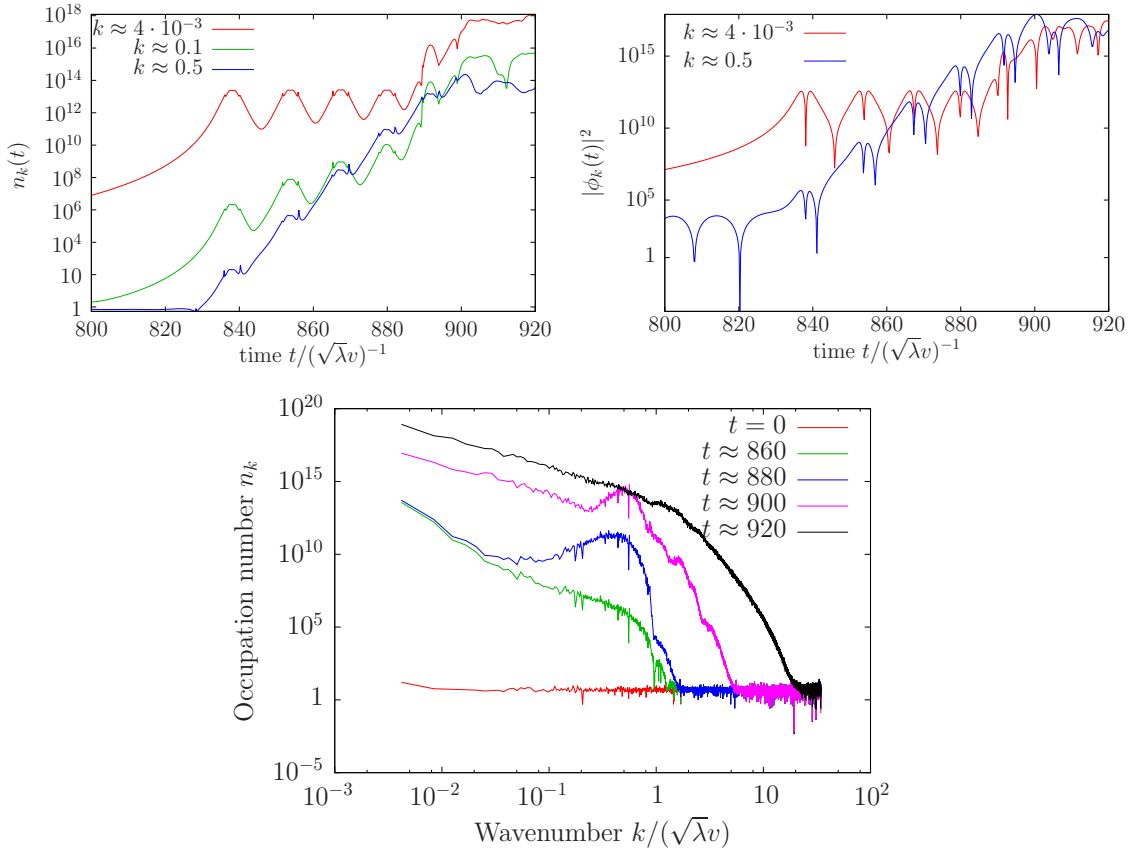


Figure 7.10.: Some results of lattice calculations within the model (5.26) at the energy scale $v = 10^{-3}m_{\text{Pl}}$. The wavenumber k is given in units of $\sqrt{\lambda}v$. Details are provided in the text.

density Eq. (B.46),

$$n_{\mathbf{k}} = \frac{1}{2} \left(\omega_k |\phi_{\mathbf{k}}(t)|^2 + \frac{1}{2\omega_k} |\dot{\phi}_{\mathbf{k}}(t)|^2 \right),$$

shows that also the number density of long-wavelength modes oscillates at the beginning of preheating. This is verified by the lattice results displayed in the upper left panel of Fig. 7.10. The small peaks before and after the maxima of $n_k(t)$ form because the frequency ω_k is zero there. For larger values of k the mode functions ϕ_k follow the behavior of $\dot{\phi}$ less closely.

7.5.3. Parametric resonance

The momentum range of tachyonic production in the UV depends on the maximal negative curvature of the potential which in the case

$$V''(\phi) = 3\lambda\phi^2 \left(\ln \frac{|\phi|}{v} + \frac{1}{3} \right) \quad (7.115)$$

is

$$V''(\phi_{\max}) = -\frac{3}{2}\lambda v^2 e^{-5/3}. \quad (7.116)$$

So the highest momenta excited tachyonically are those around $k = 0.5\sqrt{\lambda}v$. The exponential growth of these modes is weaker than for smaller k and thus there should be a different explanation for the peak at $k \approx 0.5\sqrt{\lambda}v$ and $t \approx 890$: The growth of these modes can be attributed to a period of non-adiabatic evolution around the inflection point of the potential. This is demonstrated following an estimate done in Ref. [42]: At the inflection point

$$\tilde{\phi} = v \exp(-1/3) \quad (7.117)$$

the frequency squared of fluctuations is just k^2 which leaves the low momentum modes prone to violation of adiabaticity. The corresponding condition

$$\dot{\omega} < \omega^2 \quad (7.118)$$

is indeed violated: Comparison of

$$\dot{\omega} = \frac{d}{dt} \sqrt{k^2 + V''(\phi(t))} \Big|_{\phi=\tilde{\phi}} = \frac{3}{2} \lambda \frac{\phi \dot{\phi}}{k} \Big|_{\phi=\tilde{\phi}} \quad (7.119)$$

with $\omega^2 = k^2$ gives

$$k \leq \frac{2}{3} \lambda v \quad (7.120)$$

as an approximative condition for non-adiabatic evolution around $\tilde{\phi}$. To arrive at the last inequality the field velocity is estimated from energy conservation neglecting Hubble damping. The conclusion is, that the modes around $0.5\lambda v$ can undergo strong growth as seen from Fig. 7.10. Different mechanisms leading to a peak at this momentum scale are described in Ref. [28]. Additionally, in this reference the computation of particle production is done similarly to the case in Sect. 7.2, namely by matching WKB solutions to the exact solutions of a simplified potential.

7.6. Preheating within a model with two periods of inflation

In Chapter 6 the fluctuations from inflation in the model Eq. (6.1) are discussed. The present section gives a short account on preheating within this scenario: The second inflationary period ends somewhere not too far from the origin in field space, the fields being on their way to one of the minima of the potential. This situation is similar to preheating in hilltop inflation with an additional coupling to a second field taken into account. So the evolution of the χ particle spectra is expected to resemble the one seen in Fig. 7.10. Figs. 7.11 to 7.13 depict the results of a lattice calculation using this potential.

The calculation is done within the parameter set $\lambda_0 = \lambda_1 = \lambda_2 = 10^{-13}$ and $v = 10^{-3}m_{\text{Pl}}$. As for the single field case in the preceding section, the lattice parameters are chosen following Ref. [42]: In order to cover the relevant range of momenta the necessary spatial extent of the lattice is $L \approx 1500/\sqrt{\lambda}v$. The expected momenta of growing modes range up to the scale of the curvature at the minimum of the potential, $\sqrt{\lambda}v$. Therefore, $N = 2^{14} = 16384$ lattice points¹² are necessary to resolve the whole spectrum. Assuming that the number of dimensions does not play a decisive role for the mechanisms of preheating, the computation has been done in one spatial dimension. Of course, this makes the calculation much less expensive. However, one then has to dispense with realistic statements on the late time properties of spectra being shaped by turbulence [98].

The initial values of the fields are both set to $10^{-3}v$. Presuming slow roll, the initial field velocities are set to zero. From Fig. 7.11 it is seen that the mean value of χ starts to grow whereas $\langle\phi\rangle$ stays at zero almost until χ reaches the minimum. Since all couplings λ_i are the same, the absolute values of the fields at the four minima

$$\chi_{\min} = \pm v \exp\left(\frac{\lambda_2^2}{4\lambda_0\lambda_1}\right), \quad \phi_{\min} = \pm\sqrt{\frac{\lambda_2}{2\lambda_1}}\chi_{\min}, \quad (7.121)$$

differ by a factor of $\sqrt{2}$ for the two fields. Comparison with Fig. 7.12 shows that the oscillation around these values ends when the variances have grown to almost unity. The increase of the variance is mainly because of the growth of low momentum modes, which are governed by the same equation of motion as the field velocity $\dot{\phi}$, see Sec. 7.5.

Fig. 7.13 contains the spectra of inhomogeneities of the field χ at some moments of time. The time unit is again taken as $(\sqrt{\lambda}v)^{-1}$ being the time scale of oscillations around the minimum. As has been done for Fig. 7.10, the noise of the spectra is reduced by averaging over some sets of different initial vacuum fluctuations, see App. B.2.

The shape of the spectra in Figs. 7.10 and 7.13 differs only in details. The characteristic momentum scale of the transient maximum of the spectrum shows the same dependence on the parameters of the potential. In both cases the scattering of particles out of the maximum appears as a small amplification of the modes with the approximately double momentum. Scattering processes drive the front of the spectrum to higher

¹²LATTICEASY requires the number of points to be of the form 2^n .

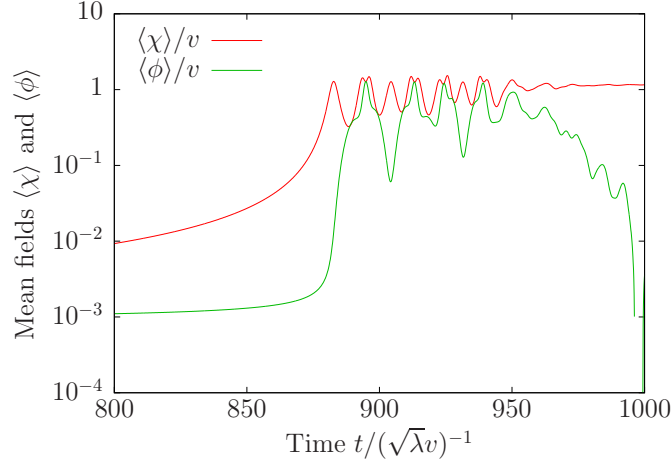


Figure 7.11.: Evolution of the means $\langle\chi\rangle$ and $\langle\phi\rangle$ after the end of inflation. In this calculation both fields start at $10^{-3}v$ with zero initial velocity. As already observed in the case of one field, Fig. 7.9, after a few oscillations the zero mode of χ is at rest in the potential minimum. The mean of ϕ can also switch between different values of minimal energy. Here and for the following Figures 7.12 and 7.13, the couplings are $\lambda_0 = \lambda_1 = \lambda_2 = 10^{-13}$ and the energy scale is $v = 10^{-3}m_{\text{Pl}}$. Field fluctuations are included.

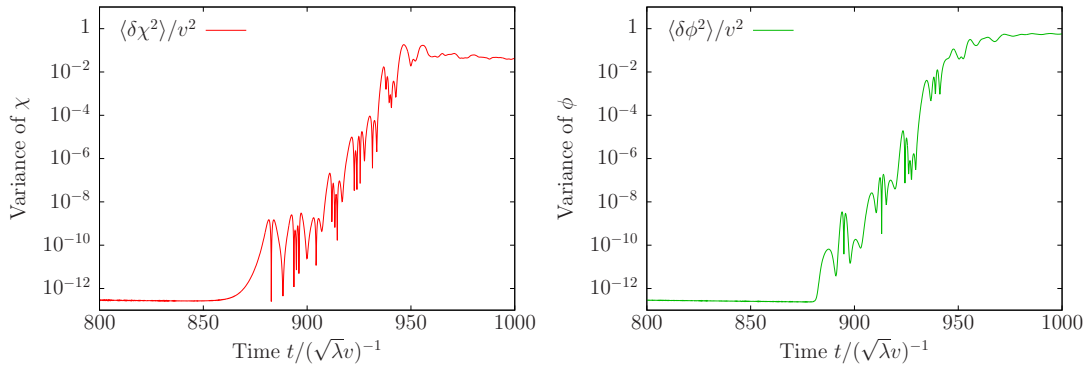


Figure 7.12.: Time dependence of the field variances in the same case as in Figs. 7.11 and 7.13. As in the single field problem discussed in Sec. 7.5, the variance of χ follows the growth of the zero mode. Inhomogeneities of ϕ evolve with a short delay, which is also observed for the mean field.

7.6. Preheating within a model with two periods of inflation

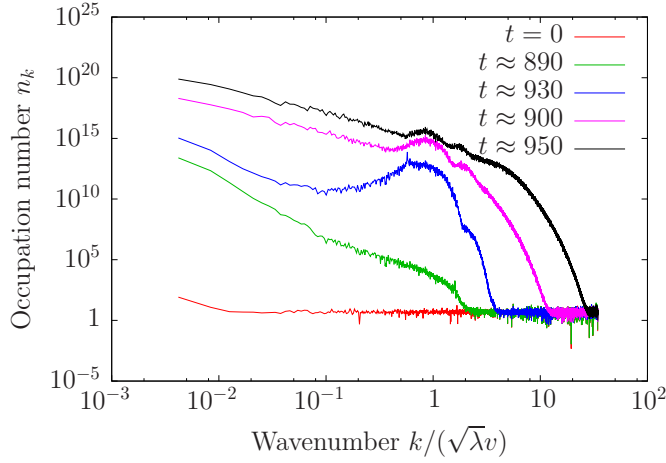


Figure 7.13.: Spectra of χ particles from the same calculation as discussed in Figs. 7.11 and 7.12. The spectra of the field ϕ are very similar and are therefore omitted. As in the case without coupling to a second scalar, a temporary maximum forms at slightly lower momenta than $\sqrt{\lambda}v$, which is the effective mass squared of χ in the minimum.

and higher momenta, finally leading to thermal equilibrium. For the field ϕ no spectra are displayed because they show no significant differences to the corresponding spectra of χ . As expected, by varying the couplings λ_i the location of the resonance scale can be moved to other values.

The calculation of preheating in the potential Eq. (6.1) has also been done for higher energy scale $v = 10^{-1}m_{\text{Pl}}$. As in the case without additional field, no efficient particle production could be observed. The variances did not grow from very small values for various combinations of the couplings.

8. Conclusion

In this thesis, calculations on the behavior of fields and particles during and after cosmological inflation have been presented. Besides a review of the results in standard inflationary models, a potential leading to two subsequent stages of inflation has been discussed. These two epochs of accelerated expansion need to correspond to two separate regions in field space where inflation is possible. In this work, the calculations concerning inflation make use of the slow-roll approximation, thus depending on the existence of two such domains, where the slow-roll conditions are fulfilled.

It has been shown that this situation is given in the potential (6.1), which is the simplified form of one that has been used to describe strongly interacting matter with effective fields. Effective field theories are motivated by their similarity to the original theory if it comes together with a significant simplification. The similarity may be measured in terms of common symmetries and other properties.

So, as it has been retraced for the example of the strong interaction, an examination of the original theory and its physics is required. Then, one can try to construct a simpler model, mimicking as much of the starting point as possible.

A lot of the symmetries of QCD are, in a similar fashion, common to other theories as well. Especially at high energies, nature seems to rediscover her inclination to unification and simplicity. Thus one might draw the conclusion that at inflationary energy scales, symmetries should play a vital role. Of course, still many possibilities remain.

For this work, the potential has been modeled on properties of QCD. Based on the linear sigma model, which incorporates chiral symmetry, an additional scalar field has been introduced to imitate the QCD-behavior under scale transformations. This has been done following the references given in Chapter 3. In one of these, Ref. [22], a dilaton-extended linear sigma model has already been used for an inflationary scenario during the cosmological QCD phase transition. In this work, the consequences of a similar potential during primordial inflation well before the QCD phase transition has been examined.

In this potential, the early stages of inflation are very similar to the corresponding ones in the quartic and quadratic potentials of large-field inflation. It has been shown that also the primordial spectrum of fluctuations that originates from this epoch does not differ significantly from the spectra produced by these inflationary models. However, as in other models of hybrid inflation, at the end of this period the fields have not reached the minimum of the potential. This occurs only after an additional waterfall

stage that can bring about a considerable number of e-foldings: In Ref. [34] such a scenario has been discussed for large amounts of inflation during the waterfall period. Then all observational inflation occurs in a small-field setting. By contrast, in Ref. [35] the second inflation is assumed to be short or absent, such that no additional e-foldings of a second inflation have to be taken into account:

Then, the first possibility is a result equivalent to chaotic inflation. This may happen when the offset of the potential has negligible effect, as it has been seen for the calculations in this thesis. It corresponds to the simplified picture of an inflaton rolling down a potential $V_0 + \lambda\phi^n/n$, where the potential is immediately set to zero when $\phi = 0$ is reached.

A second possibility is the following: The slow roll of ϕ becomes unstable much earlier. Then inflation stops at a position in the potential ϕ_{end} for which $N_e(\phi_{\text{end}}) > 1$ when computed in the respective monomic potential. The resulting spectrum resembles that from $\lambda\phi^n/n$ but its momentum scale today is shifted.

The spectra resulting from the calculations of this work are shifted, too, but towards the opposite direction: The scenario with two inflationary epochs, which is described in Chapter 6, prolongs inflation after its natural end. Instead of being interrupted early, inflation continues (after a short pause) and thus shifts the fluctuations to larger wavelengths than expected. So, the fluctuations at some physical q_0 today are similar to those which are expected from monomic inflation at some smaller momentum scale. They will enter the horizon at some time in the future. This is equivalent to the following statement: The fluctuations obtained from CMB measurements and being linked to a certain number of e-foldings subsequent to their horizon exit, exhibit features, which are expected from fluctuations connected to some significantly smaller value of N_e , when a monomic potential is assumed to drive inflation. The case with negligible second inflation ($N_e^{(2)} \ll 10$) gives spectra indistinguishable from the $\lambda\phi^n/n$ standard scenario and is therefore omitted from further discussion. It has already been justified in Chapter 6 that the discussion concentrates on parameter sets with $N_e^{(2)} \in (10, 60)$: Larger values would imply pure small-field inflation in the observable range, belonging to the standard scenarios of Section 5.5. Altogether, this means that the setting introduced here includes a transition from large-field inflation to small-field inflation after the modes constrained by CMB observations have left the horizon. This might cause a problem if it cannot be excluded that preheating sets in after the end of the first inflation, frustrating a subsequent restart of accelerated expansion.

For this thesis it has been assumed that particle production is overcome by Hubble dilution, and inflaton decay around $\phi = 0$ need not be accounted for. Taken into the extreme, one could consider the alternative of an uninterrupted inflation. However, while it proves difficult to rule out a viable scenario with one uninterrupted inflation, no parameter set has been found that allows for a smooth transition from large-field to small-field inflation such that both types of inflation with their typical features would show up in the observable range. Typically, inflation is either interrupted, where the

interruption needs to take place outside the CMB range in order not to be ruled out by measurements; or inflation continues down to $\phi = 0$ giving rise to many e-foldings for small ϕ . The evolution either gets stuck around $\phi = 0$ or there is at least such a strong expansion during this stage that there remains no possibility of observable large-field inflation. As already stated, this leads to the conclusion that parameter sets with $N_e^{(2)} \notin [10, 60]$ should be discarded. Also within this range the resulting spectra coincide better with measurements for smaller $N_e^{(2)}$.

It has been argued in this thesis that the resulting spectra should not be altered significantly when the computation includes multifield dynamics. This is because multifield effects such as entropy modes are only expected when the path in field space is curved. This curvature, however, typically occurs only at one point in the evolution and also coincides with the aforementioned interruption of inflation. For this thesis both, multifield dynamics and possible preheating during the interruption are neglected. This should be treated more thoroughly in future work.

APPENDIX

A. Equations of linearized General Relativity

In this appendix the Einstein equations for fluctuations on a FRW background are derived. In addition the derivation of the energy-momentum conservation equation for fluctuations is presented. The calculations are done within the gauge $h_{0i} = 0$. The presentation relies on [59, 60].

A.1. Linearized Einstein tensor

In this section the Einstein tensor for the metric

$$\gamma_{\mu\nu} = \eta_{\mu\nu} + h_{\mu\nu} \quad (\text{A.1})$$

is obtained. Only the linear order in $h_{\mu\nu}$ is accounted for. Then the Christoffel symbols are

$$\gamma_{\mu\nu}^{\lambda} = \frac{1}{2}\gamma^{\lambda\rho} (\partial_{\mu}\gamma_{\rho\nu} + \partial_{\nu}\gamma_{\rho\mu} - \partial_{\rho}\gamma_{\mu\nu}) \quad (\text{A.2})$$

$$= \frac{1}{2}\eta^{\lambda\rho} (\partial_{\mu}h_{\rho\nu} + \partial_{\nu}h_{\rho\mu} - \partial_{\rho}h_{\mu\nu}) \quad (\text{A.3})$$

$$= \frac{1}{2}(\partial_{\mu}h_{\nu}^{\lambda} + \partial_{\nu}h_{\mu}^{\lambda} - \partial^{\lambda}h_{\mu\nu}) \quad (\text{A.4})$$

where the different arrangement of indices of $\gamma_{\mu\nu}^{\lambda}$ prevents confusion with the metric. Here the following $\gamma_{\mu\nu}^{\lambda}$ are needed:

$$\gamma_{00}^0 = \frac{1}{2}h'_{00}, \quad \gamma_{0i}^0 = \frac{1}{2}\partial_i h_{00}, \quad \gamma_{ij}^0 = -\frac{1}{2}h'_{ij}. \quad (\text{A.5})$$

Note that they are calculated with the simplification $h_{0i} = 0$. From the formula for the Riemann tensor (2.20) the Ricci tensor is seen to be

$$R_{\mu\nu}(\gamma) = \partial_{\lambda}\gamma_{\mu\nu}^{\lambda} - \partial_{\mu}\gamma_{\lambda\nu}^{\lambda} + \gamma_{\rho\lambda}^{\lambda}\gamma_{\mu\nu}^{\rho} - \gamma_{\rho\mu}^{\lambda}\gamma_{\nu\lambda}^{\rho}. \quad (\text{A.6})$$

Only the first two terms contribute to first order. Then it is

$$R_{\mu\nu}(\gamma) = \frac{1}{2} \left(\partial_{\mu}\partial_{\lambda}h_{\nu}^{\lambda} + \partial_{\nu}\partial_{\lambda}h_{\mu}^{\lambda} - \partial_{\lambda}\partial^{\lambda}h_{\mu\nu} - \partial_{\mu}\partial_{\nu}h_{\lambda}^{\lambda} \right) \quad (\text{A.7})$$

Appendix A

and finally

$$R(\gamma) = R_\mu^\mu(\gamma) = \partial_\mu \partial_\nu h^{\mu\nu} - \partial_\mu \partial^\mu h_\nu^\nu \quad (\text{A.8})$$

for the Ricci scalar. Note that also index contraction must not entail higher order in $h_{\mu\nu}$. Let us finally note down the Einstein tensor:

$$G_{\mu\nu}(\gamma) = R_{\mu\nu}(\gamma) - \frac{1}{2}\eta_{\mu\nu}R(\gamma). \quad (\text{A.9})$$

In order to make use of the helicity decomposition described in Section 2.2.3, it is useful to write out the sum in Eq. (A.7). With the definitions $h = h_{ii}$ and $\Delta = \partial_i \partial_i$ it is

$$R_0^0(\gamma) = \frac{1}{2}(h'' + \Delta h_{00}), \quad (\text{A.10})$$

$$R_i^0(\gamma) = \frac{1}{2}(\partial_i h' - \partial_j h'_{ij}), \quad (\text{A.11})$$

$$R_j^i(\gamma) = \frac{1}{2}(\partial_i \partial_k h_{jk} + \partial_j \partial_k h_{ik} + h''_{ij} - \Delta h_{ij} + \partial_i \partial_j h_{00} - \partial_i \partial_j h), \quad (\text{A.12})$$

where the Latin indices are summed over irrespectively of being on the same level. Recall that lowering a spatial index gives a sign change. The result for the Ricci scalar is

$$R(\gamma) = h'' + \Delta h_{00} + \partial_i \partial_j h_{ij} - \Delta h. \quad (\text{A.13})$$

A.2. Conformal transformations

In the last section the calculation of geometric quantities corresponding to a perturbed metric $\gamma_{\mu\nu}$ has been presented. The next step is to connect them to their counterparts corresponding to the metric $g_{\mu\nu}$ that results from $\gamma_{\mu\nu}$ after a conformal transformation. By convention this is phrased as

$$g_{\mu\nu} = e^{2\varphi(x)} \gamma_{\mu\nu}, \quad (\text{A.14})$$

where $\varphi(x)$ is an arbitrary smooth function. Below this will be applied to $\varphi = \ln a$. The Christoffel symbols transform as

$$\Gamma_{\nu\lambda}^\mu(g) = \Gamma_{\nu\lambda}^\mu(\gamma) + \delta_\lambda^\mu \partial_\nu \varphi + \delta_\nu^\mu \partial_\lambda \varphi - g^{\mu\rho} g_{\nu\lambda} \partial_\rho \varphi. \quad (\text{A.15})$$

The Ricci tensor is obtained from the contraction of Eq. (2.20) as

$$R_{\mu\nu}(g) = \partial_\lambda \Gamma_{\mu\nu}^\lambda(g) - \partial_\mu \Gamma_{\lambda\nu}^\lambda(g) + \Gamma_{\rho\lambda}^\lambda(g) \Gamma_{\mu\nu}^\rho(g) - \Gamma_{\rho\mu}^\lambda(g) \Gamma_{\nu\lambda}^\rho(g). \quad (\text{A.16})$$

Here Eq. (A.15) has to be inserted. After reorganizing the expression the result is

$$R_{\mu\nu}(g) = R_{\mu\nu} - 2\nabla_\mu \partial_\nu \varphi - \gamma_{\mu\nu} \gamma^{\lambda\rho} \nabla_\lambda \partial_\rho \varphi + 2\partial_\mu \varphi \partial_\nu \varphi - 2\gamma_{\mu\nu} \gamma^{\lambda\rho} \partial_\lambda \varphi \partial_\rho \varphi, \quad (\text{A.17})$$

where all expressions on the right hand side are evaluated with the help of the metric $\gamma_{\mu\nu}$. Contraction with $g^{\mu\nu}$ yields the Ricci scalar $R(g)$ in terms of $\gamma_{\mu\nu}$ and the function φ ,

$$R(g) = e^{-2\varphi} (R - 6\gamma^{\mu\nu} \nabla_\mu \partial_\nu \varphi - 6\gamma^{\mu\nu} \partial_\mu \varphi \partial_\nu \varphi) \quad (\text{A.18})$$

A.3. Linearization within FRW background

Again, the right hand side is calculated in terms of $\gamma_{\mu\nu}$. This holds also for the following formula for the Einstein tensor,

$$G_{\mu\nu}(g) = G_{\mu\nu}(\gamma) - 2\nabla_\mu\partial_\nu\varphi + 2\partial_\mu\varphi\partial_\nu\varphi + \gamma_{\mu\nu}\gamma^{\lambda\rho}(2\nabla_\lambda\partial_\rho\varphi + \partial_\lambda\varphi\partial_\rho\varphi). \quad (\text{A.19})$$

Applied to the situation in cosmology, $\varphi = \ln a$, this reads

$$G_{\mu\nu}(g) = G_{\mu\nu}(\gamma) - \frac{2}{a}\nabla_\mu\partial_\nu a + \frac{4}{a^2}\partial_\mu a\partial_\nu a + \gamma_{\mu\nu}\gamma^{\lambda\rho}\left(\frac{2}{a}\nabla_\lambda\partial_\rho a - \frac{1}{a^2}\partial_\lambda a\partial_\rho a\right). \quad (\text{A.20})$$

Index raising of $G_{\mu\nu}(g)$ is done with the metric $g_{\mu\nu}$ and results in

$$a^2 G_\nu^\mu(g) = G_\nu^\mu(\gamma) - 2\gamma^{\mu\lambda}\frac{\nabla_\lambda\partial_\nu a}{a} + 4\gamma^{\mu\lambda}\frac{\partial_\lambda a\partial_\nu a}{a^2} + \delta_\nu^\mu\gamma^{\lambda\rho}\left(2\frac{\nabla_\lambda\partial_\rho a}{a} - \frac{\partial_\lambda a\partial_\rho a}{a^2}\right). \quad (\text{A.21})$$

A.3. Linearization within FRW background

The Einstein tensor after the conformal transformation $g_{\mu\nu} = a(\eta)^2\gamma_{\mu\nu}$ has been obtained in Eq. (A.21). Linearization gives

$$\begin{aligned} a^2\delta G_\nu^\mu(g) &= G_\nu^\mu(\gamma) + 2h^{\mu\lambda}\frac{\partial_\lambda\partial_\nu a}{a} - 2\eta^{\mu\lambda}\frac{\nabla_\lambda\partial_\nu a}{a} - 4h^{\mu\lambda}\frac{\partial_\lambda a\partial_\nu a}{a^2} \\ &\quad - \delta_\nu^\mu h^{\lambda\rho}\left(2\frac{\partial_\lambda\partial_\rho a}{a} - \frac{\partial_\lambda a\partial_\rho a}{a^2}\right) + 2\delta_\nu^\mu\eta^{\lambda\rho}\frac{\nabla_\lambda\partial_\rho a}{a} \end{aligned} \quad (\text{A.22})$$

$$\begin{aligned} &= R_\nu^\mu(\gamma) + 2h^{\mu\lambda}\frac{\partial_\lambda\partial_\nu a}{a} + 2\eta^{\mu\lambda}\gamma_{\lambda\nu}^\sigma\frac{\partial_\sigma a}{a} - 4h^{\mu\lambda}\frac{\partial_\lambda a\partial_\nu a}{a^2} \\ &\quad - \delta_\nu^\mu\left(\frac{1}{2}R(\gamma) + 2h^{\lambda\rho}\frac{\partial_\lambda\partial_\rho a}{a} - h^{\lambda\rho}\frac{\partial_\lambda a\partial_\rho a}{a^2} + 2\eta^{\lambda\rho}\gamma_{\lambda\rho}^\sigma\frac{\partial_\sigma a}{a}\right), \end{aligned} \quad (\text{A.23})$$

where $G_\nu^\mu(\gamma)$, $R_\nu^\mu(\gamma)$, and $R(\gamma)$ are already of first order in the perturbation. The components are obtained with the help of the previous results in Eqs. (A.10) to (A.13): Plugging in, reorganizing, and making use of $h_{0i} = 0$ yields

$$a^2\delta G_0^0 = -3h_{00}\frac{a'^2}{a^2} - \frac{1}{2}\partial_i\partial_j h_{ij} + \frac{1}{2}\Delta h - h'\frac{a'}{a}, \quad (\text{A.24})$$

$$a^2\delta G_i^0 = \frac{1}{2}\partial_i h' - \frac{1}{2}\partial_j h'_{ij} + \frac{a'}{a}\partial_i h_{00}, \quad (\text{A.25})$$

$$\begin{aligned} a^2\delta G_j^i &= \frac{1}{2}\partial_i\partial_k h_{jk} + \frac{1}{2}\partial_j\partial_k h_{ik} + \frac{1}{2}h''_{ij} - \frac{1}{2}\Delta h_{ij} + \frac{1}{2}\partial_i\partial_j(h_{00} - h) + \frac{a'}{a}h'_{ij} \\ &\quad - \delta_j^i\left\{\frac{1}{2}h'' + \frac{1}{2}\Delta h_{00} + \frac{1}{2}\partial_l\partial_k h_{lk} - \frac{1}{2}\Delta h + 2\frac{a''}{a}h_{00} - \frac{a'^2}{a^2}h_{00} + \frac{a'}{a}(h'_{00} + h')\right\}. \end{aligned} \quad (\text{A.26})$$

Now the decomposition of the metric perturbation, Eq. (2.60) is used. As in Section 2.2.3 the coordinate system is chosen such that $E = 0$ additionally to $h_{0i} = 0$ (conformal Newtonian gauge). For the scalar perturbations this means

$$h_{00} = 2\Phi, \quad h_{0i} = 0, \quad h_{ij} = -2\Psi\delta_{ij}, \quad (\text{A.27})$$

Appendix A

which simplifies Eqs. (A.24) to (A.26):

$$a^2 \delta G_0^0 = -6\Phi \frac{a'^2}{a^2} - 2\Delta\Psi + 6\Psi' \frac{a'}{a}, \quad (\text{A.28})$$

$$a^2 \delta G_i^0 = -2\partial_i\Psi' + 2\frac{a'}{a}\partial_i\Phi, \quad (\text{A.29})$$

$$a^2 \delta G_j^i = \partial_i\partial_j(\Psi + \Phi) + \delta_{ij} \left\{ 2\Psi'' - \Delta\Psi - \Delta\Phi + 2\frac{a'}{a}(2\Psi' - \Phi') - 4\frac{a''}{a}\Phi + 2\frac{a'^2}{a^2}\Phi \right\}. \quad (\text{A.30})$$

A.4. Linearized evolution equations

The components of the linearized energy-momentum tensor have been derived in Eq. (2.74),

$$\delta T_0^0 = \delta\rho, \quad (\text{A.31})$$

$$\delta T_i^0 = -(\bar{\rho} + \bar{p})v_i, \quad (\text{A.32})$$

$$\delta T_j^i = -\delta_j^i\delta p. \quad (\text{A.33})$$

Comparison of Eqs. (A.30) and (A.33) yields $\Psi = -\Phi$ for an ideal fluid because the first term in Eq. (A.30), $k_i k_j(\Psi_{\mathbf{k}} + \Phi_{\mathbf{k}})$, is independent from $\delta_{ij}\delta p_{\mathbf{k}}$.

Put together, the 00- and the 0*i*-components of the Einstein equation for scalar perturbations read

$$\Delta\Phi - 3\frac{a'}{a}\Phi' - 3\frac{a'^2}{a^2}\Phi = \frac{4\pi a^2}{m_{\text{Pl}}^2}\delta\rho \quad (\text{A.34})$$

$$\text{and } \Phi' + \frac{a'}{a}\Phi = -\frac{4\pi}{m_{\text{Pl}}^2}(\bar{\rho} + \bar{p})v, \quad (\text{A.35})$$

respectively. The remaining part of Eq. (A.30) is the one in curly brackets. Together with Eq. (A.33) it gives

$$2\frac{a''}{a}\Phi - \frac{a'^2}{a^2}\Phi = \frac{4\pi a^2}{m_{\text{Pl}}^2}\delta\rho \quad (\text{A.36})$$

The formulation of energy-momentum conservation makes use of covariant derivatives. They include the Christoffel symbols of the metric $g_{\mu\nu} = a^2(\eta_{\mu\nu} + h_{\mu\nu})$:

$$\Gamma_{00}^0 = \frac{a'}{a} + \frac{1}{2}h'_{00}, \quad (\text{A.37})$$

$$\Gamma_{0i}^0 = \Gamma_{00}^i = \frac{1}{2}\partial_i h_{00}, \quad (\text{A.38})$$

$$\Gamma_{0j}^i = \frac{a'}{a}\delta_{ij} - \frac{1}{2}h'_{ij}, \quad (\text{A.39})$$

$$\Gamma_{ij}^0 = \frac{a'}{a}(1 - h_{00})\delta_{ij} - \frac{a'}{a}h_{ij} - \frac{1}{2}h'_{ij}, \quad (\text{A.40})$$

$$\Gamma_{jk}^i = -\frac{1}{2}(\partial_j h_{ik} + \partial_k h_{ij} - \partial_i h_{jk}). \quad (\text{A.41})$$

A.4. Linearized evolution equations

Then the zero component of energy-momentum conservation is

$$\nabla_{\mu} T_0^{\mu} = \delta\rho' + 3\frac{a'}{a}(\delta\rho + \delta p) + (\bar{\rho} + \bar{p})(3\Psi' - \Delta E' + \partial_i v_i) = 0 \quad (\text{A.42})$$

and the spatial components are

$$\nabla_{\mu} T_i^{\mu} = -((\bar{\rho} + \bar{p})v_i)' - \partial_i \delta p - (\bar{\rho} + \bar{p}) \left(4\frac{a'}{a}v_i + \partial_i \Phi \right) = 0 \quad (\text{A.43})$$

for an ideal fluid. In the gauge $E = 0$ and with $\Phi = \Psi$, Eq. (A.42) simplifies to

$$\delta\rho' + 3\frac{a'}{a}(\delta\rho + \delta p) + (\bar{\rho} + \bar{p})(3\Psi' + \partial_i v_i) = 0. \quad (\text{A.44})$$

In the case of a non-ideal fluid one has to account for anisotropic stress which is added to the spatial components of the energy-momentum tensor:

$$\delta T_j^i = -\delta_j^i \delta p - \Pi_j^i. \quad (\text{A.45})$$

The additional component is traceless and symmetric and it is treated as a small perturbation. Being transverse, $\partial_i \Pi_j^i = 0$, it respects the energy-momentum conservation, which is also true for the corresponding part of the Einstein tensor, h_{ij}^{TT} in Eq. (2.60). The equation of motion for this piece of the metric is obtained by inserting the transverse traceless part of this equation, i.e. h_{ij}^{TT} , into Eq. (A.30) and equating it to Eq. (A.45). The result is

$$(h_{ij}^{TT})'' + 2\frac{a'}{a}(h_{ij}^{TT})' - \Delta h_{ij}^{TT} = -\frac{16\pi a^2}{m_{\text{Pl}}^2} \Pi_{ij}^{TT} \quad (\text{A.46})$$

Its solution is a gravitational wave. Ideal fluids do not source gravitational waves. Instead, within such a medium they propagate freely through spacetime as long as their scale is much smaller than the Hubble scale.

B. A short reference to LATTICEEASY

Many calculations being used in this work have been done with LATTICEEASY [50], an open source lattice code for C++ written by Gary Felder and Igor Tkachev. Here a short account on its properties is given using the documentation on [51] by the same authors. LATTICEEASY and also its parallel computing version CLUSTEREASY [49] can be downloaded from [51].

LATTICEEASY solves the classical Euler-Lagrange equations of scalar fields (??) on a rectangular lattice in real space with N lattice points for each spatial dimension. If needed the simulation can be done within an expanding background and with the number of dimensions reduced to $d = 2$ or 1 .

Before doing a calculation LATTICEEASY must be provided with the number of scalar fields in the problem, with their potential, and with derivatives of the potential with respect to the fields. Suitable values for the number of lattice points in real space, N , and the length of the lattice, L , have to be chosen. They determine the spectrum which can be resolved within the calculation. $1/L$ sets the smallest value of momentum k that can be resolved and N/L fixes the largest one.

Possible output includes the field values on the lattice points, means and variances of the fields, as well as spectra of energy or occupation numbers.

B.1. General lattice issues

When doing a calculation on a lattice one has to care for its finite size L and the finite spacing $\Delta x = L/N$. To do so let us start from a quantity like $\langle f^2(\mathbf{x}) \rangle$, where the brackets $\langle \dots \rangle$ stand for taking the mean over all lattice points. $\langle f^2(\mathbf{x}) \rangle$ may well depend on Δx , because the spacing sets the UV cutoff for Fourier modes, but should be independent of L . With the following definition of the Fourier transformation for infinitely large spatial Volumes,

$$F^\infty(\mathbf{k}) := \int d\mathbf{x} f(\mathbf{x}) e^{-i\mathbf{k}\mathbf{x}}, \quad (\text{B.1})$$

this leads to

$$\langle f^2(\mathbf{x}) \rangle = \frac{1}{L^d} \int_{\text{Vol.}} f^2(\mathbf{x}) d\mathbf{x} \quad (\text{B.2})$$

$$= \frac{1}{L^d (2\pi)^d} \int d\mathbf{x} d\mathbf{y} d\mathbf{k} f(\mathbf{x}) f(\mathbf{y}) e^{i\mathbf{k}(\mathbf{x}-\mathbf{y})} \quad (\text{B.3})$$

$$= \frac{1}{L^d} \int d\mathbf{k} |F^\infty(\mathbf{k})|^2 = \int d\mathbf{k} |F(\mathbf{k})|^2, \quad (\text{B.4})$$

where in the last line the finite space Fourier transformed $F(\mathbf{k}) := L^{-d/2} F^\infty(\mathbf{k})$ has been defined. So in order to keep $\langle f^2(\mathbf{x}) \rangle$ independent of the spatial extent L , for example the initial fluctuations should be set in terms of $F(\mathbf{k})$ which is the relevant quantity in our context. The implementation of the initial conditions will be discussed below. Let us now turn to the finite lattice spacing Δx : Since LATTICEEASY evolves the fields in discretized real space, the Fourier transform to be dealt with is not exactly $F(\mathbf{k})$ but

$$f(\mathbf{k}) = \sum_{\mathbf{x}} f(\mathbf{x}) e^{-2\pi i \mathbf{k} \mathbf{x} / N} \quad (\text{B.5})$$

$$\rightarrow \frac{1}{\Delta x^3} \int d\mathbf{x} f(\mathbf{x}) e^{-2\pi i \mathbf{k} \mathbf{x} / N} \quad (\text{B.6})$$

$$= \frac{1}{\Delta x^3} F^\infty(\mathbf{k}) = \frac{L^{d/2}}{\Delta x^3} F(\mathbf{k}), \quad (\text{B.7})$$

where, correspondingly to the discreteness of \mathbf{x} -space, $f(\mathbf{k})$ has a periodicity N . For Eq. (B.6) the sum has been turned into the corresponding integral in the limit $\Delta x \rightarrow 0$.

While computing the time evolution the time-steps Δt have to be small enough in order to make a stable behavior possible. More precisely, Δt should meet the Courant stability condition [40],

$$\Delta t < \frac{\Delta x}{\sqrt{\text{dim}}}, \quad (\text{B.8})$$

which for dim dimensions ensures that the physical dependence region of any space-time point $\mathbf{x}(t)$ (i.e. the region in space-time which can possibly influence the solution at $\mathbf{x}(t)$) lies inside the numerical dependence region of that point (i.e. within the numerical problem each point on the lattice can be reached by information of at least all lattice points within the corresponding physical dependence region). This is a necessary condition for convergence to the analytical solution.

B.2. The implementation of vacuum fluctuations

In Section 7.1 it is described how the spectrum of vacuum fluctuations in an expanding space can be calculated. An account on the implementation as initial conditions of some of the calculations is given here. The probability distribution of modes of a scalar field follows Eq. (7.14) which is written down again with k replaced by $\omega(k)$ in order to generalize for a massive field:

$$\mathcal{P}[\varphi(\mathbf{k}, \eta_0)] \propto \exp \left\{ -2\omega(k) |\varphi(\mathbf{k}, \eta_0)|^2 \right\}. \quad (\text{B.9})$$

B.2. The implementation of vacuum fluctuations

The corresponding normalized distribution of the absolute value is

$$\mathcal{P} [|\varphi(\mathbf{k}, \eta_0)|] = 4\omega(k)|\varphi(\mathbf{k}, \eta_0)|\exp \{-2\omega(k)|\varphi(\mathbf{k}, \eta_0)|^2\}. \quad (\text{B.10})$$

To obtain numbers which are distributed according to this Rayleigh function LAT-TICEEASY first generates a random number on the basis of a constant probability distribution in the interval $(0, 1)$

$$\mathcal{P}_{\text{uni}}[x]dx = \begin{cases} dx & \text{if } 0 < x < 1 \\ 0 & \text{otherwise.} \end{cases} \quad (\text{B.11})$$

From the transformation law to an arbitrary probability distribution,

$$|\mathcal{P} [|\varphi_{\mathbf{k}}|] d\varphi_{\mathbf{k}}| = |\mathcal{P}_{\text{uni}}[x]dx|, \quad (\text{B.12})$$

one sees

$$\mathcal{P} [|\varphi_{\mathbf{k}}|] = \mathcal{P}_{\text{uni}}[x] \left| \frac{dx}{d\varphi_{\mathbf{k}}} \right|, \quad (\text{B.13})$$

where $\varphi_{\mathbf{k}}$ is shorthand for $\varphi(\mathbf{k}, \eta_0)$. The last equation leads to

$$x = \int_0^{\varphi_{\mathbf{k}}} \mathcal{P} [|\tilde{\varphi}_{\mathbf{k}}|] d\tilde{\varphi}_{\mathbf{k}}. \quad (\text{B.14})$$

This is to be resolved for $\varphi_{\mathbf{k}}(x)$ which sets the absolute value of the mode function following the distribution (B.10). The phase of each mode function is drawn from a uniformly distributed sample.

There are some further issues connected with the time dependence of field fluctuations: So, in order to generate isotropic initial conditions one should initialize each mode as a superposition of waves moving in opposite directions, for example as a standing wave. Another point concerns calculations on lattices with one or two spatial dimensions. These can be done for different reasons: First, in order to check the theoretical predictions for a reduced number of dimensions numerically, and second in order to save computation time. If it is for the latter reason, one should correct the resulting spectra by a factor which renders the contribution of each mode to the variance equal to the amount in the three-dimensional case. In the rest of this section the corresponding calculation is presented:

From the definition of a discrete Fourier transform in Eq. (B.5) it is seen

$$f(\mathbf{x}) = \frac{1}{N^d} \sum_{\mathbf{k}} f(\mathbf{k}) e^{2\pi i \mathbf{k} \mathbf{x} / N} \quad (\text{B.15})$$

$$\Rightarrow \langle |f(\mathbf{x})|^2 \rangle = \frac{1}{N^{2d}} \sum_{\mathbf{k}} |f(\mathbf{k})|^2. \quad (\text{B.16})$$

The isotropic system allows for a reduction to a one-dimensional sum. In three dimensions this leads to the Jacobian $2\pi \mathbf{n}^2$ in the following expression,

$$\langle |f(\mathbf{x})|^2 \rangle \approx \frac{1}{N^6} \sum 2\pi \mathbf{n}^2 |f(k)|^2, \quad (\text{B.17})$$

Appendix B

where \mathbf{n} is the momentum \mathbf{k} in the units of the Fourier transformed lattice, $\mathbf{k} = \frac{2\pi}{L}\mathbf{n}$, and the sum is taken over both positive and negative k . Replacing \mathbf{n} by \mathbf{k} then gives

$$\langle |f(\mathbf{x})|^2 \rangle \approx \frac{L^2}{2\pi N^6} \sum k^2 |f(k)_{3d}|^2, \quad (\text{B.18})$$

where the dimension of the Fourier transform has been labelled. In one and two dimensions the corresponding expressions are

$$\langle |f(\mathbf{x})|^2 \rangle = \frac{1}{N^2} \sum |f(k)_{1d}|^2 \quad \text{and} \quad \langle |f(\mathbf{x})|^2 \rangle \approx \frac{L}{2N^4} \sum |k| |f(k)_{2d}|^2, \quad (\text{B.19})$$

respectively. Comparison shows

$$|f(k)_{1d}|^2 \approx \frac{L^2}{2\pi N^4} k^2 |f(k)_{3d}|^2 \quad \text{and} \quad (\text{B.20})$$

$$|f(k)_{2d}|^2 \approx \frac{L}{\pi N^2} |k| |f(k)_{3d}|^2. \quad (\text{B.21})$$

So, in order to approximate the three-dimensional occupation number one should multiply the one- or two-dimensional result with a factor

$$\frac{2\pi N^4}{L^2 k^2} \quad \text{and} \quad \frac{\pi N^2}{L k^2}, \quad (\text{B.22})$$

respectively.

B.3. Staggered leapfrog method

LATTICEEASY calculates the time evolution of the fields by use of the staggered leapfrog method which is discussed in [66]. The name refers to the fact, that within this integration scheme the function and its second derivative are evaluated at different times compared to the first derivative. This is done alternately. To see how it works let us consider a second-order differential equation

$$J[f(t)] = \ddot{f}(t) \quad (\text{B.23})$$

and the discretized version

$$J[f(t)] \approx \frac{\dot{f}(t + \Delta t/2) - \dot{f}(t - \Delta t/2)}{\Delta t} \approx \frac{f(t + \Delta t) - 2f(t) + f(t - \Delta t)}{\Delta t^2}, \quad (\text{B.24})$$

where Δt is the step-size in time. A rather stable numeric solution to this problem is to first desynchronize the time-steps for f and \dot{f} on the one hand and of \ddot{f} on the other hand,

$$\dot{f} \left(t + \frac{\Delta t}{2} \right) = \dot{f}(t) + J[f(t)] \frac{\Delta t}{2}, \quad (\text{B.25})$$

B.4. Particle number density of classical fields

to evolve $f(t)$ and its derivatives by the same time steps Δt ,

$$f(t + \Delta t) = f(t) + \dot{f}\left(t + \frac{\Delta t}{2}\right) \Delta t, \quad (\text{B.26})$$

$$\dot{f}\left(t + \frac{3}{2}\Delta t\right) = \dot{f}\left(t + \frac{\Delta t}{2}\right) + J[f(t + \Delta t)]\Delta t, \quad (\text{B.27})$$

and to resynchronize after N steps,

$$\dot{f}(t + N\Delta t) = \dot{f}\left(t + \left(N - \frac{1}{2}\right) \Delta t\right) + J[f(t + N\Delta t)]\frac{\Delta t}{2}. \quad (\text{B.28})$$

However, the advantage in stability is lost, when \ddot{f} depends also on \dot{f} . This does not occur if there is no expansion of space. But within an FRW background time and fields need to be rescaled with appropriate powers of the scale factor a in order to eliminate the contribution proportional to \dot{f} in the equation of motion.

B.4. Particle number density of classical fields

This section gives an account on how particle densities or occupation numbers can be defined within a classical calculation. For highly occupied modes this definition coincides with the quantum mechanical approach based on Bogolyubov transformations. In order to be applicable to all calculations done in this work, the derivation includes an expanding background. Let us first write down the equation of motion of a classical scalar field with potential V within a spatially flat FRW universe, see Eq. (??),

$$\ddot{\phi} + 3H\dot{\phi} - \frac{1}{a^2}\Delta\phi + \frac{\partial V}{\partial\phi} = 0. \quad (\text{B.29})$$

Here, Δ refers to comoving spatial coordinates \mathbf{x} . To write down the conformal version of this equation, one again defines $a d\eta \equiv dt$ and $\varphi \equiv a\phi$ and sees

$$\dot{\phi} = \frac{1}{a}\phi', \quad \ddot{\phi} = \frac{1}{a^2}\phi'' - \frac{a'}{a^3}\phi' \quad (\text{B.30})$$

$$\Rightarrow \phi'' + 2\frac{a'}{a}\phi' - \Delta\phi + a^2\frac{\partial V}{\partial\phi} = 0. \quad (\text{B.31})$$

Written in terms of φ , the equation does not depend on the first derivative of the field with respect to time anymore:

$$\phi' = \frac{1}{a}\varphi' - \frac{a'}{a^2}\varphi, \quad \phi'' = \frac{1}{a}\varphi'' - 2\frac{a'}{a^2}\varphi' + 2\frac{a'^2}{a^3}\varphi - \frac{a''}{a^2}\varphi \quad (\text{B.32})$$

$$\Rightarrow \varphi'' - 2\frac{a''}{a}\varphi - \Delta\varphi + a^4\frac{\partial V}{\partial\varphi} = 0. \quad (\text{B.33})$$

Now let φ_k be the Fourier transform of the conformal field, $\varphi_k = a\phi_k$, and approximate the derivative of the potential in Fourier space by

$$\left(\frac{\partial V}{\partial\varphi}\right)_k \approx \left\langle \frac{\partial^2 V}{\partial\varphi^2} \right\rangle \varphi_k. \quad (\text{B.34})$$

Appendix B

After defining the mode energy

$$\omega_k := k^2 + a^4 \left\langle \frac{\partial^2 V}{\partial \varphi^2} \right\rangle - \frac{a''}{a}, \quad (\text{B.35})$$

this leads to the oscillator equation

$$\varphi_k'' + \omega_k^2(\eta)\varphi_k = 0. \quad (\text{B.36})$$

Following [104], now the occupation numbers n_k are derived. From the theory of Bogolyubov transformations it is known that

$$n_k = |\beta_k|^2, \quad |\alpha_k|^2 - |\beta_k|^2 = 1, \quad (\text{B.37})$$

$$\alpha_k = \frac{W(u_k, v_k^*)}{2i}, \quad \beta_k = \frac{W(v_k, u_k)}{2i}, \quad W(v, u) := v'u - vu', \quad (\text{B.38})$$

where the Bogolyubov coefficients α_k and β_k are written in terms of the Wronskian W of mode functions. These are defined for example in Ref. [104], which is recommended as a more detailed presentation. Assuming large occupation numbers one can also write

$$n_k \approx \frac{|\alpha_k|^2 + |\beta_k|^2}{2} \quad (\text{B.39})$$

and then calculate

$$n_k \approx \frac{1}{8} (|W(u_k, v_k^*)|^2 + |W(v_k, u_k)|^2) \quad (\text{B.40})$$

$$= \frac{1}{4} (u_k u_k^* v_k' v_k'^* + u_k' u_k'^* v_k v_k) = \frac{1}{4} \left(\omega_k |u_k|^2 + \frac{1}{\omega_k} |u_k'|^2 \right), \quad (\text{B.41})$$

where for the last equality the initial condition

$$v_k(\eta) = \frac{1}{\sqrt{\omega_k}} e^{i\omega_k \eta} \quad (\text{B.42})$$

has been used. Writing $|\hat{A}|^2 = \hat{A}\hat{A}^+$ for a general operator, expression (B.41) can in terms of operators be rewritten as

$$\frac{1}{\text{Volume}} \left\langle 0, b \left| \frac{1}{4} \omega_k |\hat{b}_{\mathbf{k}}^- u_{\mathbf{k}}^*(\eta) + \hat{b}_{-\mathbf{k}}^+ u_{\mathbf{k}}(\eta)|^2 + \frac{1}{4\omega_k} |\hat{b}_{\mathbf{k}}^- u_{\mathbf{k}}'^*(\eta) + \hat{b}_{-\mathbf{k}}^+ u_{\mathbf{k}}'(\eta)|^2 \right| 0, b \right\rangle, \quad (\text{B.43})$$

which is arranged such that one can make use of the general solution of (B.36),

$$\hat{\varphi}_{\mathbf{k}}(\eta) = \frac{1}{\sqrt{2}} \left(\hat{b}_{\mathbf{k}}^- u_{\mathbf{k}}^*(\eta) + \hat{b}_{-\mathbf{k}}^+ u_{\mathbf{k}}(\eta) \right). \quad (\text{B.44})$$

Doing so we arrive at

$$n_{\mathbf{k}} = \frac{1}{\text{Volume}} \left\langle 0, b \left| \frac{1}{2} \omega_k |\hat{\varphi}_{\mathbf{k}}(\eta)|^2 + \frac{1}{2\omega_k} |\hat{\varphi}_{\mathbf{k}}'(\eta)|^2 \right| 0, b \right\rangle, \quad (\text{B.45})$$

and finally write down the formula which is used in the lattice calculations:

$$n_{\mathbf{k}} = \frac{1}{2} \left(\omega_k |\varphi_{\mathbf{k}}(\eta)|^2 + \frac{1}{2\omega_k} |\varphi_{\mathbf{k}}'(\eta)|^2 \right) \quad (\text{B.46})$$

where as above in Eq. (B.4) the volume has been absorbed into the definition of $\varphi_{\mathbf{k}}$.

C. An auxiliary calculation

In this section the calculation of the integral

$$\theta_k = \int_0^{\frac{\pi}{m}} dt \sqrt{k^2 + g^2 \phi^2(t)} \quad (\text{C.1})$$

in Sect. 7.2.4 is presented: Inserting $\phi(t) = \phi_0 \sin(mt)$ and defining $z = mt$ and $\varepsilon = k/(g\phi_0)$ gives

$$\frac{m}{\phi_0 g} \theta_k = \int_0^\pi dz \sqrt{\varepsilon^2 + \sin^2 z} = 2 \int_0^{r\varepsilon} dz \sqrt{\varepsilon^2 + \sin^2 z} + \int_{r\varepsilon}^{\pi-r\varepsilon} dz \sqrt{\varepsilon^2 + \sin^2 z}, \quad (\text{C.2})$$

where the integral is split such that $1 \gg r \gg \varepsilon$ in the equation above. After approximating $\sin z \approx z$ the first term is now expanded up to $O(\varepsilon^2)$ which yields

$$\varepsilon^2 \left[r \sqrt{r^2 + 1} + \ln \left(r + \sqrt{r^2 + 1} \right) \right] \quad (\text{C.3})$$

as in Eq. (7.44). The second term is expanded in terms of the small quantity $\varepsilon^2/\sin^2 z$ leading to a sum over an alternating sequence that converges to zero:

$$\sum_{n=0}^{\infty} \binom{2n}{n} \frac{(-1)^n}{4^n (1-2n)} \varepsilon^{2n} \int_{r\varepsilon}^{\pi-r\varepsilon} dz \frac{1}{\sin^{2n-1}(z)}. \quad (\text{C.4})$$

For $n = 0$ the integral results in

$$2 \cos(r\varepsilon) \approx 2 - r^2 \varepsilon^2, \quad (\text{C.5})$$

for $n = 1$ there is

$$\frac{1}{2} \varepsilon^2 \int_{r\varepsilon}^{\pi-r\varepsilon} dz \frac{1}{\sin(z)} = \frac{1}{2} \varepsilon^2 \ln \left[\frac{\tan(\pi/2 - r\varepsilon/2)}{\tan(r\varepsilon/2)} \right] \quad (\text{C.6})$$

$$\approx \frac{1}{2} \varepsilon^2 \ln \left(\frac{4}{r^2 \varepsilon^2} \right), \quad (\text{C.7})$$

and for $n > 1$ the result up to $O(\varepsilon^2)$ amounts to

$$\varepsilon^2 \sum_{n=2}^{\infty} \binom{2n}{n} \frac{(-1)^n}{4^n (1-2n)(n-1)} r^{2-2n}, \quad (\text{C.8})$$

which is negligibly small compared to the other contributions. Adding the results of Eqs. (C.3), (C.5), and (C.7), rearranging the logarithm and taking the limit $r \rightarrow \infty$ gives the result displayed in Sect. 7.2.4:

$$\theta_k = \int_0^{\frac{\pi}{m}} dt \sqrt{k^2 + g^2 \phi^2(t)} \approx \frac{2g\phi_0}{m} + \frac{\kappa^2}{2} \left(\ln \frac{g\phi_0}{m\kappa^2} + 4 \ln 2 + 1 \right). \quad (\text{C.9})$$

Bibliography

- [1] Esa webpage: <http://www.esa.int/esa>. <http://www.esa.int/ESA>.
- [2] *Metzler Philosophenlexikon*. Metzler, 2004.
- [3] L. F. Abbott and Mark B. Wise. Constraints on generalized inflationary cosmologies. *Nuclear Physics B*, 244(2):541 – 548, 1984.
- [4] Milton Abramowitz and Irene A. Stegun. *Handbook of mathematical functions with formulas, graphs, and mathematical tables*, volume 55 of *National Bureau of Standards Applied Mathematics Series*. U.S. Government Printing Office, Washington, D.C., 1964.
- [5] P. A. R. Ade et al. Detection of b -mode polarization at degree angular scales by bicep2. *Phys. Rev. Lett.*, 112:241101, Jun 2014.
- [6] P. A. R. Ade et al. A joint analysis of BICEP2/Keck array and Planck data. *Phys.Rev.Lett.*, 2015.
- [7] P. A. R. Ade et al. Planck 2015. XX. Constraints on inflation. 2015.
- [8] Stephen L. Adler. Axial-vector vertex in spinor electrodynamics. *Phys. Rev.*, 177:2426–2438, Jan 1969.
- [9] Stephen L. Adler and William A. Bardeen. Absence of higher-order corrections in the anomalous axial-vector divergence equation. *Phys. Rev.*, 182:1517–1536, Jun 1969.
- [10] Andreas Albrecht and Paul J. Steinhardt. Cosmology for grand unified theories with radiatively induced symmetry breaking. *Phys. Rev. Lett.*, 48:1220–1223, Apr 1982.
- [11] Rouzbeh Allahverdi, Robert Brandenberger, Francis-Yan Cyr-Racine, and Anupam Mazumdar. Reheating in inflationary cosmology: Theory and applications. *Ann.Rev.Nucl.Part.Sci.*, 60:27–51, 2010.
- [12] G. Barton. Quantum mechanics of the inverted oscillator potential. *Annals of Physics*, 166(2):322 – 363, 1986.

Bibliography

- [13] Bateman Manuscript Project, H. Bateman, and A. Erdélyi. *Higher Transcendental Functions*. Number Bd. 3 in Higher Transcendental Functions. McGraw-Hill, 1955.
- [14] Diana Battfeld and Patrick Peter. A critical review of classical bouncing cosmologies. *Physics Reports*, 571(0):1 – 66, 2015. A critical review of classical bouncing cosmologies.
- [15] D. Baumann and L. McAllister. Inflation and string theory. *ArXiv e-prints*, April 2014.
- [16] K. Becker, M. Becker, J. H. Schwarz, and P. Ramond. *String theory and M-theory: A modern introduction*, volume 61. 2008.
- [17] J. Beringer et al. Review of particle physics*. *Phys. Rev. D*, 86:010001, Jul 2012.
- [18] M. V. Berry and K. E. Mount. Semiclassical approximations in wave mechanics. *Reports on Progress in Physics*, 35(1):315, 1972.
- [19] Siegfried Bethke. World summary of α_s (2012). *Nucl.Phys.Proc.Suppl.*, 234:229–234, 2013.
- [20] S. Biswas, P. Misra, and I. Chowdhury. The CWKB method of particle production in a periodic potential. *General Relativity and Gravitation*, 35(1):1–16, 2003.
- [21] Tillmann Boeckel. A little inflation at the cosmological QCD phase transition. PhD Thesis. 2011.
- [22] Tillmann Boeckel and Jürgen Schaffner-Bielich. A little inflation in the early universe at the QCD phase transition. *Phys. Rev. Lett.*, 105(4):041301+, 2010.
- [23] Arvind Borde and Alexander Vilenkin. Eternal inflation and the initial singularity. *Phys. Rev. Lett.*, 72:3305–3308, May 1994.
- [24] Robert H. Brandenberger. Alternatives to the inflationary paradigm of structure formation. *Int.J.Mod.Phys.Conf.Ser.*, 01:67–79, 2011.
- [25] Robert H. Brandenberger. The matter bounce alternative to inflationary cosmology. *ArXiv e-prints*, June 2012.
- [26] Robert H. Brandenberger. Do we have a theory of early universe cosmology? *Studies in History and Philosophy of Science Part B: Studies in History and Philosophy of Modern Physics*, 46, Part A(0):109 – 121, 2014. Philosophy of cosmology.
- [27] V. M. Braun, G. P. Korchemsky, and D. Müller. The uses of conformal symmetry in QCD. *Progress in Particle and Nuclear Physics*, 51(2):311 – 398, 2003.
- [28] Philippe Brax, Jean-Francois Dufaux, and Sophie Mariadassou. Preheating after small-field inflation. *Phys.Rev.*, D83:103510, 2011.

-
- [29] Torsten Bringmann, Pat Scott, and Yashar Akrami. Improved constraints on the primordial power spectrum at small scales from ultracompact minihalos. *Phys. Rev. D*, 85:125027, Jun 2012.
- [30] I. N. Bronštejn and G. Musiol. *Taschenbuch der Mathematik*. Deutsch, 2008.
- [31] Evgeny I. Buchbinder, Justin Khoury, and Burt A. Ovrut. New ekpyrotic cosmology. *Phys. Rev. D*, 76:123503, Dec 2007.
- [32] B. A. Campbell, John Ellis, and K. A. Olive. Effective lagrangian approach to qcd phase transitions. *Physics Letters B*, 235:325 – 330, 1990.
- [33] A. Chodos, R. L. Jaffe, K. Johnson, C. B. Thorn, and V. F. Weisskopf. New extended model of hadrons. *Phys. Rev. D*, 9(12):3471–3495, 1974.
- [34] Sébastien Clesse. Hybrid inflation along waterfall trajectories. *Phys. Rev. D*, 83:063518, Mar 2011.
- [35] Sébastien Clesse and Jérémy Rekier. Updated constraints on large field hybrid inflation. *Phys. Rev. D*, 90:083527, Oct 2014.
- [36] Sidney Coleman. *Aspects of symmetry*. Cambridge University Press, 1985. Cambridge Books Online.
- [37] Sidney Coleman and Roman Jackiw. Why dilatation generators do not generate dilatations. *Annals of Physics*, 67(2):552 – 598, 1971.
- [38] Sidney Coleman and Erick Weinberg. Radiative corrections as the origin of spontaneous symmetry breaking. *Phys. Rev. D*, 7:1888–1910, Mar 1973.
- [39] John C. Collins, Anthony Duncan, and Satish D. Joglekar. Trace and dilatation anomalies in gauge theories. *Phys. Rev. D*, 16:438–449, Jul 1977.
- [40] R. Courant, K. Friedrichs, and H. Lewy. Über die partiellen Differenzgleichungen der mathematischen Physik. *Mathematische Annalen*, 100(1):32–74, December 1928.
- [41] Thibault Damour and Viatcheslav F. Mukhanov. Inflation without slow roll. *Phys. Rev. Lett.*, 80:3440–3443, Apr 1998.
- [42] Mariel Desroche, Gary N. Felder, Jan M. Kratochvil, and Andrei D. Linde. Preheating in new inflation. *Phys.Rev.*, D71:103516, 2005.
- [43] C. E. DeTar and J. F. Donoghue. Bag models of hadrons. *Annual Review of Nuclear and Particle Science*, 33(1):235–264, 1983.
- [44] R. H. Dicke, P. J. E. Peebles, P. G. Roll, and D. T. Wilkinson. Cosmic Black-Body Radiation. *Astrophysical Journal*, 142:414–419, July 1965.

Bibliography

- [45] Albert Einstein. Cosmological Considerations in the General Theory of Relativity, <http://einsteinpapers.press.princeton.edu/>. *Sitzungsber.Preuss.Akad.Wiss.Berlin (Math.Phys.)*, 1917:142–152, 1917.
- [46] George F. R. Ellis and Roy Maartens. The emergent universe: inflationary cosmology with no singularity. *Classical and Quantum Gravity*, 21(1):223, 2004.
- [47] George F R Ellis, Jeff Murugan, and Christos G Tsagas. The emergent universe: an explicit construction. *Classical and Quantum Gravity*, 21(1):233, 2004.
- [48] R. Fabbri and M.D. Pollock. The effect of primordially produced gravitons upon the anisotropy of the cosmological microwave background radiation. *Physics Letters B*, 125(6):445 – 448, 1983.
- [49] Gary Felder. Clustereasy: A program for lattice simulations of scalar fields in an expanding universe on parallel computing clusters. *Computer Physics Communications*, 179(8):604 – 606, 2008.
- [50] Gary Felder and Igor Tkachev. LATTICEEASY: A program for lattice simulations of scalar fields in an expanding universe. *Computer Physics Communications*, 178(12):929 – 932, 2008.
- [51] Gary Felder and Igor Tkachev. LATTICEEASY Home Page. <http://www.cita.utoronto.ca/felder/latticeeasy/index.html>, June 2009.
- [52] Kenneth W. Ford, David L. Hill, Masami Wakano, and John A. Wheeler. Quantum effects near a barrier maximum. *Annals of Physics*, 7(3):239 – 258, 1959.
- [53] Pietro Giuseppe Frè. *Gravity, a Geometrical Course*. Springer Netherlands, 2013.
- [54] A. Friedman. Über die Krümmung des Raumes. *Zeitschrift für Physik*, 10(1):377–386, 1922.
- [55] M. Gell-Mann and M. Lévy. The axial vector current in beta decay. *Il Nuovo Cimento*, 16(4):705–726, 1960.
- [56] J. Goldstone. Field theories with superconductor solutions. *Il Nuovo Cimento*, 19(1):154–164, 1961.
- [57] Jeffrey Goldstone, Abdus Salam, and Steven Weinberg. Broken symmetries. *Phys. Rev.*, 127:965–970, Aug 1962.
- [58] A. S. Goncharov, Andrei D. Linde, and Viatcheslav F. Mukhanov. The global structure of the inflationary universe. *Int. J. Mod. Phys. A*, 1987(02):561, 1987.
- [59] Dmitry S. Gorbunov and Valery A. Rubakov. *Introduction to the theory of the early universe: Cosmological perturbations and inflationary theory*. World Scientific, 2011.

-
- [60] Dmitry S. Gorbunov and Valery A. Rubakov. *Introduction to the theory of the early universe: Hot Big Bang theory*. World Scientific, 2011.
- [61] Christopher Gordon, David Wands, Bruce A. Bassett, and Roy Maartens. Adiabatic and entropy perturbations from inflation. *Phys. Rev. D*, 63:023506, Dec 2000.
- [62] Izrail Solomonovich Gradshteyn and Iosif Moiseevich Ryzhik. *Table of integrals, series and products*. Academic Press, San Diego, sixth edition, 2000. The relevant integrals are 3.249.7 on page 321 and 3.251.1 on page 322.
- [63] Patrick B. Greene, Lev Kofman, Andrei D. Linde, and Alexei A. Starobinsky. Structure of resonance in preheating after inflation. *Phys.Rev.*, D56:6175–6192, 1997.
- [64] Alan H. Guth. Inflationary universe: A possible solution to the horizon and flatness problems. *Phys. Rev. D*, 23:347–356, Jan 1981.
- [65] Alan H. Guth and Erick J. Weinberg. Could the universe have recovered from a slow first-order phase transition? *Nuclear Physics B*, 212(2):321 – 364, 1983.
- [66] Ernst Hairer, Christian Lubich, and Gerhard Wanner. *Geometric numerical integration illustrated by the Strmer-Verlet method*, volume 12. 4 2003.
- [67] E. Halyo. Is $f_0(975)$ a QCD dilaton? *Physics Letters B*, 271:415 – 420, 1991.
- [68] E. R. Harrison. Fluctuations at the threshold of classical cosmology. *Phys. Rev. D*, 1:2726–2730, May 1970.
- [69] S. W. Hawking. The development of irregularities in a single bubble inflationary universe. *Physics Letters B*, 115(4):295 – 297, 1982.
- [70] S. W. Hawking, I. G. Moss, and J. M. Stewart. Bubble collisions in the very early universe. *Phys. Rev. D*, 26:2681–2693, Nov 1982.
- [71] G. Hinshaw, D. Larson, E. Komatsu, D. N. Spergel, C. L. Bennett, J. Dunkley, M. R. Nolta, M. Halpern, R. S. Hill, N. Odegard, L. Page, K. M. Smith, J. L. Weiland, B. Gold, N. Jarosik, A. Kogut, M. Limon, S. S. Meyer, G. S. Tucker, E. Wollack, and E. L. Wright. Nine-year Wilkinson Microwave Anisotropy Probe (WMAP) Observations: Cosmological Parameter Results. *ApJS*, 208:19, October 2013.
- [72] Edwin Hubble. A relation between distance and radial velocity among extragalactic nebulae. *Proc.Nat.Acad.Sci.*, 15:168–173, 1929.
- [73] J.-C. Hwang. Perturbations of the Robertson-Walker space - Multicomponent sources and generalized gravity. *Astrophysical Journal*, 375:443–462, July 1991.

Bibliography

- [74] B. L. Ioffe. Axial Anomaly: the Modern Status. *International Journal of Modern Physics A*, 21:6249–6266, 2006.
- [75] Nemanja Kaloper, Matthew Kleban, Albion Lawrence, and Stephen Shenker. Signatures of short distance physics in the cosmic microwave background. *Phys. Rev. D*, 66:123510, Dec 2002.
- [76] Dmitri Kharzeev, Eugene Levin, and Kirill Tuchin. Broken scale invariance, massless dilaton and confinement in qcd. *Journal of High Energy Physics*, 2009(06):055, 2009.
- [77] S. Yu. Khlebnikov and I. I. Tkachev. Classical decay of the inflaton. *Phys. Rev. Lett.*, 77:219–222, Jul 1996.
- [78] Justin Khoury, Burt A. Ovrut, Paul J. Steinhardt, and Neil Turok. Ekpyrotic universe: Colliding branes and the origin of the hot big bang. *Phys. Rev. D*, 64:123522, Nov 2001.
- [79] Volker Koch. Aspects of Chiral Symmetry. *Int. J. Mod. Phys.*, E6:203–250, 1997.
- [80] Lev Kofman, Andrei D. Linde, and Alexei A. Starobinsky. Towards the theory of reheating after inflation. *Phys.Rev.*, D56:3258–3295, 1997.
- [81] C. Kounnas, H. Partouche, and N. Toumbas. Thermal duality and non-singular cosmology in d-dimensional superstrings. *Nuclear Physics B*, 855(2):280 – 307, 2012.
- [82] H. S. Kragh. *Conceptions of cosmos: From myths to the accelerating universe*. OUP Oxford, 2006.
- [83] H. S. Kragh. Historical aspects of post-1850 cosmology. volume 1632 of *American Institute of Physics Conference Series*, pages 3–26, November 2014.
- [84] N. W. M. Lachlan. *Theory and application of Mathieu functions*. Dover books on engineering and engineering physics. Dover, 1947.
- [85] C. B. Lang and N. Pucker. *Mathematische Methoden in der Physik*. Spektrum Akademischer Verlag, 2005.
- [86] H. S. Leavitt and E. C. Pickering. Periods of 25 Variable Stars in the Small Magellanic Cloud. *Harvard College Observatory Circular*, 173:1–3, March 1912.
- [87] G. Lemaître. Un Univers homogène de masse constante et de rayon croissant rendant compte de la vitesse radiale des nébuleuses extra-galactiques. *Annales de la Société Scientifique de Bruxelles*, 47:49–59, 1927.
- [88] Andrei D. Linde. Phase transitions in gauge theories and cosmology. *Reports on Progress in Physics*, 42(3):389, 1979.

-
- [89] Andrei D. Linde. A new inflationary universe scenario: A possible solution of the horizon, flatness, homogeneity, isotropy and primordial monopole problems. *Phys.Lett.*, B108:389–393, 1982.
- [90] Andrei D. Linde. Chaotic inflation. *Physics Letters B*, 129(3-4):177 – 181, 1983.
- [91] Andrei D. Linde. Eternally existing self-reproducing inflationary universe. *Physica Scripta*, 1987(T15):169, 1987.
- [92] Andrei D. Linde. Axions in inflationary cosmology. *Physics Letters B*, 259(1-2):38 – 47, 1991.
- [93] Andrei D. Linde. Fast-roll inflation. *Journal of High Energy Physics*, 2001(11):052, 2001.
- [94] Andrei D. Linde. Inflationary cosmology. volume 738 of *Lecture Notes in Physics*, Berlin Springer Verlag, page 1, 2008.
- [95] David H. Lyth and Andrew R. Liddle. *The primordial density perturbation: Cosmology, inflation and the origin of structure; rev. version*. Cambridge University Press, Cambridge, 2009.
- [96] Jérôme Martin and Robert H. Brandenberger. Trans-planckian problem of inflationary cosmology. *Phys. Rev. D*, 63:123501, May 2001.
- [97] Émile Mathieu. Mémoire sur le mouvement vibratoire d’une membrane de forme elliptique. *Journal de Mathématiques Pures et Appliqués*, pages 137–203, 1868.
- [98] Raphael Micha and Igor I. Tkachev. Turbulent thermalization. *Phys.Rev.*, D70:043538, 2004.
- [99] I. Mishustin, J. Bondorf, and M. Rho. Chiral Symmetry, Scale Invariance and Properties of Nuclear Matter. *Nuclear Physics A*, 555(1):215 – 224, 1993.
- [100] Ulrich Mosel. *Fields, symmetries, and quarks; 2nd ed*. Springer, Berlin, 1999.
- [101] Viatcheslav F. Mukhanov. *Physical foundations of cosmology*. Cambridge University Press, 2005.
- [102] Viatcheslav F. Mukhanov and G. V. Chibisov. Quantum Fluctuation and Nonsingular Universe. (In Russian). *JETP Lett.*, 33:532–535, 1981.
- [103] Viatcheslav F. Mukhanov, H. A. Feldman, and Robert H. Brandenberger. Theory of cosmological perturbations. *Physics Reports*, 215(5-6):203–333, 1992.
- [104] Viatcheslav F. Mukhanov and Sergei Winitzki. *Introduction to quantum effects in gravity*. Cambridge University Press, 2007.

Bibliography

- [105] Ali Nayeri, Robert H. Brandenberger, and Cumrun Vafa. Producing a scale-invariant spectrum of perturbations in a Hagedorn phase of string cosmology. *Phys. Rev. Lett.*, 97:021302, Jul 2006.
- [106] Emmy Noether. Invariante Variationsprobleme. *Nachr. Ges. Wiss. Göttingen, Math.-Phys. Kl.*, 1918:235–257, 1918.
- [107] K.A. Olive et al. Review of Particle Physics. *Chin.Phys.*, C38:090001, 2014.
- [108] Tomás Ortín. *Gravity and strings*. Cambridge University Press, 1 edition, January 2007.
- [109] P. Papazoglou, J. Schaffner, S. Schramm, D. Zschiesche, H. Stöcker, and W. Greiner. Phase Transition in the Chiral σ - ω Model with Dilatons. *Phys. Rev. C*, 55(3):1499–1508, 1997.
- [110] Arno A. Penzias and Robert W. Wilson. A measurement of excess antenna temperature at 4080 Mc/s. *Astrophysical Journal*, 142:419–421, July 1965.
- [111] Michael E. Peskin and Daniel V. Schroeder. *An introduction to quantum field theory (Frontiers in physics)*. Perseus Books, 2008.
- [112] Patrick Peter and Nelson Pinto-Neto. Cosmology without inflation. *Phys. Rev. D*, 78:063506, Sep 2008.
- [113] Planck Collaboration, P. A. R. Ade, N. Aghanim, C. Armitage-Caplan, M. Arnaud, M. Ashdown, F. Atrio-Barandela, J. Aumont, C. Baccigalupi, A. J. Banday, and et al. Planck 2013 results. XXII. Constraints on inflation. *Astronomy and Astrophysics*, 571:A22, November 2014.
- [114] David Polarski and Alexei A Starobinsky. Semiclassicality and decoherence of cosmological perturbations. *Classical and Quantum Gravity*, 13(3):377, 1996.
- [115] J. Polchinski. *String theory*. Cambridge University Press, 2001.
- [116] Matts Roos. *Introduction to cosmology*. John Wiley and Sons, 2003.
- [117] V. A. Rubakov, M. V. Sazhin, and A. V. Veryaskin. Graviton creation in the inflationary universe and the grand unification scale. *Physics Letters B*, 115(3):189 – 192, 1982.
- [118] Karl Schwarzschild. On the permissible curvature of space (Über das zulässige Krümmungsmaß des Raumes, 1900). *Classical and Quantum Gravity*, 15(9):2539, 1998.
- [119] Vesto M. Slipher. Nebulae, <http://www.roe.ac.uk/~jap/slipher/>. *Proc.Am.Phil.Soc.*, 56:403–409, 1917.

- [120] M. Srednicki. *Quantum field theory*. Cambridge University Press, 2007.
- [121] A. A. Starobinsky. A new type of isotropic cosmological models without singularity. *Physics Letters B*, 91(1):99 – 102, 1980.
- [122] Paul J. Steinhardt and Neil Turok. Cosmic evolution in a cyclic universe. *Phys. Rev. D*, 65:126003, May 2002.
- [123] Michael S. Turner. Coherent scalar-field oscillations in an expanding universe. *Phys. Rev. D*, 28:1243–1247, Sep 1983.
- [124] Alexander Vilenkin. Birth of inflationary universes. *Phys. Rev. D*, 27:2848–2855, Jun 1983.
- [125] David Wands. Multiple field inflation. In Martin Lemoine, Jerome Martin, and Patrick Peter, editors, *Inflationary Cosmology*, volume 738 of *Lecture Notes in Physics*, pages 275–304. Springer Berlin Heidelberg, 2007.
- [126] Kyu Hwang Yeon, Shou Zhang, Yong Dae Kim, Chung In Um, and Thomas F. George. Quantum solutions for the harmonic-parabola potential system. *Phys. Rev. A*, 61:042103, Mar 2000.
- [127] Yakov B. Zeldovich. A Hypothesis, unifying the structure and the entropy of the universe. *Mon.Not.Roy.Astron.Soc.*, 160:1P–3P, 1972.
- [128] B. Zwiebach. *A first course in string theory*. Cambridge University Press, 2004.

Dank

Ich möchte mich bei allen bedanken, die zu dieser Arbeit beigetragen haben. Dabei geht der erste, große Dank an Jürgen Schaffner-Bielich, in dessen Gruppe ich die letzten Jahre gearbeitet habe. Jürgen hat mir die Möglichkeit gegeben, unter seiner Betreuung ein spannendes Forschungsgebiet kennenzulernen. Seine motivierende und inspirierende Begleitung haben mir sehr geholfen.

Die entspannte und freundschaftliche Atmosphäre in Jürgens Arbeitsgruppe habe ich sehr genossen. Für diese Erfahrung bedanke ich mich bei Kreso Baotic, Thomas Beisitzer, Till Boeckel, Debarati Chatterjee, Thorben Graf, Margit Maly, Giuseppe Pagliara, Rainer Stiele, Simon Weissenborn und Andreas Zacchi.

Gemeinsam mit Jürgen haben Jan-Martin Pawlowski und Matthias Bartelmann meine Arbeit betreut. Ich bin dankbar für ihre hilfreichen und freundlichen Hinweise und Vorschläge.

Für die Begutachtung dieser Arbeit bedanke ich mich besonders bei Jürgen und Matthias. Ich habe mich außerdem sehr darüber gefreut, dass ich mit Werner Aeschbach-Hertig und Klaus Reygers meine Prüfungskommission vervollständigen konnte. Ihre große Bereitschaft zur Terminfindung hat die Organisation der Disputation sehr erleichtert.

Mein Dank gilt den Mitgliedern des Instituts für theoretische Physik der Universität Heidelberg: Den Mitarbeiterinnen des Sekretariats und der Bibliothek, Franziska Binder, Tina Birke, Jeannette Bloch-Ditzinger, Isolde Dobhan, Angela Haag, Irene Illi, Anja Kamp und Manuela Wirschke, und Elmar Bittner für die Betreuung des Computernetzwerks. Organisatorische Fragen fanden menschliche Antworten bei Jürgen Berges und Eduard Thommes. Vielen Dank dafür.

Den Mitarbeiterinnen des HGSFP-Prüfungssekretariats, Gesine Heinzemann, Elisabeth Miller und Karina Schönfeld, danke ich für die freundliche Besprechung vieler organisatorischer Fragen.

Während meiner Zeit als Doktorand in Heidelberg war ich Mitglied der IMPRS-PTFS (International Max Planck Research School for Precision Tests of Fundamental Symmetries in Particle Physics, Nuclear Physics, Atomic Physics and Astroparticle Physics at the University of Heidelberg). Für die freundliche Aufnahme danke ich Manfred Lindner, Klaus Blaum und Werner Rodejohann. Besonderer Dank gilt Britta Schwarz für ihre Herzlichkeit, die ihre Arbeit am MPIK prägt.

Bei Philipp Merkel möchte ich mich herzlich für seine Freundschaft und Hilfsbereitschaft, die gemeinsame Zeit und viele neue Ideen bedanken.

Meine Familie war mit ihrer bedingungslosen Unterstützung in vielen Situationen ein Segen. Meine Dankbarkeit ist ihr sicher. Hannah, Amelia, Elijah und Philemon sind der beste Beweis dafür, dass Physik nicht das Wichtigste ist. Sie werden immer einen Platz in meinem Herzen haben.